



<https://theses.gla.ac.uk/>

Theses Digitisation:

<https://www.gla.ac.uk/myglasgow/research/enlighten/theses/digitisation/>

This is a digitised version of the original print thesis.

Copyright and moral rights for this work are retained by the author

A copy can be downloaded for personal non-commercial research or study, without prior permission or charge

This work cannot be reproduced or quoted extensively from without first obtaining permission in writing from the author

The content must not be changed in any way or sold commercially in any format or medium without the formal permission of the author

When referring to this work, full bibliographic details including the author, title, awarding institution and date of the thesis must be given

Enlighten: Theses

<https://theses.gla.ac.uk/>
research-enlighten@glasgow.ac.uk

"VISCOELASTIC RELAXATION IN POLYMERS WITH
SPECIAL REFERENCE TO BEHAVIOUR AT AUDIO
FREQUENCIES"

A thesis submitted to the
Faculty of Engineering
of the
University of Glasgow
for the degree of
Ph. D.
(Electrical Engineering)
by
Peter Lindon

September 1965

ProQuest Number: 10835588

All rights reserved

INFORMATION TO ALL USERS

The quality of this reproduction is dependent upon the quality of the copy submitted.

In the unlikely event that the author did not send a complete manuscript and there are missing pages, these will be noted. Also, if material had to be removed, a note will indicate the deletion.



ProQuest 10835588

Published by ProQuest LLC (2018). Copyright of the Dissertation is held by the Author.

All rights reserved.

This work is protected against unauthorized copying under Title 17, United States Code
Microform Edition © ProQuest LLC.

ProQuest LLC.
789 East Eisenhower Parkway
P.O. Box 1346
Ann Arbor, MI 48106 – 1346

SUMMARY

An electromagnetic transducer has been developed to measure the complex dynamic shear modulus of viscoelastic liquids as a function of frequency in the range $20\text{c/s} - 1.5\text{Kc/s}$. The test liquid is subjected to an oscillatory shear strain in an annular gap, and the variation of loading on the moving boundary as a function of the height of liquid in the annulus is reflected as a change in transfer impedance at the transducer terminals. This change in electrical impedance may then be used to calculate the shear properties of the test liquid.

The liquids investigated were four polydimethyl siloxane fluids of differing molecular weight. Measurements previously made on these fluids at higher frequencies have been extrapolated to low frequencies on the basis of a modified theory of Rouse and it is shown that these extrapolations coincide well with the low frequency experimental determinations.

A theory has also been developed to attempt a correlation between the non-Newtonian behaviour of viscoelastic liquids under the influence of steady shear flow with the dynamic shear moduli. It appears that there is a functional relationship connecting the shear and normal stresses as a function of shear rate with the real and imaginary parts of the complex shear modulus as a function of angular frequency. In addition, the recoverable elastic shear strain in steady flow appears in the resulting equations and shows that the

properties in oscillatory shear do not completely specify the behaviour in steady shear flow. Some comparison of the theory with experiment is given.

Finally, some attention has been given to means of automatically calculating relaxation spectra from dynamic modulus data. Although various methods of performing this calculation have already been described, they usually involve laborious hand computation and are not amenable to direct programming for use on a computer. Two new methods are described one of which need involve only a simple hand calculation after a certain matrix has been pre-calculated. This matrix does not depend on the data values and so needs only to be calculated once.

ACKNOWLEDGEMENTS

I am grateful to my colleagues of the 'Viscoelastics' laboratory for discussion and assistance throughout this work and especially to my supervisor, Professor J. Lamb, who suggested the project and who gave every encouragement during its execution.

My thanks are due to Dr. A. J. Barlow and Dr. G. Harrison of this laboratory and also to Mr. J. L. den Otter of the Central Laboratorium T. N. O. for making results available to me.

The work of this project forms part of a research programme supported by the Department of Scientific and Industrial Research and their assistance is gratefully acknowledged.

Finally, I am indebted to the Institution of Electrical Engineers for maintenance during the session 1960-61 by granting me an Oliver Lodge Scholarship.

Summary	2
Acknowledgements	4
Contents	5
Symbols	8
Chapter 1 Introduction	9
Chapter 2 Some introductory theory	
2.1 Descriptions of viscoelasticity	15
2.2 Derivation of an equation of state	16
2.3 The response in the time domain	21
2.4 The frequency response	23
2.5 Three dimensional equation of state	28
2.6 Frequency - temperature superposition	31
Chapter 3 The electromagnetic transducer	
3.1 Survey of techniques	35
3.2 The audio frequency range	37
3.3 General considerations of transducer design	38
3.4 Design of the transducer	41
3.5 Assembly	54
3.6 Theory of the transducer	55
3.7 Calibration	62
Chapter 4 The measuring system	
4.1 Introduction	64
4.2 The system layout	65
4.3 Electronic design	69

4.4	Measurement procedure	88
4.5	Calculation of the measured quantities	89
4.6	Typical calculation	90
4.7	Limitations of the apparatus	93
Chapter 5	Experimental results	
5.1	Description of the siloxanes	95
5.2	Density	96
5.3	Static viscosity	96
5.4	Dynamic measurements	97
Chapter 6	Interpretation of experimental results	
6.1	Introduction	103
6.2	The Rouse theory and undiluted polymers	104
6.3	Generalisation to polydisperse polymers	107
6.4	Comparison with experiment	109
6.5	Viscosity - molecular weight relationship	117
6.6	Modification of the theory for entanglements	121
6.7	Discussion	124
Chapter 7	A theory of steady shear flow for viscoelastic liquids	
7.1	Introduction	128
7.2	Equations of state and coordinate systems	130
7.3	Theory	131
7.4	Discussion of the theory	138
7.5	An extension of the theory	141
7.6	Comparison with experiment	143

Chapter 8	Automatic computation of relaxation spectra	
8.1	Nature of the problem	148
8.2	Numerical methods	151
8.3	First method	152
8.4	Second method	161
8.5	The second method as an analogue of the Barlow and Lamb procedure	170
8.6	Discussion	171
Appendix A	Analysis of shear wave propagation in cylindrical coordinates	173
Appendix B	Numerical integration of propagation equations	
B.1	Description of integration process	178
B.2	Table of values for the integrated propagation equations	180
B.3	Algol programme for the integration procedure	207
Appendix C	Calculation of the cylindrical impedance z	212
	General view of apparatus	214
	References	215

D	Differentiating matrix
e	Strain
G	Complex shear modulus(dyne.cm ⁻²), Spectrum vector(dyne.cm ⁻²)
f	Frequency(sec ⁻¹)
g	Shear modulus vector(dyne.cm ⁻²)
h	Liquid height(cm)
J	Polar moment of inertia(gm.cm ²)
K	Shear rate(sec ⁻¹)
K ²	Transducer constant(dyne.cm.ohm.sec)
M	Kernel matrix, Loop gain(db)
Q	Friction coefficient magnification factor
q	Molecular chain length
R,r	Radius(cm)
s	Relaxation frequency(sec ⁻¹)
T	Torque(dyne.cm)
t	Time(sec)
x	Friction coefficient(dyne.sec.cm ⁻¹)
Z _E , Z _{EO}	Electrical impedance(ohm)
Z _T , Z _O	Torsional mechanical impedance(dyne.cm.sec)
z	Torsional liquid impedance per unit height(dyne.sec)
α	Frequency shift factor, angle
β	Frequency shift factor, angle
ε	Deviatoric strain tensor component
η	Viscosity(dyne.cm ⁻² .sec)(poise)
ν	Kinematic viscosity(cm ² .sec ⁻¹)
ρ	Density(gm.cm ⁻³)
σ	Stress tensor component(dyne.cm ⁻²)
τ	Time(sec), Relaxation time(sec)
ψ	Relaxation function(dyne.cm ⁻²)
ω	Angular frequency(sec ⁻¹)

CHAPTER 1INTRODUCTION

The original studies of deformable media were concerned with purely viscous fluids and purely elastic solids. Fluids as investigated by Newton are incapable of supporting a shear stress without continuously deforming. Moreover, when the shear stress is removed the fluid instantaneously attains equilibrium in the new deformed state. The ratio of shear stress to strain rate is defined as the viscosity and is independent of these two quantities. In the case of elastic solids a shear stress induces a unique shear strain which is completely recovered upon removal of the stress. The main difference therefore between the elastic solid and the viscous fluid is that the former possesses an undeformed reference configuration while for the latter, the reference configuration is its instantaneous state.

This may be described in other terms with reference to the concept of 'memory'. The elastic solid may be said to have perfect memory since when the stresses are removed after whatever time, the material always returns to its reference state. The viscous fluid has no memory since upon removal of the stresses at time t_1 the configuration remains the same for all times for which $t \gg t_1$ i.e. it does not 'remember' any previous state.

A class of materials exists that falls between these two extremes and exhibits imperfect or fading memory. These visco-elastic materials, which may be either solid or liquid, have no

absolute reference configuration but nevertheless show elastic or rubberlike behaviour. Under the influence of a steady shear stress, the material deforms apparently like a viscous fluid; but upon removal of the stresses, a partial recovery takes place which depends on the history of deformation. The reference configuration thus lags behind the instantaneous configuration and the material is therefore partially elastic and partially viscous.

Maxwell (1867) was the first to postulate such a material in which the total deformation is the sum of an elastic and a viscous deformation. Such a material has a characteristic (relaxation) time given by the ratio of a viscosity to an elastic shear modulus. In experiments involving time scales much shorter than the relaxation time, the Maxwell fluid tends towards the characteristics of an elastic solid, while for large time scales it approaches the behaviour of a purely viscous liquid. It is doubtful that any real materials are approximated by the Maxwell hypothesis but they may be described by a generalisation which involves superposing a number of Maxwell bodies in such a way that for a given strain, the stress is the sum of the stresses in a distribution of Maxwell elements. The rheological properties may thus be defined by a distribution of viscosities, rigidity moduli and relaxation times. In fact only two of these three quantities are necessary to completely specify the viscoelastic properties of the material.

The rheological properties so far described are linear in that the principle of superposition of stress and strain applies. In the case of small strains this assumption is realistic and the

theory of viscoelasticity is well developed in this context and is reviewed by Hunter (1960). In the case of large strains a material may still be linear but a more complex theory is necessary to describe finite strain. Such theories have been developed by Murnaghan (1951) and Rivlin (1956). Finally, there are the inherently non-linear materials for which only elementary theories have been developed (Reiner, 1949).

One of the most convenient methods of determining the visco-elastic properties for small strains is that of subjecting the material to sinusoidal variations of shear stress or strain. Part of the work with which this thesis is concerned has been to develop an apparatus capable of measuring these properties in the frequency range 20c/s – 1.5Kc/s and the description of this method is contained in Chapters 3 and 4.

The advantage of this method of testing is that the mechanical properties of the material in its equilibrium or ground state are ascertained by small perturbations, and information may thus be gained as to the kinetics of molecular flow. Measurements have been taken on a series of polydimethyl siloxane fluids of differing molecular weight. In the case of long chain polymers, at low frequencies the flow may be considered to involve the co-operative motion of the complete molecule, and the drag that the molecules exert upon each other manifests itself as a purely viscous effect. At higher frequencies segments of the molecule are capable of partially independent motion and the restraining effect of one segment on another of the same molecule gives rise to an elasticity. At very high frequencies this effect is dominant and the behaviour tends to that of a perfectly elastic solid.

Several theories have been put forward to explain these mechanical properties on the basis of molecular models, for dilute solutions of long chain polymers (Bueche, 1954., Rouse, 1953., Zimm, 1956). For undiluted polymers Ferry, Landel and Williams (1955) have suggested a modification of the Rouse theory which is discussed in Chapter 6, and which appears to satisfactorily explain the observed properties of the polydimethyl siloxanes when due allowance is made for the polydispersity of molecular weight in these fluids. The molecular picture of long chain polymers is complicated by the occurrence of temporary cross links above a certain critical molecular weight. These have the effect of immobilising parts of the molecule and greatly enhancing the static viscosity. However as the frequency of an oscillatory excitation is increased, since smaller parts of the molecule are involved in the motion, the 'pinning' points of the molecules play a less significant part in the dynamic properties. For the same reason the chain length itself becomes less important in determining the high frequency properties, and experiment shows that at the higher frequencies the complex shear moduli of the different molecular weight siloxanes converge to a single curve (Barlow, Harrison and Lamb, 1964).

Although the viscoelastic properties of a material are important for the purposes of understanding molecular kinetics, it is beginning to emerge that they do not completely define the mechanics of a material in steady flow. In particular, it is observed that when a viscoelastic material is subjected to steady shear flow, the viscosity, measured as the ratio of shear stress to strain rate,

diminishes with increasing shear rate. Also, stresses normal to the direction of shear develop, which are also functions of shear rate. Many theories have been formulated to account for these effects based on empirical equations of state for which the molecular interpretations remain to be investigated. Very often, as a result of the experimental difficulty, it is impossible to distinguish one theory from another.

In general, it appears that these empirical equations contain parameters in addition to those required for exhibiting viscoelastic behaviour in oscillatory shear; and consequently the data from oscillatory experiments would not be sufficient to completely determine the steady flow behaviour. Nevertheless, correlations have been observed between the normal and shear stresses as a function of shear rate, and the real and imaginary parts of the dynamic shear modulus as a function of angular frequency (Padden and de Witt, 1954., Markovitz and Williamson, 1957). An advantage, therefore, of being able to take measurements in the audio frequency range is that the corresponding angular frequencies are of the same order of magnitude as shear rates obtainable with a variety of viscometers. For this reason it appears desirable to attempt a theoretical correlation and two appear in the literature (Pao, 1957., de Witt, 1955). The former theory however does not predict the presence of normal stresses in steady flow while the latter is confined to materials with a single relaxation mechanism. A theory developed by the author and described in Chapter 7 allows for a distribution of relaxation times and predicts the occurrence

of normal stresses. However, because only the viscoelastic properties have been included in the original equation of state the stresses result in not being completely kinematically determined. The resulting equations nevertheless may be checked for consistency in the light of experimental data.

The remainder of the work of this thesis is concerned (Chapter 8) with simple methods of obtaining relaxation spectra from dynamic data, that are suitable for programming on a digital computer. Although various methods have already been described in the literature, they are primarily designed for hand computation and are not suitable for direct conversion to a computer programme. The amount of labour involved in these calculations makes it desirable to formulate a method that is simple to programme and at the same time does not contain complicated convergence requirements. Two methods are described the second of which is amenable to simple hand calculation, after the initial matrices that are required have been pre-calculated.

Note: Wherever reference is made in this thesis to automatic calculations, the associated numerical work has been carried out on the University of Glasgow KDF 9 computer using Algol as a programming language.

CHAPTER 2

SOME INTRODUCTORY THEORY

2.1 Descriptions of Viscoelasticity

Theoretical work in the field of materials may begin from one of two starting points, the microscopic or the macroscopic. The two methods lead to results which inevitably overlap, (since they must be compatible) but the emphasis in each case is rather different. The macroscopic approach seeks to generalise the results obtained by experiment and so be able to predict behaviour in a diversity of situations. A consequence of this method is that, subject to the appropriate assumptions being made in the theory, general forms of equations are obtained of which the results from microscopic theory are special cases. The microscopic approach however involves the prediction of bulk properties from the behaviour of the individual molecules that compose the material, and the assumptions in this method though by nature more specific must be compatible with those of the phenomenological theory. By comparing the results of such theories with experimental a greater understanding of molecular processes is obtained. An example of this approach is given in Chapter 6.

In viscoelasticity the elementary bulk or phenomenological theory of flow is well understood in the restricted situations of small strain and strain rate. Outside these restrictions the possible forms for the equation of state are very numerous especially

if non-linearity is allowed in the formulation. Even in the linear situation the formulation requires extensive use of topology and the theory of function spaces (Coleman and Noll, 1959). The other main branch of phenomenological theory is that of predicting behaviour under diverse experimental conditions starting with an equation of state as a postulate. Unfortunately, the difficulty of this subject is often increased by the various means available of specifying strain. Lodge (1964) has attempted to rationalise this by the use of what he terms 'shape variables' with a resulting elegance and simplicity in the form of his equations.

The present chapter is concerned with the development of elementary small strain linear theory as it applies to the remainder of this thesis. The results obtained are not new but the approach is considered unconventional and leads to the desired results in an economical way.

2.2 Derivation of an equation of state

It is the concern of this section to derive a relation between quantities (to be defined more precisely later), σ representing a deforming stress and ϵ the deformation or shear strain which in general may both be functions of the independent variable time, t . For the present discussion it is assumed that the relationship will be linear so that if

$$\sigma_1 = f(\epsilon_1) \quad \text{and} \quad \sigma_2 = f(\epsilon_2)$$

then $\sigma_1 + \sigma_2 = f(\epsilon_1 + \epsilon_2)$

We further assume at this stage that there are a finite number of discrete processes that will describe the viscoelastic system.

With these two assumptions the relation between σ and ϵ must be of

$$\text{the form } f_1(D) \sigma = f_2(D) \epsilon \quad 2.1$$

where f_1 and f_2 are linear total differential operators. By taking the Laplace transform of both sides of equation 2.1 with zero initial conditions, we obtain

$$\bar{\sigma}(p) = \phi(p) \cdot \bar{\epsilon}(p) \quad 2.2$$

where the superscript bar denotes a transformed variable. $\phi(p)$ is the ratio of two polynomials in p and is of the form

$$\phi(p) = \frac{p + a_2 p^2 + a_3 p^3 + \dots + a_m p^m}{b_0 + b_1 p + b_2 p^2 + \dots + b_n p^n} \quad 2.3$$

The absence of a constant term in the numerator is based on the physical fact that in any fluid, no stress function can cause constant strain.

The polynomials in equation 2.3 may be factorised to give

$$\phi(p) = \frac{p(p - p_1') (p - p_2') \dots (p - p_m')}{(p - p_1) (p - p_2) \dots (p - p_n)}$$

where p_1 and p_j' are the poles and zeros of the function. This form may now be written after use of the Heaviside expansion (Cheng, 1959,

p. 185)
$$\phi(p) = \frac{k_1 p}{p - p_1} + \frac{k_2 p}{p - p_2} + \dots + \frac{k_n p}{p - p_n} \quad 2.4$$

or alternatively,

$$\begin{aligned}\phi(p) &= \sum_{r=1}^n K_r + \frac{K_1 p_1}{p-p_1} + \frac{K_2 p_2}{p-p_2} + \dots + \frac{K_n p_n}{p-p_n} \\ &= C + \frac{C_1}{p-p_1} + \frac{C_2}{p-p_2} + \dots + \frac{C_n}{p-p_n} \quad 2.5\end{aligned}$$

The roots of the polynomial p_j are either real or appear in complex conjugate pairs. Since the fluid system is evidently stable, the the real parts of all the roots must be negative and we now divide the n poles of ϕ into x real roots and y complex conjugate roots.

Equations 2.4 and 2.5 now become

$$\phi(p) = \sum_{r=1}^x \frac{K_r p}{p+s_r} + \sum_{r=x+1}^{x+y} \frac{2K_r p(p+\alpha_r)}{(p+\alpha_r)^2 + \omega_r^2} \quad 2.6$$

$$\phi(p) = C + \sum_{r=1}^x \frac{C_r}{p-s_r} + \sum_{r=x+1}^{x+y} \frac{2C_r(p+\alpha_r)}{(p+\alpha_r)^2 + \omega_r^2} \quad 2.7$$

respectively, when the real roots are $-s_j$ and the complex conjugate roots are $-\alpha_j \pm j\omega_j$.

It is thus seen that the original system has been decomposed into x first order systems and y second order systems. In the study of relaxation behaviour in general and viscoelasticity in particular it is usual to neglect the second order systems on the grounds that the damping of the first order systems masks the presence of any natural modes. No experimental evidence has been found for the existence of natural modes and consequently viscoelastic behaviour is universally interpreted in terms of first order systems only. An interesting discussion of this topic by Gross is to be found in

Harrison (1954, p. 227). We thus have the simplified equations:

$$\phi(p) = \sum_{r=1}^{\infty} \frac{K_r p}{p + s_r} = C + \sum_{r=1}^{\infty} \frac{C_r}{p + s_r} \quad 2.8$$

which give two possible representations of the same system. The advantage of these forms over the polynomial form of equation 2.3 is that the system may be seen to be describable in terms of x systems of identical simple form but with different parameters. (In the second representation, an additional system, C , is required also). These simple forms occur in network theory and are termed canonical forms. Mechanical and electrical canonical forms having the transfer functions occurring in equation 2.8 are shown in Figure 2.1.

In the electrical models the most common transfer functions are impedance (voltage/current) and admittance (current/voltage). For mechanical models two different types of transfer function are found: the modulus (force/displacement) and its inverse, compliance; and impedance (force/velocity) and its inverse, admittance.

Two types of analogue appear from the comparison in Figure 2.1

1) Electrical impedance \equiv Mechanical modulus

Electrical admittance \equiv Mechanical compliance

It then follows in this case that the analogous quantities are:-

Voltage \equiv Force

Resistor \equiv Dashpot

Current \equiv Displacement

Inductor \equiv Spring

for models 1, 4, 5 and 8.

2) Electrical admittance \equiv Mechanical impedance

Electrical impedance \equiv Mechanical admittance

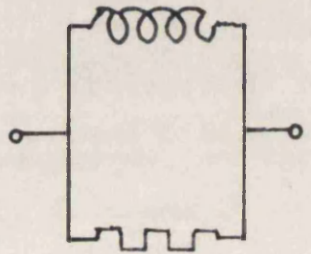
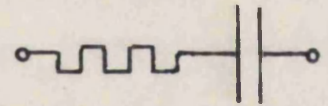
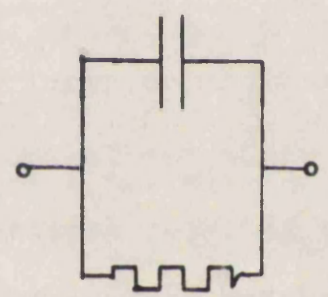
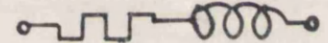


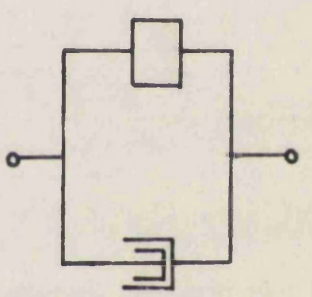
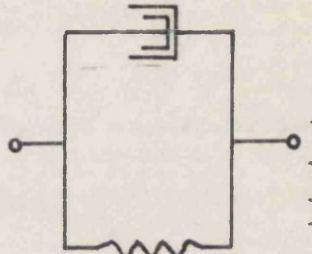
	$cp/p - \alpha$		$c/p - \alpha$	
	Impedance	Admittance	Impedance	Admittance
Electrical	 1	 2	 3	 4
	Modulus	Impedance	Admittance	Compliance
Mechanical	 5 Maxwell	 6	 7	 8 Voigt

Fig.2.1 Networks with Equivalent Transfer Functions

This analogue concerns models 2, 3, 6 and 7 whence the analogous quantities are

$$\begin{array}{ll} \text{Voltage} \equiv \text{velocity} & \text{Resistor} \equiv \text{dashpot} \\ \text{Current} \equiv \text{force} & \text{Capacitor} \equiv \text{spring} \end{array}$$

An interesting consequence of this type of analogue is that the networks are topologically equivalent, which is not the case in the other representation.

The electrical models of Figure 2.1 are all known as Foster canonical forms (Guillemin, 1957) whereas only two of the mechanical models are distinguished by a title: the Maxwell and the Voigt elements. Although both these models occur in viscoelasticity, the present work is mainly concerned with the Maxwell representation i.e. transfer functions of the form $\sum \frac{K_r p}{p + s_r}$. This has been chosen

because one such model could represent a hypothetical fluid whereas the Voigt element needs an extra dashpot in series corresponding to the quantity C in equation 2.8.

2.3 The response in the time domain

Now that the form of $\phi(p)$ appropriate to viscoelastic materials has been determined, we may substitute into equation 2.2 to give

$$\bar{\sigma}(p) = \sum_{r=1}^{\infty} \frac{K_r p}{p + s_r} \bar{\epsilon}(p) \quad 2.9$$

The response in the time domain is determined by finding the inverse

transform of this equation. We first note a theorem of the Laplace transform:

$$\text{If } \mathcal{L}\{f_1(t)\} = \overline{f_1}(p) \text{ and } \mathcal{L}\{f_2(t)\} = \overline{f_2}(p) \\ \text{then } \mathcal{L}^{-1}\{\overline{f_1}(p) \cdot \overline{f_2}(p)\} = \int_{-\infty}^t f_1(t-\gamma) f_2(\gamma) d\gamma$$

where the right hand side is the convolution integral which commonly occurs in the theory of linear systems.

$$\text{In equation 2.9 let } \overline{f_2}(p) = p \cdot \overline{\xi}(p) \text{ and } \overline{f_1}(p) = \sum_{r=1}^{\infty} \frac{K_r}{p-s_r}.$$

The inverse transforms of these two functions are (Cheng, 1959, p. 165, 175)

$$f_2(t) = \frac{d\xi(t)}{dt} \\ f_1(t) = \sum_{r=1}^{\infty} K_r \exp(-s_r t)$$

Taking the inverse transform of both sides of equation 2.9 therefore gives

$$\sigma(t) = \sum_{r=1}^{\infty} \int_{-\infty}^t K_r \exp(-s_r [t-\gamma]) \frac{d\xi(t)}{dt} dt \quad 2.10$$

Equation 2.10 therefore gives the stress function of time σ in terms of the rate of change of the strain function ξ . It may be seen that the state of stress at time t is dependent on the strain history from $-\infty$ to the present time t . The lower limit of integration of $-\infty$ ensures that the assumption of zero initial conditions in going from equation 2.1 to equation 2.2 does not limit the generality of equation 2.10.

A quantity called the relaxation function may be introduced at this stage defined by

$$\psi(t) = f_1(t) = \sum_{r=1}^{\infty} K_r \exp(-s_r t)$$

so that equation 2.10 becomes

$$\sigma(t) = \int_{-\infty}^t \psi(t-\tau) \frac{d\varepsilon(\tau)}{d\tau} d\tau$$

which is a form of the well known Boltzmann superposition integral given by Gross (1953).

2.4 The frequency response

For the purposes of measuring the viscoelastic properties of a liquid equation 2.10 is not suitable for calculation of the K_r and s_r , since the process involves separating out the contributions of x exponential functions, when simple step or impulse functions of strain are applied. This procedure is extremely imprecise (Lanczos, 1957, p. 272) and the method of testing adopted is that of frequency response determination i.e. the use of sinusoidal functions of time. The frequency response may be simply obtained by substituting $j\omega = p$ into equation 2.9, where ω is the radian frequency of the disturbance, to give

$$\sigma(j\omega) = \sum_{r=1}^{\infty} K_r \frac{j\omega \varepsilon(j\omega)}{s_r + j\omega}$$

We may now define a complex modulus $G(j\omega)$ by the ratio of stress to strain:

$$G(j\omega) = G'(j\omega) + G''(j\omega) = \frac{\sigma}{\varepsilon} = \sum_{r=1}^{\infty} K_r \frac{j\omega}{s_r + j\omega} \quad 2.11$$

It may be noted that at very high frequencies where $\omega \gg s_r$, $G \rightarrow G_\infty = \sum K_r$. G_∞ is termed the high frequency, impulse or indicial modulus and is the elastic modulus observed in a fluid when experimental time scales are very short compared to all the relaxation times ($1/s_r$) of the fluid. It is also apparent that each K_r corresponds to the high frequency modulus of each Maxwell element and equation 2.11 may be more appropriately written:

$$G(j\omega) = \sum_{r=1}^{\infty} G_{\infty r} \frac{1}{s_r + j\omega} \quad 2.12$$

which, when separating into real and imaginary parts, gives

$$\begin{aligned} G' &= \sum_{r=1}^{\infty} G_{\infty r} \frac{\omega^2}{s_r^2 + \omega^2} \\ G'' &= \sum_{r=1}^{\infty} G_{\infty r} \frac{\omega s_r}{s_r^2 + \omega^2} \end{aligned} \quad 2.13$$

A dynamic viscosity η_d is also defined as

$$\eta_d = \frac{G''(j\omega)}{\omega} = \sum_{r=1}^{\infty} \frac{G_{\infty r} s_r}{s_r^2 + \omega^2}$$

In the special case where there is one relaxation frequency s_r i.e. $x = 1$, Figure 2.2 shows the variations of G' , G'' and η_d with the radian frequency ω .

The dynamic viscosity defined above must converge to the static viscosity η_s at frequencies where $\omega \ll s_r$. Hence we have

$$\eta_s = \sum_{r=1}^{\infty} \frac{G_{\infty r}}{s_r} \quad 2.14$$

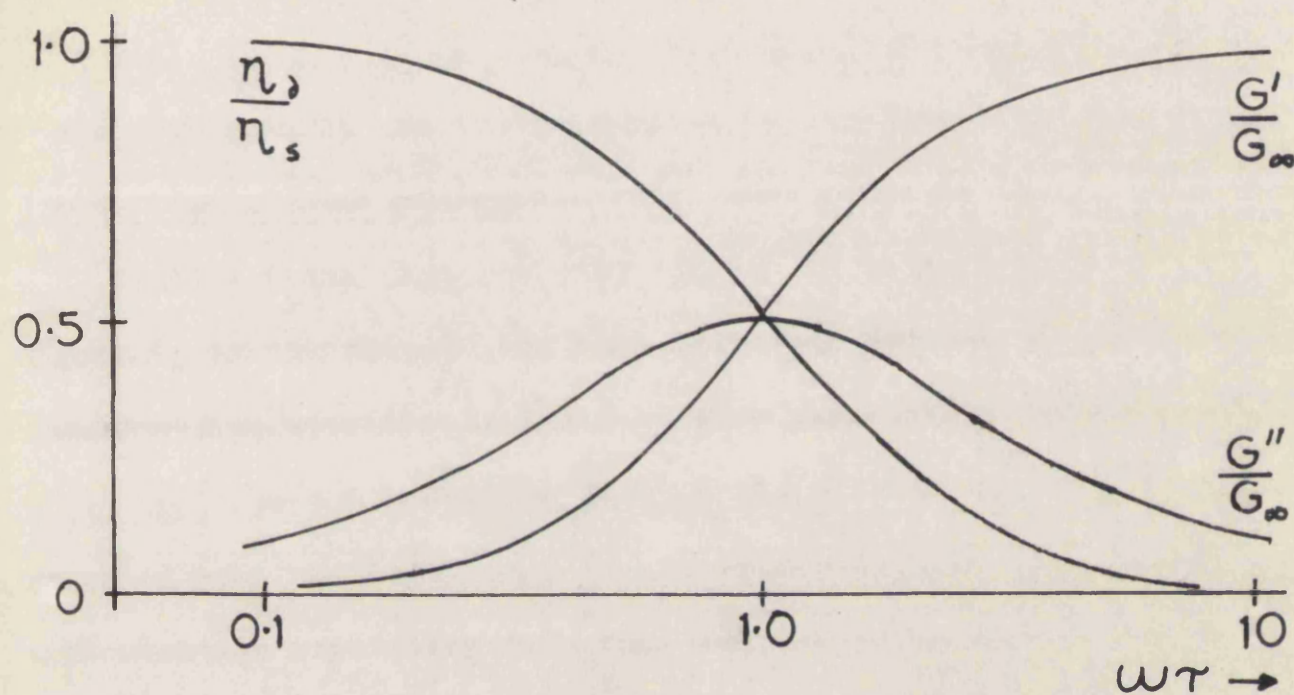


Fig.2.2 Shear Properties of a Liquid having a Single Relaxation Time

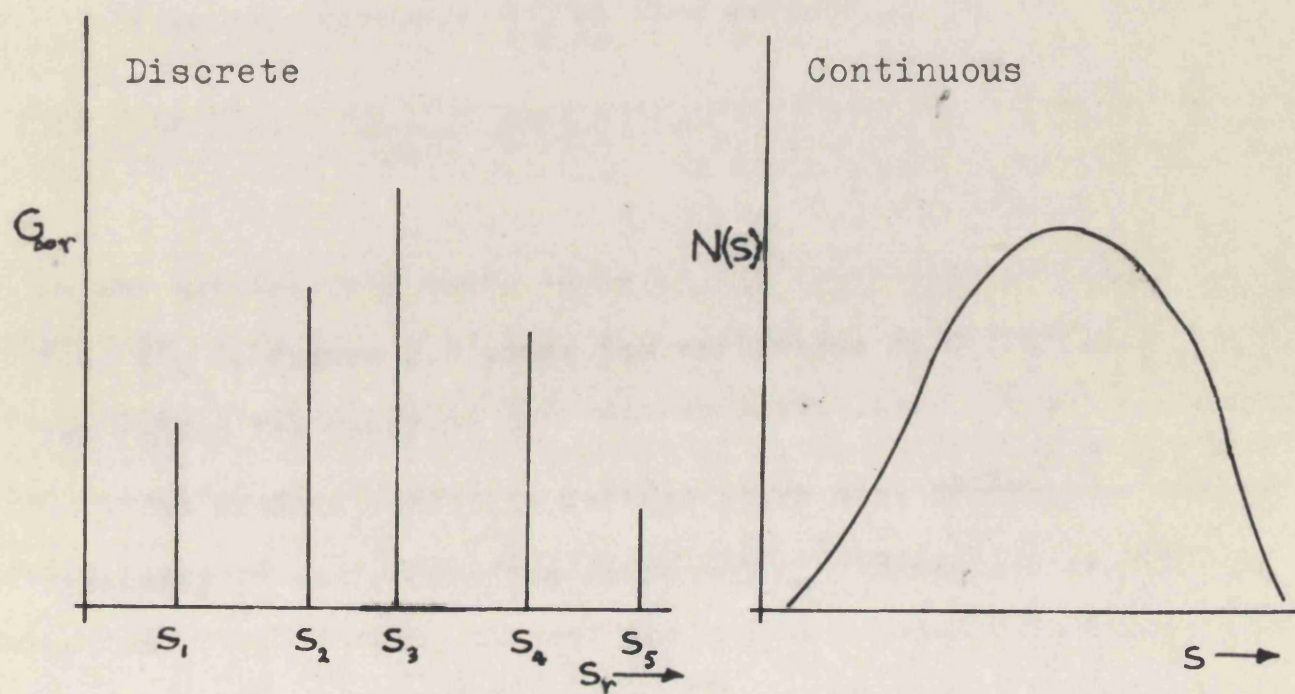


Fig.2.3 Discrete and Continuous Spectra

For a single relaxation time $\tau (= 1/s)$ we therefore have

$$\eta_s = G_\infty \cdot \tau$$

2.4.1 Continuous systems

Until now the properties of the viscoelastic system have been deduced under the assumption that there are a finite number of discrete relaxation processes each contributing (equation 2.11) an amount $G_\infty \cdot \frac{j\omega}{s + j\omega}$ to the modulus. Because the viscoelastic liquid may be regarded as a continuum and the observed relaxation behaviour is an agglomeration of statistical processes, it is more realistic to consider a continuous distribution of G over s , i.e. $G_r \rightarrow G_\infty(s)$. In the elemental range $(s, s+ds)$, the contribution of the indicial modulus is $dG_\infty(s) = \frac{dG_\infty(s)}{ds} ds$. The contribution to the overall modulus is therefore

$$dG = \frac{dG_\infty(s)}{ds} \cdot \frac{j\omega}{s + j\omega} ds$$

By putting $N(s) = \frac{dG_\infty(s)}{ds}$ and integrating we obtain for the modulus

$$G(j\omega) = \int_0^\infty N(s) \frac{j\omega}{s + j\omega} ds \quad 2.15$$

where the upper and lower limits of integration allow of all relaxation frequencies in the semi-infinite range. $N(s)$ is known as the distribution or spectrum of relaxation frequencies (or times), and a liquid may be completely specified viscoelastically by means of this function. A comparison of the representation with discrete and continuous spectra is shown in Figure 2.3.

In general it may be said that the results obtained for the

discrete system may be applied to the continuous system except that integrals occur in the place of summations. Practically, there is little difference between the two representations because the continuous system may always be approximated to any desired degree of accuracy by the use of a sufficiently large number of discrete Maxwell elements; though for numerical and analytical work it may be more convenient to work with one rather than the other.

It is as well to note however that there is an analytical difficulty if it is attempted to represent a line spectrum as a continuous spectrum. We have by definition $N(s) = \frac{dG_{\infty}(s)}{ds}$

If $G_{\infty}(s)$ is a line spectrum it may be represented by

$$G_{\infty}(s) = \sum_r \int G_{\infty r} \delta(s-s_r) ds$$

where δ is the delta function of zero width, infinite height and unit area at the point $s = s_r$.

Differentiating this equation we obtain

$$N(s) = \frac{dG_{\infty}(s)}{ds} = \sum_r G_{\infty r} \delta(s-s_r)$$

Thus when representing a line spectrum as a continuous spectrum the resulting function consists of a series of pulses with area $G_{\infty r}$, infinite height and zero width. For this reason it is often more convenient to represent the spectrum in discrete terms although in real materials where line spectra are not found either representation may be used.

2.4.2 Calculation of the viscoelastic properties

The method of oscillatory testing is to obtain measurements of

the complex ratio of stress to strain over a frequency range. Thus in equations 2.11 and 2.13 the complex function $G(j\omega)$ is an experimentally known function. From these measurements it is then necessary to determine the distribution of relaxation times which, in the case of the continuous system, is buried in the integrand of the integral equation 2.15. Various methods have been devised to facilitate this calculation and this subject is more fully dealt with in Chapter 8.

2.5 Three dimensional equation of state

Until now we have been considering the simple case of a deformation ξ and a stress σ , which are related by equation 2.10 assuming linearity and the presence of first order mechanisms only. For a useful description of viscoelasticity this is not sufficient as the variables σ and ξ will in general be functions of spatial coordinates. Thus to describe the behaviour in a variety of situations the equation of state in three dimensions is required. Although the end result is similar in form to equation 2.10 the process by which it is achieved is not trivial and a variation of the method is capable of giving corresponding results for anisotropic viscoelasticity although this is not pursued here.

For the purposes of the three dimensional formulation we may consider σ and ξ to be stress and strain tensors respectively of the second order. Now a second order tensor T may be split into three

parts (Long, 1961, p. 21)

$$T = \frac{1}{3} U \operatorname{tr} T + T^a + T^s \quad 2.16$$

where U is the unit tensor and $\operatorname{tr} T$ is the trace of the tensor T . T^a is an antisymmetric tensor and T^s is a symmetric tensor with zero trace. If it is assumed that these are no body couples acting and no rigid body rotation it follows that both the stress and strain tensors are symmetric, so that

$$\sigma = \frac{1}{3} U \operatorname{tr} \sigma + \sigma^s = \sigma^i + \sigma^d$$

$$\xi = \frac{1}{3} U \operatorname{tr} \xi + \xi^s = \xi^i + \xi^d$$

and the tensors can be split into only two parts. The first terms are isotropic tensors and are associated with hydrostatic pressure for σ and dilatation for ξ . The second terms are deviatoric tensors (by definition) and are associated with change of shape.

If the material is assumed isotropic and the stress and strain tensors may be related by a linear transformation, then de Groot and Mazur (1962, Chapter 6) show that the deviatoric part of σ is uniquely related to the deviatoric part of ξ by a constant multiplier; and similarly for the isotropic parts. Hence

$$\begin{aligned} \sigma^i &= K_i \xi^i \\ \sigma^d &= K_d \xi^d \end{aligned} \quad 2.17$$

where the superscripts and subscripts refer to isotropic and deviatoric relationships. This result is derived from the work of Curie (1908) which is based on the fact that the properties of an isotropic system

are invariant under a rotation or inversion, and is known as Curie's Theorem.

The work of de Groot and Mazur however is concerned with linear, time invariant, thermodynamic systems and the quantities K in equations 2.17 are true constants. For the time varying system of a viscoelastic fluid the result may be generalised by the use of Laplace transformed tensor components $\bar{\sigma}$ and $\bar{\epsilon}$ which are related by a linear transformation in the Curie sense. Therefore we may write for equation 2.17,

$$\begin{aligned}\bar{\sigma}^i &= K_1(p) \bar{\epsilon}^i \\ \bar{\sigma}^d &= K_d(p) \bar{\epsilon}^d\end{aligned}\tag{2.18}$$

Both equations imply that each component of the tensor $\bar{\sigma}$ is related to the corresponding component of the tensor $\bar{\epsilon}$ by means of the multiplier K and that only two quantities K_1 and K_d are necessary for the complete formulation of the isotropic and deviatoric behaviour. We therefore have for any given component

$$\begin{aligned}\bar{\sigma}^i &= K_1(p) \bar{\epsilon}^i \\ \bar{\sigma}^d &= K_d(p) \bar{\epsilon}^d\end{aligned}\tag{2.19}$$

Since on the basis of assumptions made in section 2.2 the form of these equations must be the same as that obtained in equation 2.9 it follows that $K(p)$ must be of the form

$$K(p) = \sum_{r=1}^{\infty} \frac{K_r p}{p + s_r}\tag{2.20}$$

Both of equations 2.19 are of the same form and we may write a single equation to describe both isotropic and deviatoric behaviour.

Substituting from equation 2.20 gives

$$\bar{\sigma}_{\alpha\beta} = \sum_{r=1}^{\infty} \frac{K_r p}{p + s_r} \bar{\epsilon}_{\alpha\beta} \quad 2.21$$

Although this equation applies to both isotropic and deviatoric situations, the constants K_r and s_r will be different. In particular, for the isotropic case one of the s_r is infinite because fluids have a static compressional modulus. By analogy with equation 2.10, equation 2.21 may be rewritten in the time domain to give:

$$\sigma_{\alpha\beta} = \sum_{r=1}^{\infty} \int_{-\infty}^t K_r \exp(-s_r [t - \gamma]) \frac{d\epsilon_{\alpha\beta}}{d\gamma} d\gamma \quad 2.22$$

These same results have been obtained by Bland (1960) who postulates a viscoelastic material of which the microscopic structure consists of a number of randomly arranged dashpots and springs. Alfrey (1948) and many other authors suggest that the one-dimensional stress-strain law may be generalised a-priori to three dimensions, but this approach is open to the objection that it assumes a three dimensional system cannot exhibit features not evident in the one dimensional system.

2.6 Frequency - Temperature superposition

The viscoelastic properties so far discussed have been defined in terms of a spectrum of relaxation frequencies $N(s)$. Since the bulk properties of materials depend on other external variables such as temperature and pressure, it is interesting to investigate how the relaxation spectrum will be affected. This was originally

carried out by Tobolsky and Andrews (1943) and Leaderman (1943) in connection with stress relaxation, and Ferry et al. (1952) used the method for frequency response testing. The two postulates on which the superposition principle is based are:

a) The variation of the relaxation frequency of any one relaxation process with temperature is the same for all relaxation processes in any given material.

b) The variation of the high frequency modulus of any one relaxation process with temperature is the same for all relaxation processes.

From postulate (a) it may be interpreted that we may write $\alpha(T) = \frac{s_{T_0}}{s_T}$ where the suffices T and T_0 refer to two different temperatures of which the latter may be considered a reference temperature. $\alpha(T)$ is a function that represents the temperature variation of the relaxation frequencies s. In a similar way we may write for postulate (b) that $\beta(T) = \frac{G_{\omega T}}{G_{\omega T_0}}$

$$\text{Now } N_T = \frac{dG_{\omega T}}{ds_T} = \beta \alpha \frac{dG_{\omega T_0}}{ds_{T_0}} = \alpha \beta N_{T_0}$$

Substituting these results into equation 2.15 we obtain

$$\begin{aligned} G_T(j\omega) &= \int_0^{\infty} \alpha \beta N_{T_0} \frac{j\omega}{s_{T_0}/\alpha + j\omega} d(s_{T_0}/\alpha) \\ &= \beta \int_0^{\infty} N_{T_0} \frac{j\alpha\omega}{s_{T_0} + j\alpha\omega} ds_{T_0} \\ &= \beta G_{T_0}(j\alpha\omega) \end{aligned}$$

Equation 2.23 may be separated into real and imaginary parts to give

$$\frac{G_T'(\omega)}{\beta} = G_{T_0}'(\alpha\omega)$$

$$\frac{G_T''(\omega)}{\beta} = G_{T_0}''(\alpha\omega) \quad 2.24$$

It may be seen from these equations that if α and β are known, experimentally determined functions G' and G'' at one temperature T may be referred to a reference temperature T_0 . Of practical interest is the fact that if $G(\omega)$ is plotted on a log-log scale the factors α and β occur in such a way that the slopes of the curves are not altered by a change in temperature but only their position relative to the axes.

Consider equation 2.23 when $\alpha\omega \ll s_{T_0}$ i.e. at very low frequencies. Then

$$\lim_{\omega \rightarrow 0} \frac{G_T(j\omega)}{j\omega} = \eta_{s_T} = \alpha\beta \int_0^\infty N_{T_0} ds_{T_0}$$

$$= \alpha\beta \eta_{s_{T_0}}$$

Thus

$$\alpha\beta = \frac{\eta_{s_T}}{\eta_{s_{T_0}}}$$

It is therefore shown that the product $\alpha\beta$ may be obtained by finding the ratio of the static viscosities at different temperatures. We may also note from equations 2.24 that

$$\frac{G_T''(\omega)}{G_T'(\omega)} = \frac{G_{T_0}''(\alpha\omega)}{G_{T_0}'(\alpha\omega)} \quad 2.25$$

which eliminates β . It is therefore shown to be possible to find both α and β . In practice, the reduction principle may be used to obtain results over a wide range of ω with a relatively restricted range of ω by variation of the temperature. This is of great advantage because it lessens the necessary frequency range required of the apparatus in order to explore the overall relaxation behaviour. Unfortunately the form of equation 2.25 is such that for a given frequency range the possible variations in temperature are limited because of the G' and G'' values becoming too small at low values of ω for accurate measurement.

. Often because the expected variation of an elasticity modulus with temperature is small β is made unity, in which case α is determined from the ratio of the static viscosities.

CHAPTER 3

THE ELECTROMAGNETIC TRANSDUCER

3.1 Survey of techniques

The measurement of the viscoelastic properties of a material as defined in Chapter 2 reduces to the problem of measuring the complex ratio of stress to strain over a wide frequency range. In principle, there is no difference between a method suitable for measuring the viscoelastic properties of solids or of liquids but in practice a liquid requires to be constrained between boundaries and often the mechanical properties of a liquid are more temperature dependent; hence a greater degree of temperature control is normally required.

Unfortunately, it is found that real materials have relaxation times extending over several decades and it impossible for a single apparatus to cover the required frequency range. In practice it is found that any one apparatus can rarely cover more than two decades of frequency, the limits being set by measurement accuracy and the occurrence of spurious modes of operation. Below 10c/s purely mechanical methods are usually favoured (Morrisson et al., 1955., Russell, 1946) in which the stress and strain are measured directly together with the phase difference between them. At higher frequencies the inertia of the reciprocating masses causes excessive backlash and the various parts of the apparatus can no longer be considered

rigid, resulting in spurious measurements of stress and strain.

Between 10c/s and 10Kc/s the mass of the apparatus is decreased and its stiffness increased by minimising the size of the moving members. The most appropriate means of driving such a system is through the use of an electromagnetic method (Benbow, 1953; Hopkins, 1951; Fitzgerald and Ferry, 1953). A variety of methods is used to measure the stress-strain ratio; these usually involve transforming the mechanical quantities into electrical quantities before measurement. The apparatus to be described later falls into this category, its limitation at high frequencies being spurious modes of oscillation set up in the vibrating member.

Above 10Kc/s the transducer is almost invariably in the form of a crystal such as quartz or barium titanate (Mason, 1948) that is set into resonance by an applied electric field. Under these conditions the vibrating member cannot be considered as a rigid body and elastic theory is required to calculate the mechanical behaviour of the transducer. A characteristic of some of these techniques is the propagation of pulsed oscillations rather than a continuous wave. The pulses must be short enough not to set up standing waves in the vibrating member but long enough for the effect of transients to have died away, in order that the steady state behaviour of the test sample may be observed. A survey of the available methods for measuring viscoelastic properties is given in the literature (Ferry, 1958).

3.2 The audio frequency range

The recent interest shown in the possible correlation between static (continuous shear) and dynamic measurements on viscoelastic materials (de Witt, 1955; Cox and Merz, 1958; Dyson, 1965) requires that radian frequencies ω in dynamic experiments should be used that are within an order of magnitude of shear rates K . By virtue of the reduction principle (Ferry et al., 1952) it is possible to predict results obtained at any one temperature and frequency from some other specified temperature and frequency. In the laboratory with which the author has been associated, several methods have been developed for measuring viscoelastic properties at frequencies above 10Kc/s and the reduction principle has been applied to predict behaviour at audio frequencies (Barlow and Lamb, 1959). It is therefore desirable to have some experimental check on the validity of the reduction principle.

More particularly, in the case of the present work, an experimental check on the low frequency behaviour of certain polymers predicted (Barlow, Harrison and Lamb, 1964) on the basis of a modified theory of coiling polymers (Rouse, 1953), is required. Also, in the case of correlation with steady shear measurements, the upper limit of shear rate is of the order of 10^4 sec^{-1} corresponding approximately to a frequency of 1500c/s, however viscometers operating at even higher shear rates have been developed (Barber, Muenger and Villforth, 1955). The apparatus designed by the author operates in the range 20c/s - 1.5Kc/s at temperatures between 10°C and 50°C

although all measurements reported herein were taken at 30°C.

3.3 General considerations of transducer design

For reasons already explained the possibility of using a purely mechanical system in the audio frequency range was discounted. The use of quartz crystals at frequencies below their natural resonance has received some attention (McSkimin, 1952), although their use below 10Kc/s has not been reported. One method is to use a quartz crystal to propagate pulses of oscillations down a rod. The pulses are reflected at the end and are reconverted into electrical energy by the crystal transducer. The properties of the test liquid are deduced from the loading effect caused by immersing the rod. An apparatus of this type has been developed in the author's laboratory (Barlow et al., 1961) consisting of a crystal capable of torsional vibration bonded to a Nickel-Silver rod. One result of the loading effect of the rod on the crystal is to lower the 'Q' hence increasing the available bandwidth of the system; and frequencies down to 10Kc/s have been obtained using a crystal with a natural resonance of 20Kc/s.

Lower frequencies may be obtained only by increasing the size of the crystal in order to decrease its resonant frequency and also increasing the length of the rod. The velocity of torsional waves in Nickel-Silver is 2.10^5 cm/sec., thus at a frequency of 10Kc/s a pulse of 20 cycles occupies a space of 400 cms. In order that a standing wave is not set up in the rod, the overall length of the rod

must be greater than 400 cms. Since the rod must increase in length in inverse proportion to the frequency, it can be seen that a system operating down to low audio frequencies would be very cumbersome, unless materials with significantly lower velocities could be found.

Although a lower velocity might be obtainable by using a rod with distributed inertia, a very large crystal would be necessary and it was therefore decided that an electromagnetic method would be most suitable. The difficulty with this latter type of system is that of achieving high frequency rather than low frequency capability as opposed to the torsional rod method. This is because one of the systems may be regarded as of the lumped parameter variety whereas the other (torsional rod) is of the distributed parameter type. The lumped parameter electromagnetic system must be such that the natural modes of the individual members of the apparatus are well above the operating range of the instrument. In practice this means that the parts must have a high stiffness to mass ratio i.e. the velocities of all possible acoustic waves in the various parts of the apparatus must be as high as possible.

Another consideration is the form of the vibrating member that will excite shear waves in the test liquid. Three principle methods appear in the literature:

- 1) Axial vibration of a cylinder (Fitzgerald and Ferry, 1953).

In this arrangement, the viscoelastic material is contained in the annulus between two cylinders, one of which executes axial oscillatory motion. The test material is therefore under conditions of

oscillatory shear but unfortunately the boundaries are such that they are not suitable for constraining a liquid.

2) Axial vibrations of a rod (Smith, Ferry and Shremp, 1949). In this method a rod is forced to oscillate axially as a solid body while immersed in a test liquid. Cylindrical shear waves are propagated radially into the test medium. The distance of propagation is so short compared to the distance to the outer boundary that the mechanical impedance observed from the rod is the cylindrical characteristic impedance.

At high frequencies the rod breaks up into modes of standing waves and meaningful results can no longer be obtained. One criticism is that the end of the rod inevitably generates compressional waves in the test material and a correction has to be made. This however may be overcome by taking several measurements using different depths of immersion. Another difficulty when the oscillating and fixed boundaries are too close is the pumping effect which must then be allowed for.

3) Torsional oscillations. With these methods the moving boundary is an oscillating sphere, disc or cylinder (Sittel et al., 1954; Goldberg and Sandvik, 1947). The fixed boundary may be either of arbitrary shape, in which case it must be 'infinitely distant' from the moving boundary, or of the same shape as the moving boundary. In the case of one instrument (Oldroyd, Strawbridge and Toms, 1951), both boundaries, which are cylindrical, are movable, and the effect of propagating a shear wave from one boundary to the other and

observing the resultant motion of the second boundary is the means of measuring the shear properties of the intervening medium.

It will be noted that the non-spherical systems all suffer from end effects but the spurious propagation is all in the form of shear waves and is thereby more easily allowed for.

3.4 Design of the transducer

In view of the above considerations it was decided to design an apparatus using torsional oscillations with cylindrical boundaries. The method of eliminating the end effect is discussed in Section 3.6. Figure 3.1 shows a horizontal cross section of the system. The central cylinder or core is held stationary while the outer cylinder or cup is excited into forced torsional oscillations. The test liquid is in the annular gap between the two boundaries and shear waves are propagated radially inwards and are reflected at the inner boundary. A standing shear wave is thereby set up in the liquid and the loading effect at the moving boundary is related to the shear properties of the liquid by means of equations derived in Appendix A.

3.4.1 The oscillating cup

As has been previously pointed out, the rigidity of the moving boundary must be as great as possible and from this standpoint spherical symmetry would be most appropriate. However, in view of the difficulty of designing a spherically symmetric electromagnetic

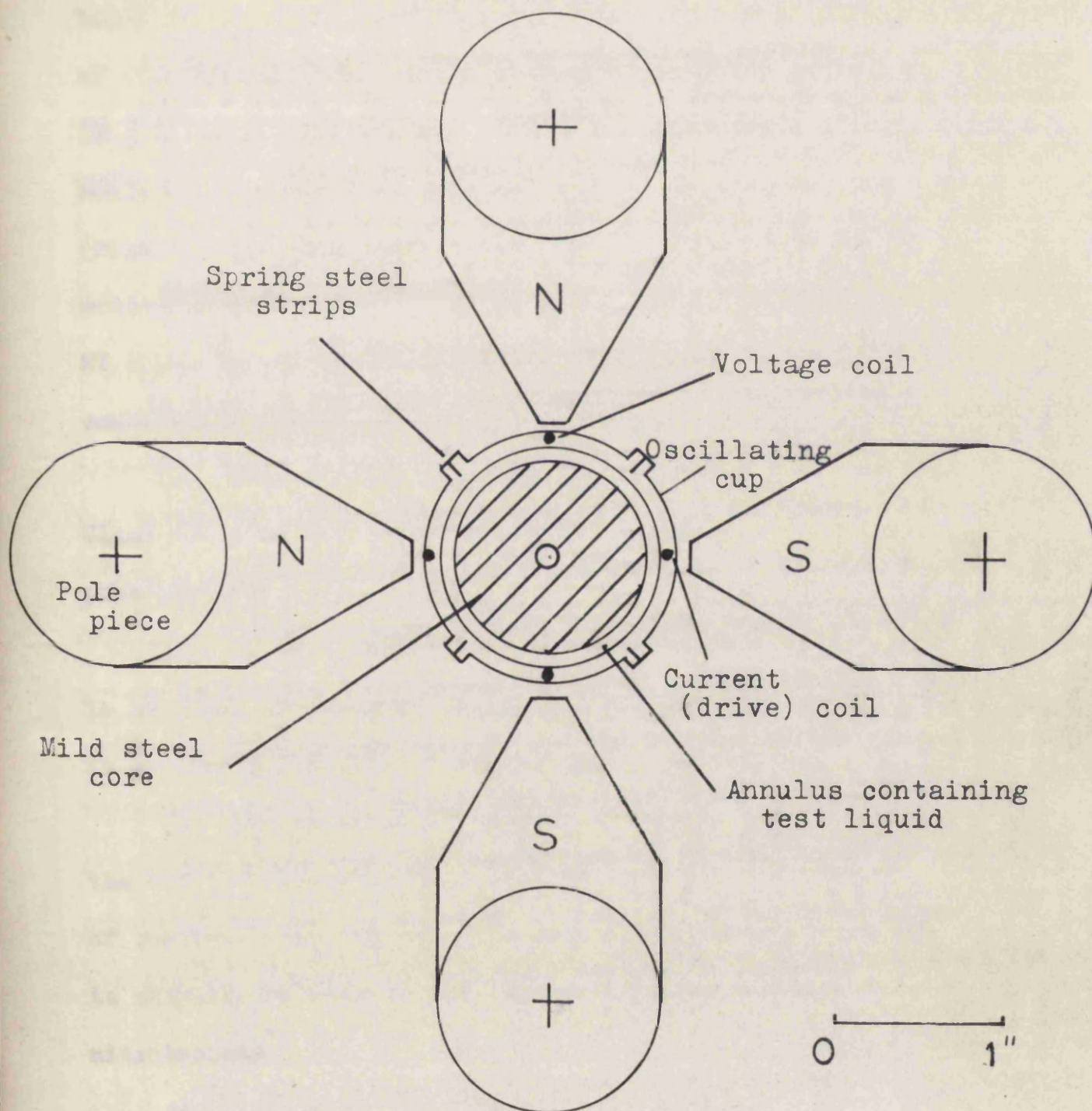


Fig.3.1 Horizontal Cross Section of Transducer

system, the cylindrical system was finally adopted. The outer boundary is in the form of a cup which is held in position by means of four spring steel strips clamped at each end as in a cantilever (Figure 3.2). The cup was cast in an epoxy resin using a brass mould for the outer surface and a P.T.F.E. plug for the inner surface (Figure 3.3). The epoxy resin was 'Araldite' type MY 753 and the mould was cured at 60°C for 24 hours using 'Araldite' hardener type HY 951. The choice of 'Araldite' was based on the following considerations.

1) The velocity of sound is reasonably high in this material. Glass would be more appropriate but the difficulty of machining prevented its use.

2) It is translucent. For reasons that will appear later it is necessary to measure the height of test liquid in the cup and this is obviously facilitated if the cup is translucent.

3) The material is chemically inert. It is desirable that the range of possible test liquids is not restricted by the possibility of chemical reaction with the containing vessel. 'Araldite' however is slightly soluble in the heavier organic solvents such as nitrobenzene.

4) 'Araldite' is dimensionally stable.

5) The mechanical damping in this material is quite high relative to metals or glasses. This implies that any natural modes set up in the cup will tend to be damped and thereby reduce the possibility of spurious measurements.

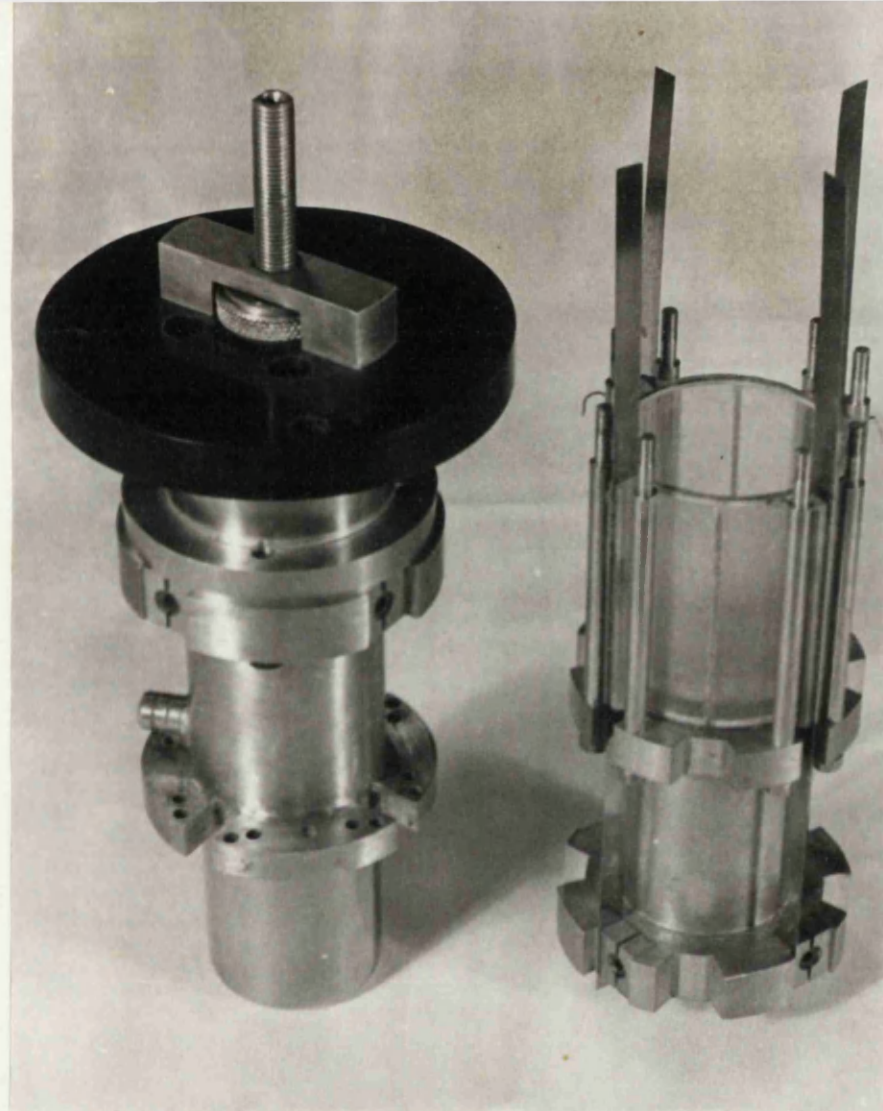


Fig. 3.2
Centre Unit of
Transducer

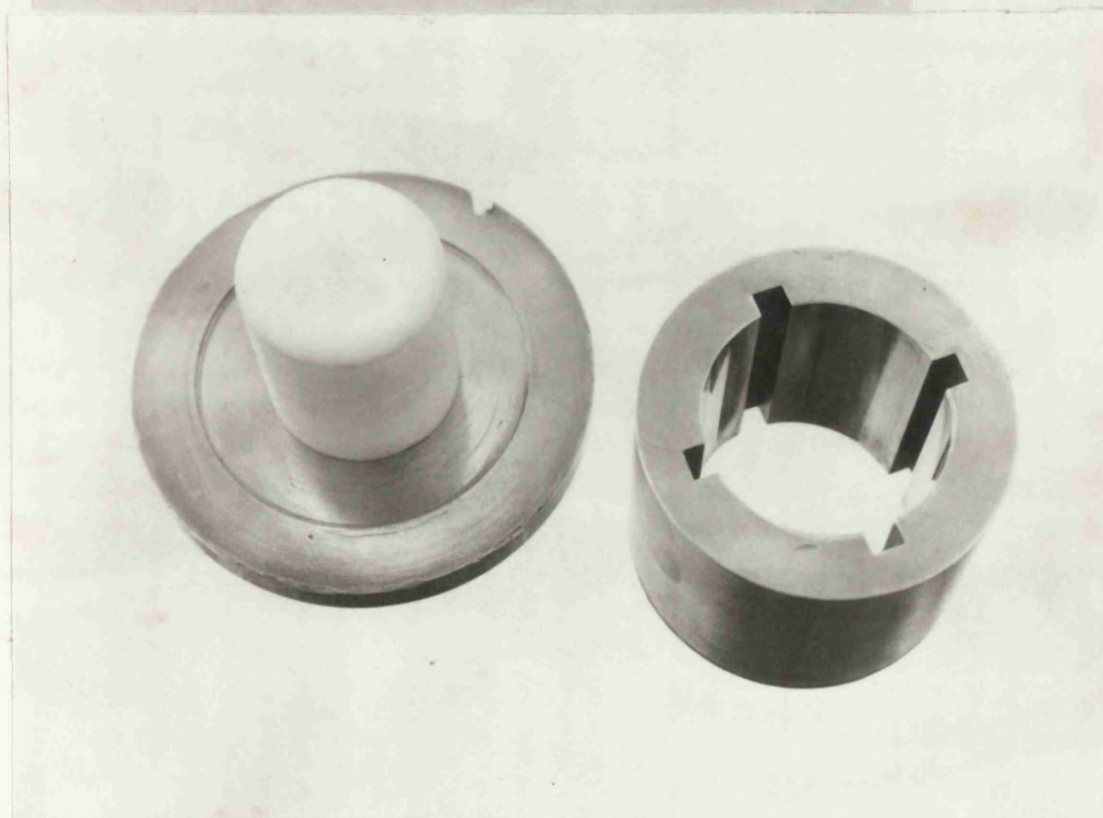
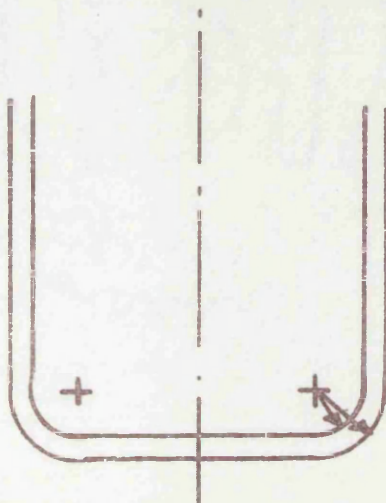


Fig. 3.3 Mould for Oscillating Cup

The necessity to use P.T.F.E. for the central part of the mould arises from the high adhesive strength of 'Araldite'/metal surfaces. The adhesion to P.T.F.E. however is substantially less and the central plug was extracted without difficulty. After extraction from the mould, slots to take the spring steel strips were machined in the centre of each lug by means of a 0.005" thick diamond milling wheel. Slots to take the various coils to be mounted on the cup were then machined as indicated in Figure 3.4.

The curvature at the bottom of the cup was incorporated for the following reason. In torsional oscillation, shear waves are not only propagated inwards radially but also upwards from the bottom of the cup. In the absence of curvature, the upward propagating waves interfere with the radially propagating waves giving rise to unpredictable effects. In order to minimise this, the inner surface of the cup and the central core are given a curvature at their lower end such that their centres of curvature are at the same point (see below).



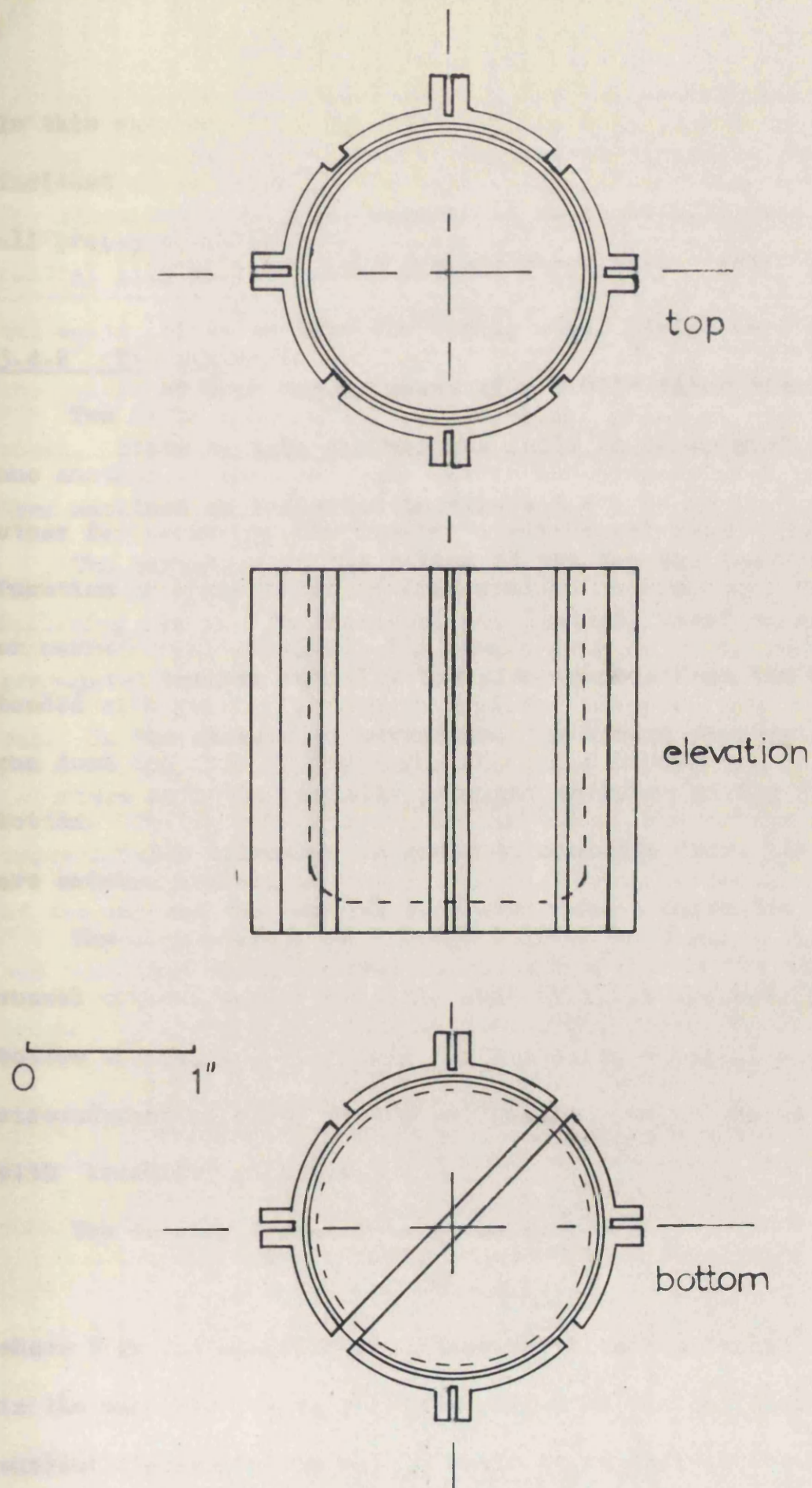


Fig.3.4 Details of Oscillating Cup

In this way the fixed boundary is at all places normal to the incident shear waves and in particular, shear waves in the annulus all propagate radially.

3.4.2 The cup coils

Two coils are mounted in a vertical plane at right angles to one another on the cup. One is for the purpose of driving and the other for measuring the angular displacement rate. The precise function of these coils is discussed in Section 3.6. The driving or current coil consists of a single loop of 26 s.w.g. copper wire bonded with general purpose 'Araldite' adhesive into the slots that run down the side of the cup, and a slot diametrically across the bottom. The loop terminates at the top of the cup in two hooks which are cadmium plated.

The displacement or voltage coil is 30 turns of 47 s.w.g. enamel covered copper wire the ends of which are brought out to the bottom of the cup. The coil fills the two other side slots and the circumferential slots at top and bottom, and is bonded to the cup with 'Araldite' adhesive.

The driving torque T is given by

$$T = B l r i \quad 3.1$$

where B is the magnetic flux density, l is the length of the coil in the magnetic field, r is the radius of the coil and i is the current flowing in the coil. While it is desirable to obtain the maximum torque for a given current by increasing the number of turns,

the total inertia of the cup would thereby be increased. It was therefore decided to use a single turn and pass as much current as possible without the wire heating unduly. For this design the maximum current is 4 A.

For the voltage coil the e.m.f.e induced by the motion of the cup is given by

$$e = B l r \dot{\theta} \quad 3.2$$

where $\dot{\theta}$ is the angular displacement rate. The sensitivity of the instrument will be directly related to the ratio $e/\dot{\theta}$ and it is important to make this as high as possible. Since the coil does not have to pass any current if e is to be measured directly, the wire may be as thin as desired consistent with mechanical strength. As many turns as would fit into the slots were used. The width of the slots is limited so that throughout the motion of the cup, the coils may be considered linked with a magnetic field of constant intensity.

3.4.3 The cup support

Four spring steel strips 0.25" wide 0.007" thick and 8" long were bonded into the lug slots with 'Araldite' adhesive. These are clamped top and bottom in flat jaws and form the means of supporting the cup. The torsional stiffness of this system depends on the thickness of the strip and any tension that may be induced in the strip. The purpose of using strip is to substantially increase the stiffness in lateral directions and thereby raise the frequency of the corresponding resonant mode above the desired operating range.

A cross section of the assembled unit including the oscillating cup, the clamps and the central core is shown in Figure 3.5 and is hereafter referred to as the centre unit.

3.4.4 The electromagnet

A diagram of the electromagnet configuration is shown in Figure 3.6. Four pole pieces are energised by means of eight coils of 6000 turns of 30 s.w.g. high temperature enamel covered copper wire. The yoke was machined from mild steel and the pole posts were ground into the conical holes of the top and bottom retaining rings for good magnetic contact. A plug of mild steel is disposed centrally with respect to the pole pieces and fixed on the centre unit to reduce the air gap in the magnetic circuit. This plug also acts as the fixed cylindrical boundary for the torsional shearing motion.

It is evident from equations 3.1 and 3.2 that the sensitivity of the system is greatly improved if a greater flux density can be achieved. This may be arranged in two ways: the magnetomotive force can be made as high as possible; and the reluctance of the magnetic circuit can be made low. The first consideration is limited by the space requirements and the heating of the coils while the second is mainly determined by the length of the air gap. By virtue of the method adopted, the air gap is determined by the annulus size and the thickness of the cup together with some clearance. The minimum annulus width is mainly limited by its allowable tolerance over the height of the cup and round its circumference. An annulus width

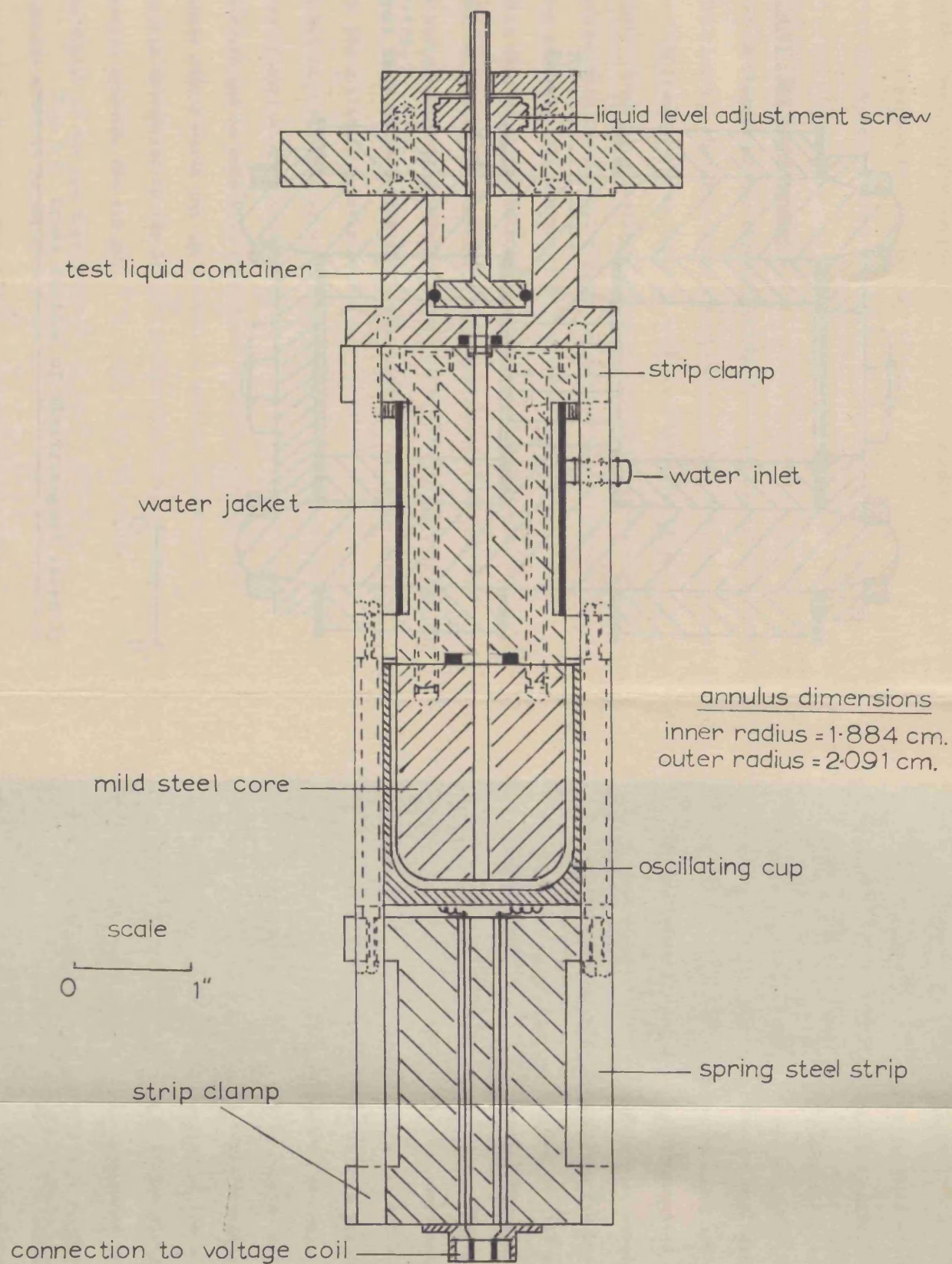


Fig.3.5 Centre Unit of Transducer

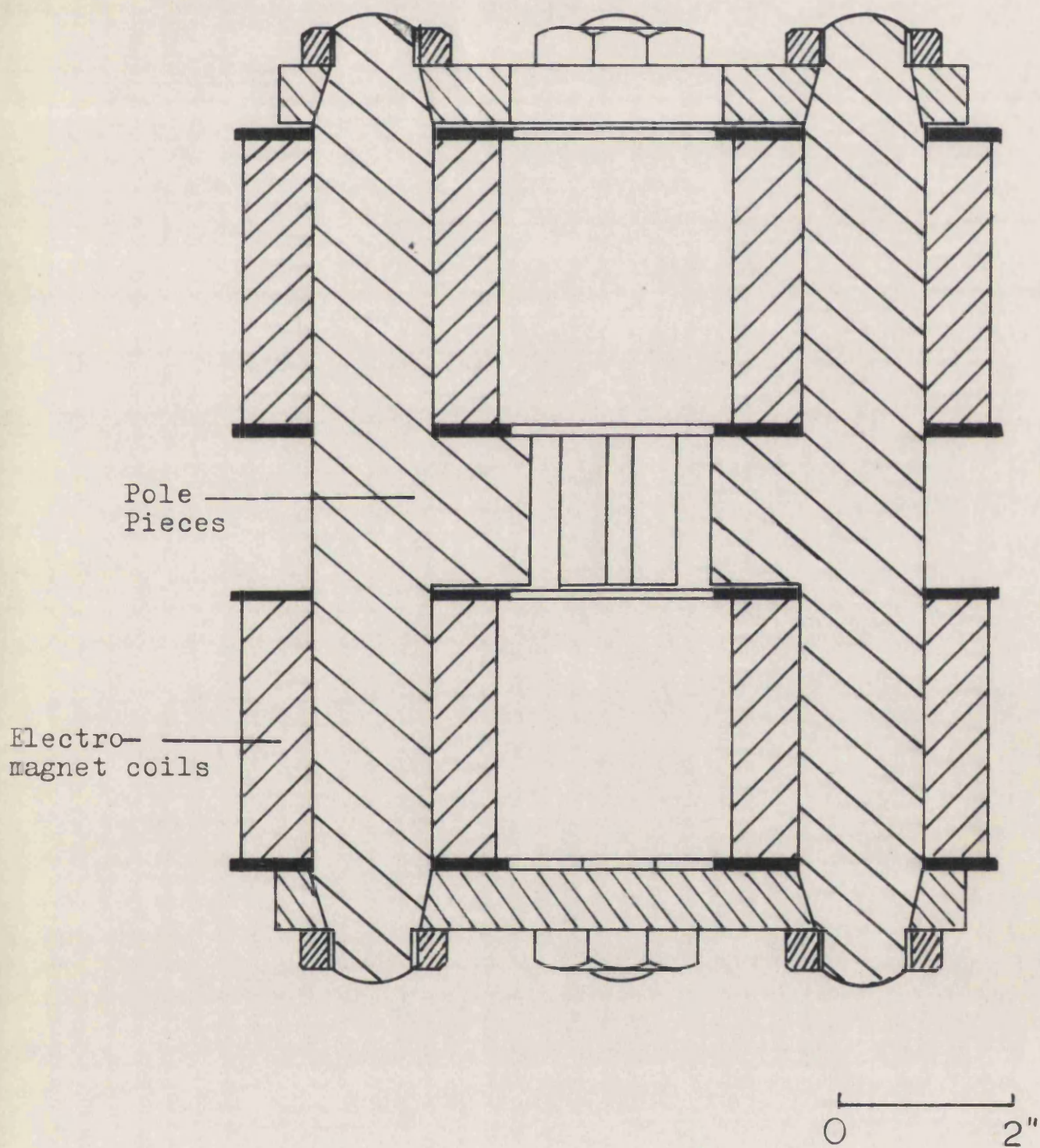


Fig.3.6 Cross Section of Electromagnet Assembly

of 0.0815" was finally used with a total air gap of 0.25" per pole. With the designed electromagnet current of 0.3 A. an estimated flux density of 0.1 Wb/m^2 is obtainable in the air gap.

3.4.5 Electrical connections

Connections to the voltage coil are obtained through a screened two-pole socket mounted on the bottom of the centre unit. A hole drilled centrally upwards from the socket allows the flying leads of the voltage coil to be soldered to the socket.

For the current coil, connection is made to the hook ends of the coil by means of small pots of mercury mounted on two of the pole pieces. With the central unit inserted into the electromagnet, the hooks dip into the mercury. The pots are made of 'Tufnol' and connection to the mercury is made by a small pin passing through the wall of the pot. All metallic pieces in contact with the mercury are cadmium plated to prevent erosion.

The connections must be such that they interfere as little as possible with the motion of the cup. In the case of the voltage coil, the wire is so fine that connection by flying leads causes little damping. For the current coil however a mercury connection provides a large current carrying capacity together with minimum frictional loss.

3.4.6 Temperature control

Owing to the marked temperature dependence of the mechanical

properties of most liquids it is necessary to ensure that the test liquid in the annulus is closely defined in temperature. The upper part of the centre unit is provided with a jacket through which water at the required temperature is pumped. In Figure 3.2 the inlet nozzle of this jacket is visible. The water is pumped from a thermostat bath in which the temperature is maintained stable to within 0.1°C , through the jacket and back to the bath. Thermometers at the input and output of the jacket indicate any significant temperature drop. The upper part of the centre unit including the mild steel plug is thus maintained at the required temperature.

The test liquid is in intimate contact with the mild steel plug and tends to assume the same temperature as the plug. However because of the outward radial heat flow, a temperature drop across the annulus may be expected; but this will be minimised to a certain extent by the fact that the surrounding cup wall is a very poor thermal conductor. Because of the size of the annulus it is impossible to measure the temperature distribution across it, but a measure of the thermostating efficiency is obtained by comparing the mean annulus temperature with the thermostat bath temperature. A thermistor bridge employing one thermistor situated in the annulus and one in the thermostat tank recorded a difference in temperature of less than 0.05°C at 30°C . The time necessary to achieve stability after switching on the pump was two hours.

3.4.7 Liquid level adjustment

It is shown in Section 3.6.3 that measurements with this system involve varying the height of liquid in the annulus during an experiment. Above the water jacket (Figure 3.5) in the centre unit is a small chamber to contain the test sample and a piston controlled by a knurled screw at the top of the apparatus. A $\frac{1}{8}$ " diameter hole passes from the chamber down to the end of the steel plug and by moving the piston, liquid may be expelled into the cup or removed from it. 30 cc. of test liquid is required to fill the apparatus of which 25 cc. is recoverable. The height of liquid in the annulus is measured by means of a travelling telescope situated 18 in. distant from the apparatus.

3.5 Assembly

Each time a different test liquid is to be measured the following procedure is necessary. The centre unit must first be withdrawn from the electromagnet and separated into the two halves indicated in Figure 3.2, after loosening the upper set of strip clamps. The inside of the oscillating cup can then be cleaned. The upper section is in three parts consisting of the steel plug, the water jacket and the liquid chamber. These are separated and cleaned, followed by filling the chamber with new test liquid and reassembling. A small extra amount of test liquid is poured into the cup before the two halves of the centre unit are bolted together.

The lower set of clamps are then slackened and four circular section feeler gauges of diameter equal to the annular thickness are inserted from the top of the cup. This ensures that the cup and the steel plug are concentric. The height of the cup is adjusted and the lower and upper clamps are then tightened. It is then necessary to give each of the steel strips a tension in order to ensure the absence of buckling in any one strip, which would cause severe non-linearity in the torque/displacement relationship. Also a slight adjustment of the fundamental resonant frequency may be achieved in this way. The tensioning is effected by passing a current of approximately 12 A. through the steel strips causing heating and therefore longitudinal expansion. When thermal equilibrium is reached, the upper clamps are momentarily loosened and then re-tightened after which the current is switched off. A tension develops in the strips when they return to room temperature. The process is repeated cyclically on each strip several times in order to ensure that the four strips have equal tension.

Finally the gauges are removed from the annulus and the centre unit can be inserted into the electromagnet assembly.

3.6 Theory of the transducer

3.6.1 The single coil transducer

The torque and e.m.f. equations have already been given (equations 3.1 and 3.2). In the case of a transducer with a single

coil the torque is given by

$$T = K i$$

and the e.m.f. by $e = K \dot{\theta}$

where K is a parameter depending on the flux density and the geometry. We now define a torsional mechanical impedance:

$$Z_T = T/\dot{\theta} = K^2 i/e$$

In general the coil will have some internal electrical impedance Z_c and because of the current i flowing, the potential difference v across the coil will be different from e . In fact,

$$v = e + Z_c i$$

giving

$$Z_T = \frac{K^2 i}{v - Z_c i}$$

Rearranging, and defining the total electrical impedance of the coil as Z_e ($= v/i$) we have,

$$Z_e - Z_c = K^2/Z_T \quad 3.3$$

It will be noted that the electrical and mechanical impedances are inversely proportional with K^2 as a transducer constant. The disadvantages of the single coil system are twofold: the internal impedance Z_c of the coil is a difficult quantity to measure in an electromagnetic system since it implies that the mechanical system must be rigidly clamped ($Z_T = \text{infinity}$) while electrical measurements are being made. This is especially difficult at the higher frequencies and moreover it is necessary to obtain a calibration curve of Z_c over the complete operating frequency range of the instrument. Another difficulty occurs when the transducer is heavily loaded. In this case the difference between Z_e and Z_c

is very small compared to the value of Z_0 itself, and large inaccuracy inevitably arises in the calculation of Z_T .

It will be shown that these difficulties are greatly reduced in the two-coil transducer.

3.6.2 The two-coil transducer

For the two-coil transducer the torque and current is associated with one of the coils while the voltage and displacement rate is associated with the other.

We have,

$$T = K_1 i_1$$

$$e_2 = K_2 \dot{\theta}$$

which gives

$$Z_T = \frac{T}{\dot{\theta}} = K_1 K_2 \frac{i_1}{e_2}$$

where the suffices 1 and 2 refer to the current and voltage coils respectively. Now the difference between this and the single coil transducer equation is that e_2 is available directly, since no current need be passed through coil 2. Referring to the ratio e_2/i_1 as the transfer impedance Z_{12} , we have

$$Z_{12} = K^2 / Z_T \quad 3.4$$

where $K^2 = K_1 K_2$

In practice, the transfer impedance does not depend solely on the mechanical loading Z_T because some of the e.m.f. induced in coil 2 arises from mutual electrical coupling between the two coils i.e. mutual inductance and capacitance. Equation 3.4 may be modified to

allow for this effect to give

$$Z_{12} = K^2/Z_T + M_{12} \quad 3.5$$

where M_{12} is the mutual impedance between coils 1 and 2.

3.6.3 Effect of liquid loading

Equation 3.5 gives the electrical transfer impedance in terms of the torsional mechanical impedance of the apparatus and the impedance of the liquid sample. We may write

$$Z_T = Z_0 - zh$$

where Z_0 is some 'base line' mechanical impedance, h is the height of liquid in the annulus measured from the top of the cup, and z is the torsional impedance per unit height of the annular sample of test

liquid. Hence

$$Z_{12} = \frac{K^2}{Z_0 - zh} + M_{12} \quad 3.6$$

Consider two separate measurements of Z_{12} , Z_{E0} and Z_E at different heights of the test liquid. We may regard Z_{E0} as a measurement with $h = 0$ and some mechanical impedance Z_0 . It is a matter of convention that in the present work $h = 0$ is taken to be the case when the cup is full of test liquid, and h increases positively as the level of liquid is reduced.

From equation 3.6 we have

$$Z_{E0} = \frac{K^2}{Z_0} + M_{12} \quad 3.7$$

and

$$Z_E = \frac{K^2}{Z_0 - zh} + M_{12} \quad 3.8$$

when the change from Z_{E0} to Z_E is solely due to a change in liquid

height h . It will be noticed that in this way the end effects of the apparatus may be included in the quantity Z_o . Equations 3.7 and

3.8 give
$$\Delta Z_E = Z_{Eo} - Z_E = \frac{K^2}{Z_o} - \frac{K^2}{Z_o - zh}$$

Rearranging, we obtain

$$\frac{h}{\Delta Z_E} = \frac{Z_o \cdot h}{K^2} - \frac{Z_o^2}{K^2 z} \quad 3.9$$

Appendix C indicates how it is possible to extract the value of z from the knowledge of a set of values of ΔZ_E and h . If graphs of $h \times \text{Re} (1/\Delta Z_E)$ and $h \times \text{Im} (1/\Delta Z_E)$ are plotted against h where Re and Im are real and imaginary parts of a complex argument, the following results are obtained:

$$\begin{aligned} \tan \beta &= S_2/S_1 & \tan (2\beta + \alpha) &= I_2/I_1 \\ |z| &= \frac{K^2 (S_1^2 + S_2^2)}{\sqrt{I_1^2 + I_2^2}} & 3.10 \end{aligned}$$

where $\beta = \angle Z_o$ and $z = |z| \angle -\alpha$. The suffices 1 and 2 refer to the graphs of real and imaginary parts which are straight lines with slope S and intercept I .

3.6.4 Mechanical impedance and resonance

Although it is shown in equations 3.10 that the effect of the 'background' impedance Z_o may be eliminated in the calculations it nevertheless, by being sufficiently large, reduces the sensitivity of the measurement. In other words it is desirable that the changes in mechanical impedance caused by changing the height of the liquid in

the annulus should be as large as possible compared with the mechanical impedance of the apparatus when empty.

The moving system may be characterised by a polar inertia J , a torsional stiffness λ and a damping constant η . The equation of motion is then

$$T(t) = \lambda \theta + \eta \dot{\theta} + J \ddot{\theta}$$

where $T(t)$ is a time varying torque and θ is the angular displacement.

In the special case of sinusoidal vibration the equation may be rewritten

$$T = \lambda \theta + j\omega \eta \theta - \omega^2 J \theta$$

The torsional impedance Z_A is therefore given by

$$Z_A = \frac{T}{\theta} = \frac{T}{j\omega \theta} = \eta + j(\omega J - \frac{\lambda}{\omega}) \quad 3.11$$

The real part η of the impedance is independent of frequency and in the present apparatus its effect has been minimised. The imaginary part becomes zero at the resonant frequency defined by

$$\omega_0 J = \lambda / \omega_0$$

giving $\omega_0^2 = \lambda / J$

Rewriting equation 3.11 and eliminating λ :

$$Z_A = \eta + jJ\omega_0 \left(\frac{\omega}{\omega_0} - \frac{\omega_0}{\omega} \right) \quad 3.12$$

A graph of the function $(R - 1/R)$ where $R = \omega/\omega_0$ is shown in Figure 3.7 and it may be seen that the curve is antisymmetric about $R = 1$ when R is on a logarithmic scale. It therefore follows that if the apparatus is to be used in the radian frequency range (ω_1, ω_2) , the optimum position for the resonant frequency is given by $\omega_0 = \sqrt{\omega_1 \omega_2}$ i.e. the harmonic mean of the two limits.

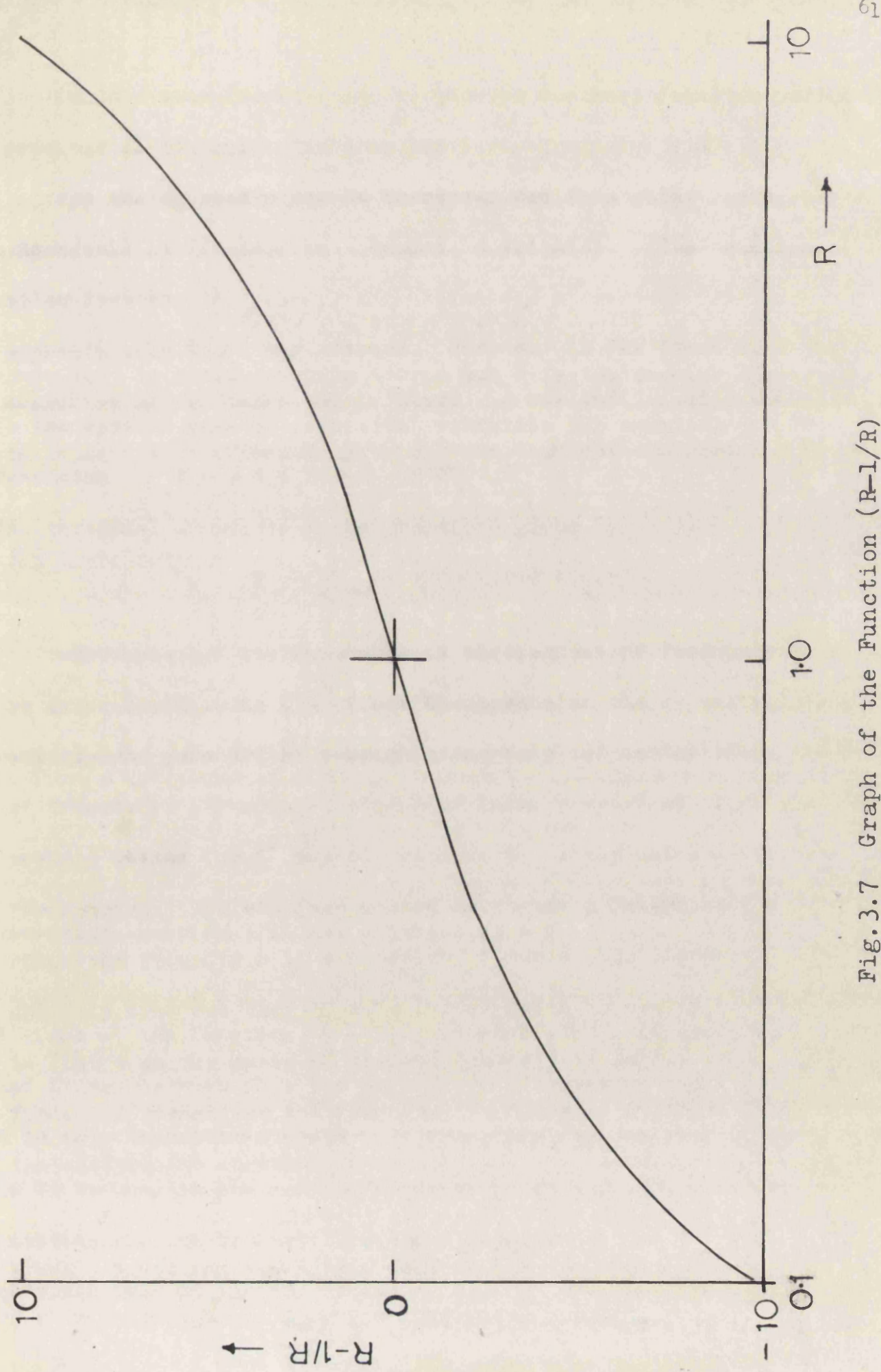


Fig. 3.7 Graph of the Function $(R-1/R)$

Under these conditions $|Z_A|$ has the smallest possible magnitude over the given range. In practice for a frequency range of 20c/s - 1.5Kc/s the optimum resonant frequency would be 173c/s. It was found impossible to increase the tension in the steel strips sufficiently to achieve this frequency, and ultimately a resonant frequency of approximately 60c/s was adopted. However, it was found that the measuring system described in Chapter 4 was sufficiently sensitive not to be seriously affected by this lower than optimum resonant frequency.

3.7 Calibration

The only calibration constant needing independent determination in equations 3.10 is K^2 . Since K^2 depends on the magnetic flux density and geometrical configuration only, it is therefore independent of frequency. By using a liquid of known properties (i.e. z is known) several values for K^2 may be obtained by simply using different frequencies. The simplest method is to use a Newtonian fluid for which the property z is a function of the static viscosity. The fluid actually used was the 350 cS siloxane which is nearly Newtonian up to 10Kc/s on the basis of the measurements of Barlow et al. (1959). Table 3.1 summarises the measurements taken to estimate the value of the calibration constant.

3.7.1 Units and dimensions

Throughout this work the centimetre-gramme-second system is used

for all the mechanical properties of the viscoelastic fluids. The electrical units of volts, amperes and ohms are used for the transducer but no ambiguity arises since the calibration constant K^2 contains all the necessary conversion factors when the electrical and mechanical quantities are always as stated.

Table 3.1

Determination of calibration constant K^2

Frequency (c/s)	25	60	160	350
Number of determinations	5	8	4	4
Mean value of K^2	180	172	168	181
Standard deviation	7	4	7	10

$$\text{Weighted mean } K^2 = 174$$

(weights taken in inverse proportion to standard deviation)

CHAPTER 4

THE MEASURING SYSTEM

4.1 Introduction

In Chapter 3 (equation 3.9) it was shown that in order to find the impedance per unit height of the liquid in the annulus, it is necessary to measure small changes ΔZ_E of the transducer transfer impedance. Thus the measuring system must be capable of determining small changes in relative amplitude and phase of the applied current and the resulting e.m.f. Because the observed changes are so small especially when operating at frequencies well away from the mechanical resonance of the transducer, very stringent requirements are placed upon the various amplifiers and phase sensitive devices in the measuring system. It may be noted that in the case of the e.m.f. induced in the voltage coil, not only are the changes observed small on a percentage basis but also in absolute magnitude. As an example, at the high frequency end of the range a signal of only $70 \mu V$ may be obtained. The magnitude and phase of two signals cannot be compared directly at this level, and high gain, stable, low noise amplification is required to raise these quantities to some suitable voltage level. Similarly, in the case of phase determination, changes of phase of the order of 0.1° need to be measured and so stability with respect to phase is as important as gain stability. Further, especially when signal levels are low, the measuring system

must be capable of ignoring the effects of noise both in the phase as well as the amplitude measurement.

The principle of measurement is that of measuring incremental quantities, Z_E , whenever possible in addition to one absolute quantity, Z_{E0} , which acts as a magnifying factor.

$$\text{i.e.} \quad Z_E = Z_{E0} - Z_E = Z_{E0} \left(1 - \frac{Z_E}{Z_{E0}} \right) \quad 4.1$$

Z_{E0} is the magnifying factor and Z_E/Z_{E0} is measured as $|(1 + \Delta) \angle \delta|$, δ and Δ being the measured quantities. (Often the driving current

is kept constant throughout the experiment and the quantities Z in equation 4.1 may then be replaced by voltages).

The necessary calculations to obtain the quantity Z_E from the various readings on the apparatus is shown in Section 4.5 and the present chapter is concerned mainly with the practical details of the system.

4.2 The system layout

A block diagram of the system is shown in Figure 4.1. An audio frequency oscillator drives a power amplifier which in turn drives the transducer in series with a standard one ohm non-inductive resistor. This resistor enables a reference signal to be derived which is proportional to and in phase with the input current. The voltage coil which is isolated from earth is connected at one end to a compensator which adds to the coil e.m.f. a proportion of the

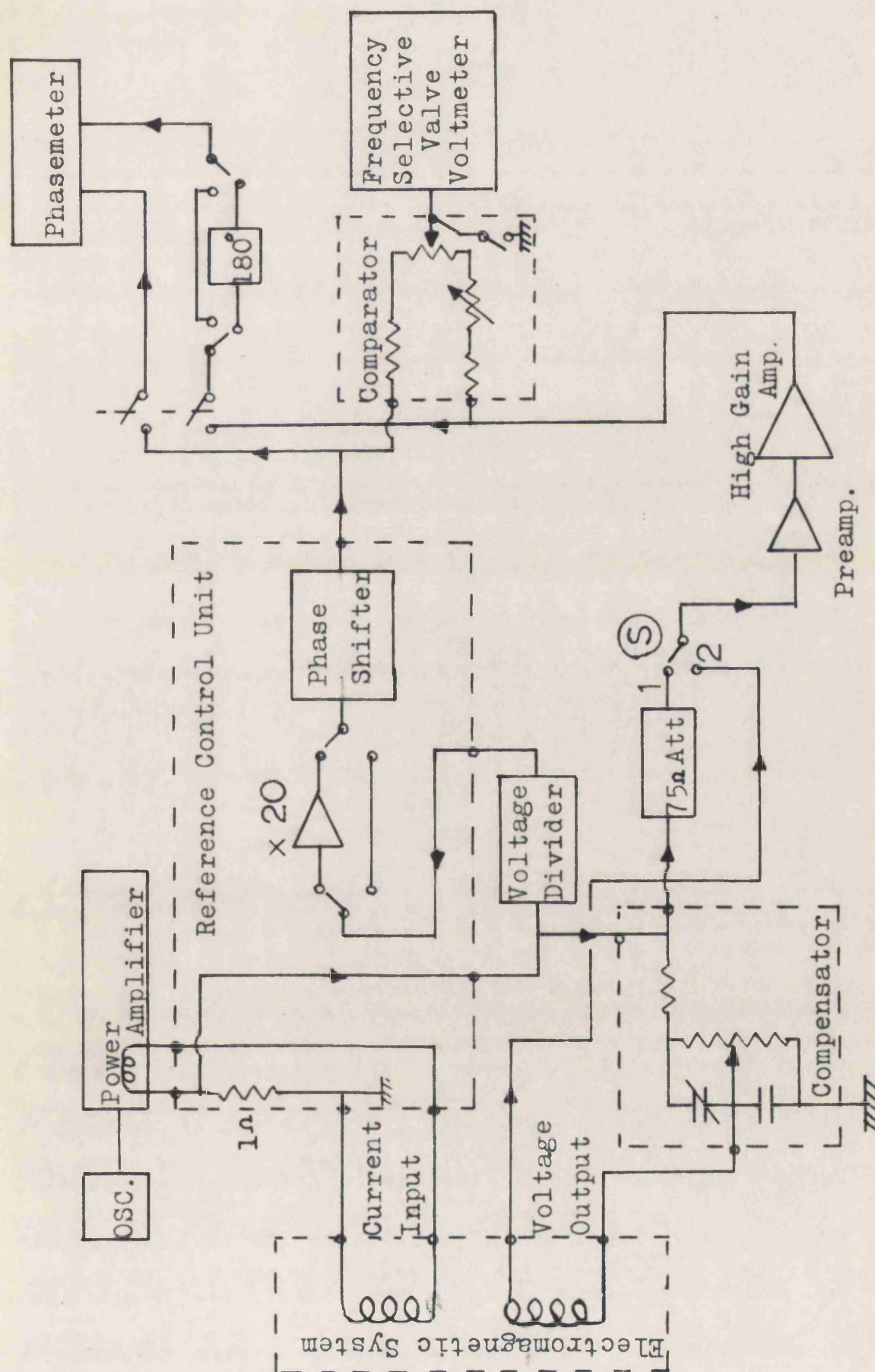


Fig. 4.1 Block Diagram of Measuring System

reference signal. The resultant signal is then taken with respect to earth from the other end of the coil. The purpose of this compensation will be explained in Section 4.2.3.

The remainder of the system may be regarded as having two channels: the reference and the signal channel.

4.2.1 The reference channel.

The single ended reference signal obtained from the one ohm resistor passes into a precision voltage divider and thereafter into an uncalibrated but highly stable phase shifter. Provision is made for the insertion of a 20x gain amplifier into the reference channel when necessary. The signal then passes to the comparator and phasemeter for comparison in amplitude and phase with the signal channel.

4.2.2 The signal channel

The voltage signal after compensation has no further phase shift except that introduced by the high gain amplifier. The preamplifier is only used when the signals are below a level of approximately 1 mV. The output of the amplifier is applied directly to the phase and amplitude comparison units and the comparison is carried out at a level of approximately 10 V. The output of the 75 ohm attenuator may also be applied to the signal channel by means of the switch so that the loop gain and phase may be measured.

4.2.3 Compensation

It was shown in Chapter 3 that the e.m.f. generated in the voltage coil is not solely due to the motion of the cup. The electrical pickup represented in equation 3.5 by the quantity M_{12} in addition to the background mechanical impedance Z_0 , while not explicitly affecting the measurement, reduces its accuracy if their effect is much larger than that due to changing the height of liquid in the annulus. The accuracy of the measurement may be much improved by introducing an 'artificial pickup', M'_{12} , which partially cancels the effects of M_{12} and Z_0 at a reference height of liquid $h = 0$. i.e.

$$Z_{E0} = \frac{K^2}{Z_0} + M_{12} - M'_{12} \rightarrow 0 \quad 4.2$$

Again since M'_{12} is of the same form as M_{12} , its effect is cancelled out in the measurement and the compensator needs no calibration. In practice the compensator is adjusted so that at the beginning of the measurement ($h=0$), the output signal from the coil and compensator is as small as possible, consistent with a satisfactory signal to noise ratio. In cases where this is not a limitation the amount of compensation is determined by the maximum gain available. The result is that a much larger percentage change in the signal voltage is observed as h is increased than would be the case without compensation.

In order to achieve compensation, advantage is taken of the fact that the voltage coil on the transducer is isolated from earth and the compensation voltage is introduced between earth and one end of the coil. The other end of the coil thus provides a compensated

single ended signal. The compensating signal is derived from the reference signal by means of a potentiometer with two shunt capacitors as shown in Figure 4.1. Magnitude and phase of the compensating signal may thus be adjusted.

4.3 Electronic design

4.3.1 Reference signal amplifier

This amplifier is in the reference channel and provides a fixed gain of 20 in situations when the required driving current is small (i.e. near the frequency of resonance). The circuit is shown in Figure 4.2 and is a conventional 3-stage amplifier with negative feedback applied to the cathode of the first stage. The open loop gain is approximately 10^3 and the feedback is derived from two wire-wound manganin resistors in the cathode circuit of the output cathode follower.

The input network is designed to curtail the response above 20Kc/s and prevent low frequency instability when the input is disconnected. The output cathode follower which is direct coupled to the previous stage consists of two halves of an ECC 91 strapped in parallel.

4.3.2 Phase shifter

Figure 4.3 shows the design of the phase shifter. The important

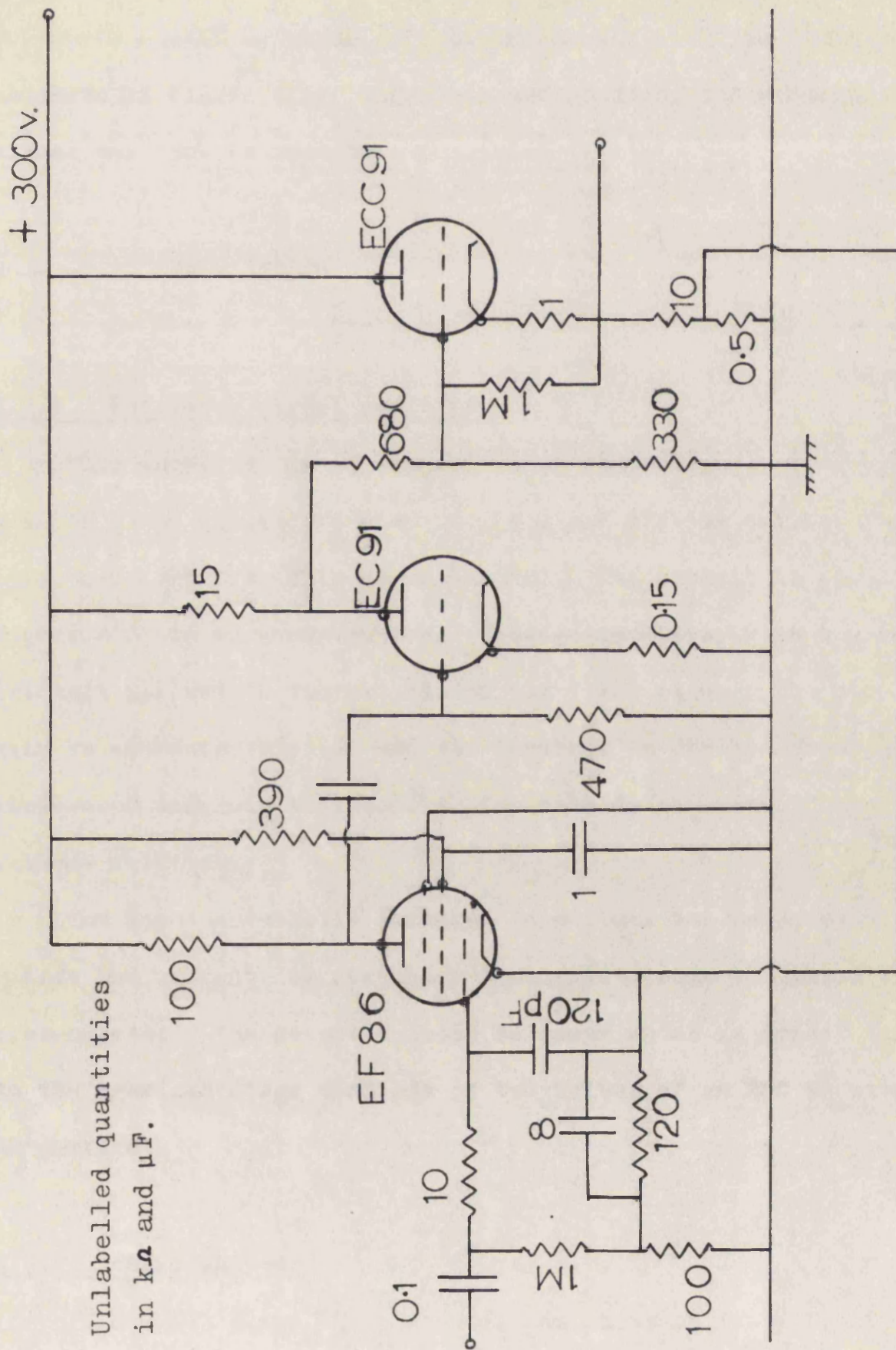


Fig. 4.2 Circuit Diagram of Reference Signal Amplifier

consideration here is that variation of phase should have the minimum possible effect on the amplitude of the output signal. This may be achieved by applying a balanced signal to a series R C combination and taking the output from the R-C junction. As either R or C is varied, so the phase of the output signal changes without the amplitude changing. In the present design the balanced signal is obtained from a triode phase splitter at the input, the two outputs of which are a.c. coupled to two similar cathode follower circuits. Each cathode follower consists of two halves of an ECC 81 strapped in parallel and drives each end of the R C network. A switch enables the polarity of the network to be reversed thus allowing a 180° phase shift. The phase may be continuously varied from $0 - 180^\circ$ or $180^\circ - 360^\circ$ by means of the switched capacitors and the variable resistor; and the output of the network is applied to a cathode follower output stage which negligibly loads the network and provides a low output impedance.

A 100 ohm potentiometer in the cathode circuit of the input phase splitter allows final trimming of the balancing so that with large phase changes negligible amplitude changes are observed. The passive components of the phase shift network do not have to be calibrated but their stability is improved as much as possible by the use of polystyrene capacitors and wire-wound resistors. For amplitude stability wire-wound resistors are used throughout the circuit and special (manganin) types are used in the phase splitter. The overall mid-band gain of the circuit is 0.9 and can change phase from $0 - 360^\circ$ down to 20c/s.

4.3.3 Power amplifier

A standard 'Mullard' design (Figure 4.4) has been modified to give a current drive at its output. An output transformer with two 3 ohm windings connected in parallel is capable of driving approximately 3.6 A into a 1.5 ohm load at the full power of 20 watts. The low frequency limit of operation which is determined mainly by the distortion caused in the transformer is 15c/s. The feedback is applied in the same way as in the conventional design but it is derived from the standard one ohm resistor in the output circuit which provides a single ended voltage signal proportional to the load current. The feedback components were calculated so that the 100mV input voltage which gives full power output in the original design also gives full power in the present design.

It should be noted that although for most of the experiments the amplifier is required to deliver full power, only a fraction of this is dissipated in the transducer since the resistive part of its impedance is very small. Most of the power is in fact dissipated in the one ohm standard resistor and the connecting leads which together have a d.c. resistance of 1.5 ohms. The maximum current that can therefore be delivered is 3.6 A but is usually limited to 3 A to ensure linear operation.

4.3.4 Preamplifier

The primary consideration in this circuit (Figure 4.5) is that of low noise. This requirement is more easily met because the source

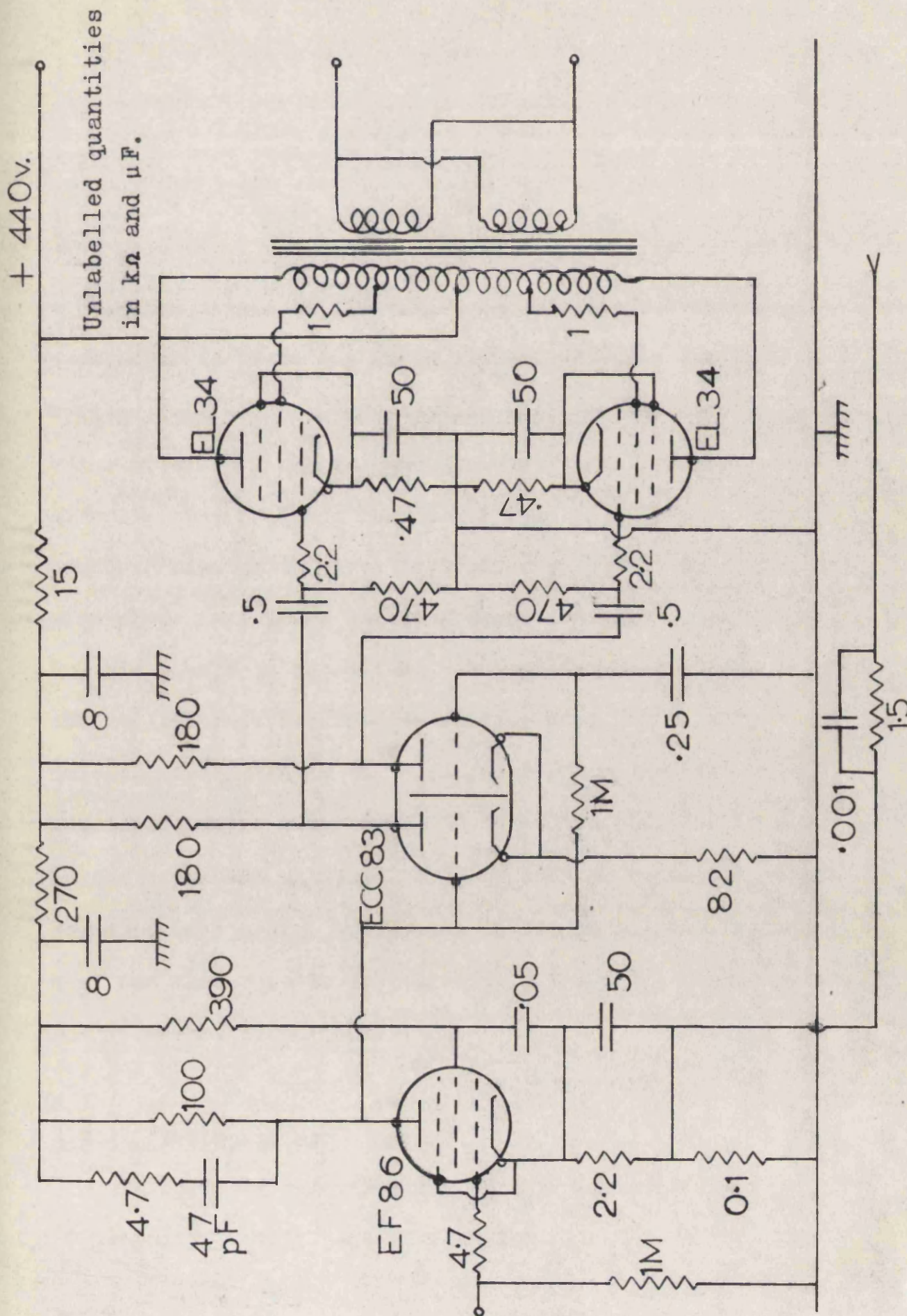


Fig.4.4.4 Circuit Diagram of Power Amplifier

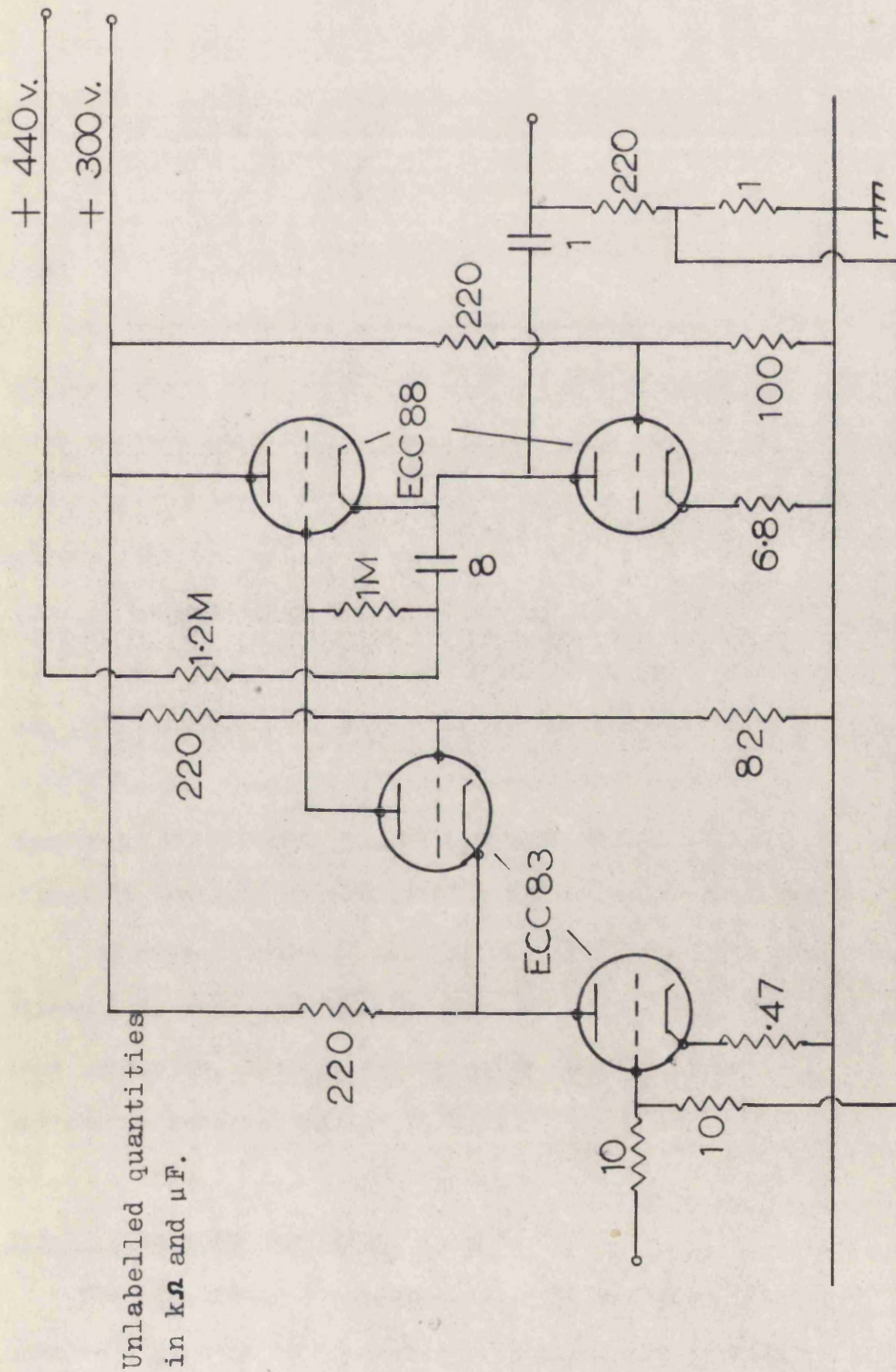


Fig.4.5 Circuit Diagram of Preamplifier

impedance for the amplifier i.e. the voltage coil and compensator, is typically only a few hundred ohms, and the input impedance of the amplifier need not be especially high. Gain stability is achieved by using a high forward gain and negative feedback; and in order to obtain the necessary gain together with low noise, an unusual circuit design has been used.

The input stage is a low noise cascode circuit (Valley and Wallman, 1948) using two halves of an ECC 83 double triode operating under current starvation conditions (Ferguson, 1954). This stage is loaded by the input impedance of a cathode follower of which the cathode load is another triode. In this way the gain of the cathode follower becomes very nearly unity and the effective load of the cascode amplifier is of the order of 100 megohms giving an open loop gain of 10^4 . The output of the cathode follower is a.c. coupled to the feedback potentiometer consisting of two high stability wire-wound resistors; and the feedback signal is added to the input signal at the grid of the first valve by means of a resistive adder.

The overall gain of the circuit is 200 and the response is flat within 1 db over a frequency range of 10/s - 100Kc/s. With the input load connected, the equivalent noise input voltage is $1.5 \mu\text{V}$ and the maximum undistorted output is 5 V.

4.3.5 High gain amplifier

The overriding consideration in this design (Figure 4.6) was to achieve a gain of 10^4 together with high gain stability. In order

to obtain the necessary stability all feedback resistors are manganin wire-wound types and the forward gains of the various stages are so high that the overall gain is almost entirely determined by the feedback components. This has the undesirable feature that with so much gain and feedback, there is a strong tendency to oscillatory instability and therefore most of the stages are decoupled at the h.t. as well as interstage phase advance networks being incorporated. A consequence of this design is that the resultant frequency response of the complete amplifier is much better than that required but the property of gain stability is maintained only over a narrower frequency range.

The complete amplifier consists of two cascaded feedback amplifiers with overall feedback. Each amplifier has an open loop gain of approximately 5×10^4 and 10^3 with feedback. The cascaded combination thus has a gain of 10^6 and with feedback the complete amplifier has a gain of 10^4 . The input stage consists of two triodes with a common anode load thus forming an adding circuit. The input is applied to one grid the other being a.c. grounded, while the local and overall feedback signals are applied to the cathodes. The output of this stage is applied to a pentode of which the anode load is the input impedance of a cathode follower, in much the same manner as that described in Section 4.3.4. This completes the first half of the amplifier, local feedback being derived from a potentiometer in the cathode circuit of the cathode follower.

The second half of the amplifier is of a similar design except

that the output cathode follower is of the two-triode variety as in the preamplifier. The output stage of the complete amplifier consists of two halves of a double triode strapped in parallel, the input to the grid being via a filter network. Without the filter network, the bandwidth extends from 0.05c/s -- 1Mc/s, with sufficient gain stability in the range 10c/s -- 5Kc/s. To reduce the noise at the output in the working frequency range, the filter network is included to curtail the response at about 50Kc/s. Under these conditions the equivalent noise input voltage is $12\mu\text{V}$ and the maximum output level is 50 V. before the onset of serious distortion.

It was not found possible to measure the gain stability of this amplifier in isolation, but the gain stability of the complete system could be assessed by observing the variations in loop gain over a period of time. Since the percentage changes observed during a measurement are small the loop gain stability during the measuring period is important. This was found to vary by less than 0.005 db (a ratio of 1.0006:1) over a period of ten minutes after allowing half an hour to elapse after switching on.

4.3.6 Comparator

The signals from the two channels are compared in amplitude by applying them 180° out of phase to a comparator consisting simply of a resistive adding network. The precision voltage divider and the phase shifter in the reference channel are adjusted until a null is obtained at the output of the comparator. This is detected

by means of a 'Brüel and Kjaer' frequency selective valve voltmeter type 2107 having a maximum sensitivity of $100 \mu\text{V}$ full scale. The resistive network is of manganin wire-wound resistors throughout.

During construction the network was trimmed so that a balanced signal obtained from a 'Gertsch' inductive ratio box gave a null at 500c/s. It was found necessary to include some small capacitance to earth in one of the arms of the network to maintain proper balance within 0.1% over the operating frequency range. Owing to the finite output impedances of the phase shifter and the high gain amplifier (Figure 4.1), provision is made to earth the output of the comparator by means of a switch in order that the interaction of the two signals is eliminated when taking a phase measurement. For the same reason the phasemeter is isolated from the circuit when making an amplitude comparison.

4.3.7 The phasemeter

It has already been stated (Section 4.1) that small phase changes of the order of 0.1° have to be measured, and the presence of noise and hum in the two signals to be compared will result in short term fluctuations in the apparent phase giving rise to 'jitter'. The method used to minimise this effect is to relate the relative phase to the mark-space ratio of a square wave, the mean d.c. level of which is measured on a potentiometer. The time constant

associated with the potentiometer may be made as large as required in order to average out the effects of jitter. A block diagram of the system is shown in Figure 4.7.

The two sine waves voltage signals whose relative phase is to be measured are fed into comparator circuits which emit a negative step at the time when the sine waves pass through zero with negative slopes. These negative steps, which occur at different times if a phase difference exists between the two signals, are differentiated at the two inputs of a bistable circuit which is only sensitive to negative pulses. The output of the bistable is thus a square wave of the same frequency as the input sine waves but having a mark-space ratio proportional to the phase difference. The d.c. component of this square wave is then measured on a potentiometer.

The waveforms occurring in this circuit are shown in Figure 4.8. It will be noted that the time at which the comparator produces a positive step is not important in the measurement, and the form of the output square wave is determined by only one point in each of the input sine waves per cycle. An ambiguity occurs in the output waveform when the phase difference is zero, since the bistable is then required to respond to two simultaneous input pulses. Also inaccuracies arise at very small phase differences because of the finite resolution time of the bistable and the phase jitter. To avoid these difficulties a monostable circuit may be switched into one of the channels by means of S 2 (Figure 4.7) and the delay in one

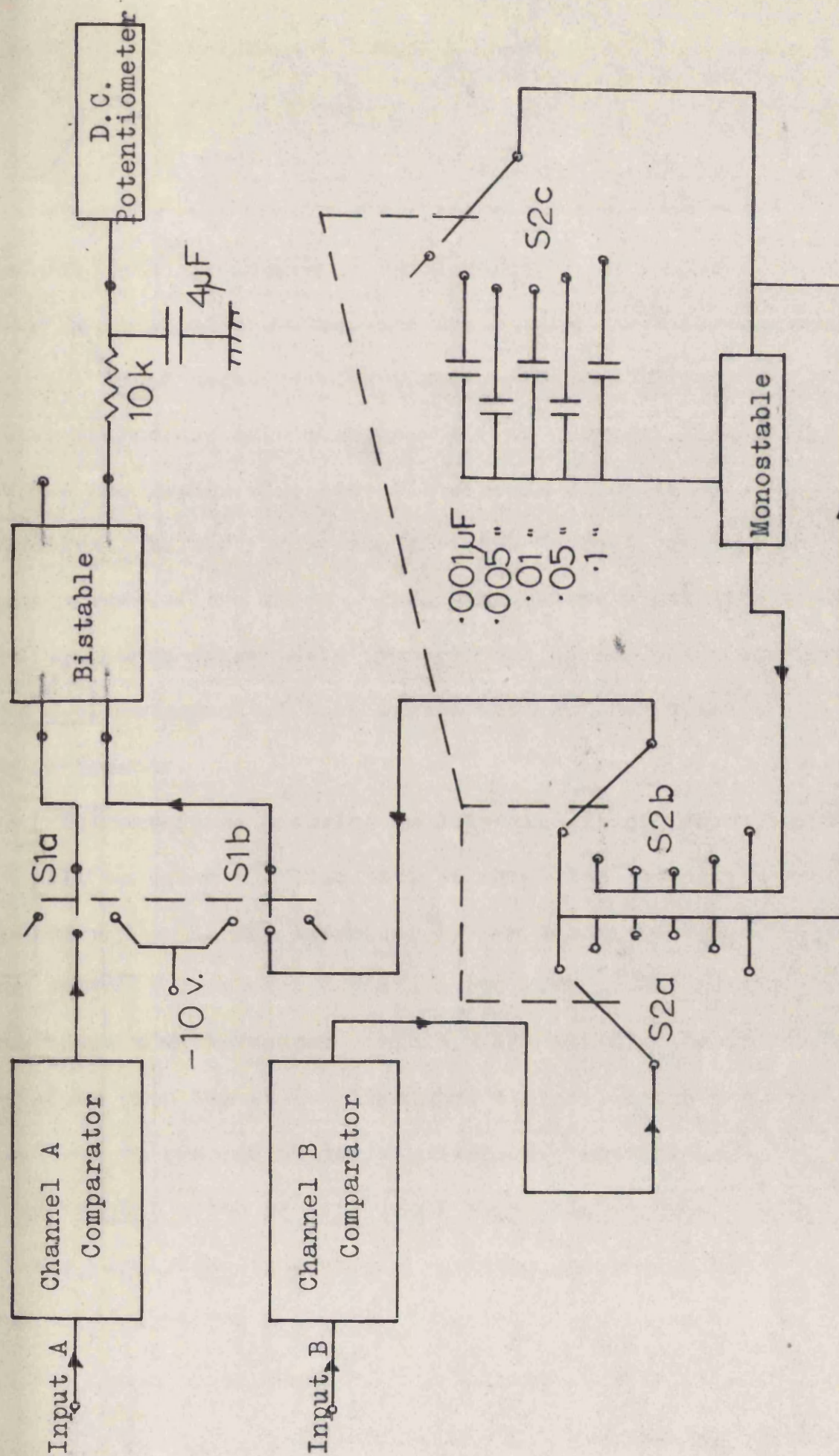


Fig.4.7 Block Diagram of Phasemeter

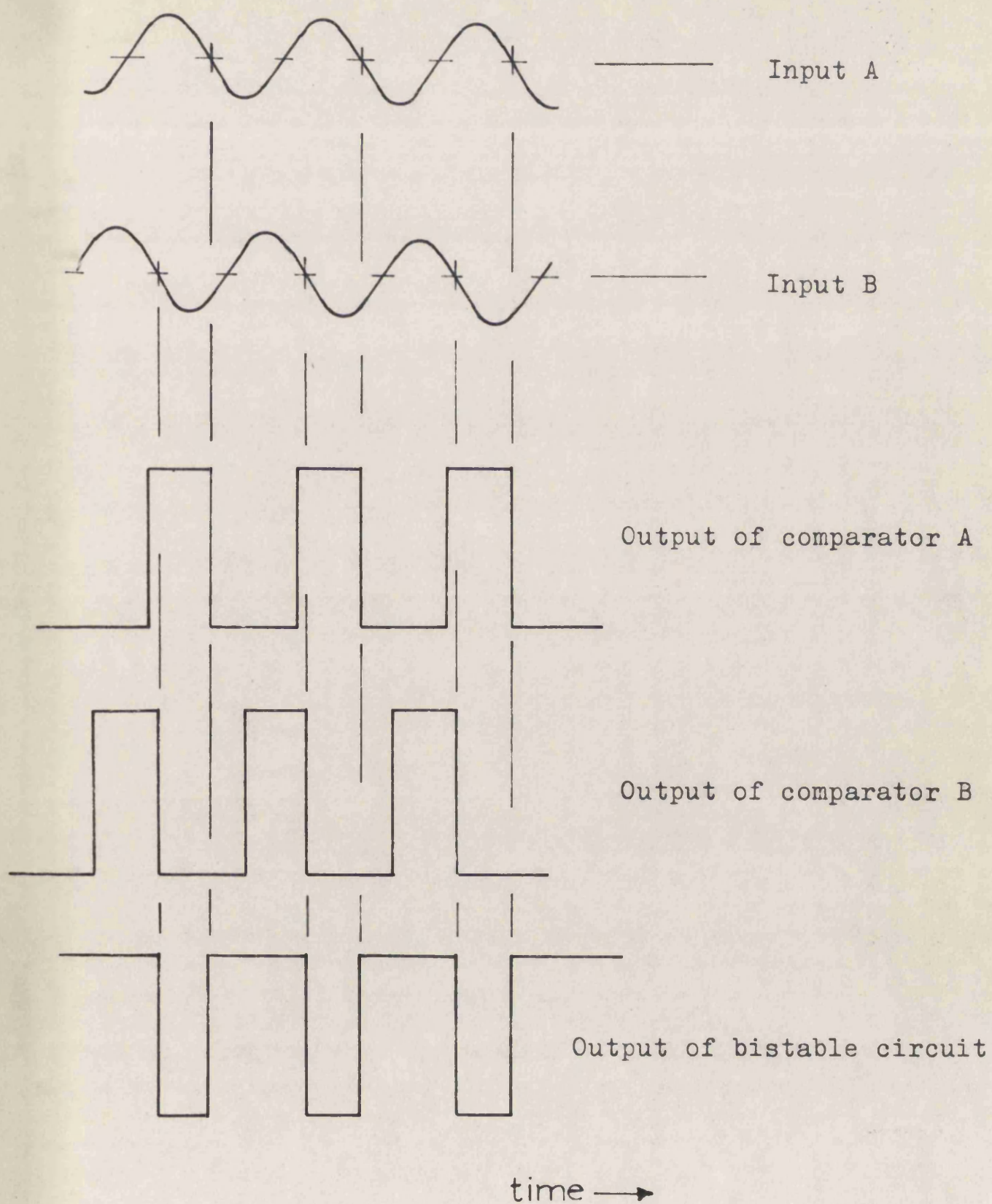


Fig.4.8 Phasemeter Waveforms

channel varied. Since only changes of phase are being measured, the values of delay need not be known exactly. The circuits of the various units comprising the phasemeter are shown in Figure 4.9.

Comparator circuit. Because it is required to select a certain voltage level on the input sine wave it is important that no distortion should occur wherever there is a.c. coupling, since the result would be a shift in d.c. level of the waveform. For this reason a cathode follower is required to isolate the inevitably a.c. coupled preceding stages to the following d.c. coupled design. The output of the cathode follower drives an emitter follower which in turn drives a common emitter stage. The load of the common emitter stage is a combination of resistors and a tunnel diode which is designed to function in a bistable mode. The output excursion of this combination is 300 mV and is sufficient to switch the base of the output transistor when suitably biased. Silicon transistors are used to minimise the effects of temperature variation on the bias current of the tunnel diode. This current is adjusted by means of the cathode follower grid potentiometer so that the circuit triggers at the point where the sine wave passes through zero. The diode and zener diode protect the solid state circuitry from excessive voltages that may be applied. The stability of the tunnel diode characteristics together with the very fast switching time ensures that the circuit has little drift or inherent jitter. The trigger level potentiometers of the two comparators are adjusted as follows. A common signal is applied to

both inputs, the square wave outputs being connected to the trigger- and Y-inputs of an oscilloscope. The amplitude of the signal in one of the channels is then varied and the trigger level potentiometer is adjusted until the amplitude of the waveform does not affect the lateral position of the negative step displayed on the oscilloscope screen. Under these conditions triggering occurs at the point where the sine wave passes through zero, and the process is then repeated on the other channel.

Bistable and monostable circuits. These are conventional n p n silicon transistor circuits, in which the collector excursions are approximately 8.5 V. Diode triggering is used on the bistable circuit and is only sensitive to negative voltage steps which appear as spikes on the bases of the transistors. The monostable has five available delays of 7.5, 15, 75, 150 and 750 μ S selected by switch S 2.

Potentiometer. A common supply of 9 V. is used for all the pulse circuits and also the potentiometer. Calibration of the 0° and 180° positions is carried out by switching S 1 to either of the positions A or B (Figure 4.9) and adjusting the appropriate preset 100 ohm resistor. The effect of the switch is to maintain the bistable in one of its states and to compare its output voltage with the high or low end of the potentiometer. The potentiometer itself is a ten turn 1 K helical type with a linearity of 0.1%. By means

of switch S 3 a range of 180° or 10° may be covered by the ten turns of the potentiometer. A galvanometer of maximum sensitivity $1 \mu\text{A}$ full scale is used for the null detection and a relative overall precision of 0.01° is attainable in the phase measurement.

4.3.8 Ancillary equipment

Power supplies. All h.t. supplies are stabilised commercial types and valve heaters are supplied from heavy duty d.c. supplies run from constant voltage transformers. This ensures stability and maximum freedom from hum.

The transducer electromagnet is powered by a 'Brandenburg' constant current unit operating at 300 mA and approximately 470 V.

Oscillator. A 'Solartron' oscillator type CO 546 is used to supply signal to the power amplifier. The frequency calibration on this instrument was checked with an electronic counter and found sufficiently accurate for direct reading of frequency.

Oscilloscopes. Two oscilloscopes are used for monitoring the various waveforms. They are a 'Telequipment' type D 31 general purpose oscilloscope and a 'Solartron' type CD 568 for pulse work.

4.4 Measurement procedure

After setting up the various parts of the apparatus as previously described, the electromagnet coil current is switched on and adjusted to 300 mA, and the test liquid is raised to its highest level in the annulus. Its height h_0 is recorded with the measuring telescope. With the switch S (Figure 4.1) in position 2, the compensator is adjusted as indicated in Section 4.2.3. The gains of the two channels are then arranged so that the output of both channels is approximately 10 V. The voltage divider and phase shifter in the reference channel are then varied to obtain a null on the comparator and the voltage divider setting P_0 is noted. The switch S is then switched to position 1 and a null is now obtained on the comparator by varying the attenuator and phase shifter. The attenuator setting M is noted. A phasemeter measurement is now made and then repeated after switching S to position 2 again, giving the loop phase shift ϕ . The comparator is then rebalanced using the phase shifter only and a phasemeter measurement is then made. This completes the loop gain and phase measurements.

The liquid level is then reduced to height h_1 and another phasemeter measurement is taken to give a phase change ϕ_1 . The amplitudes are now compared using the phase shifter and voltage divider which results in the new setting P_1 . Another phasemeter measurement is then taken before reducing the height of the liquid again and repeating the procedure. Typically measurements at five

different heights are taken.

4.5 Calculation of the measured quantities

The change in transfer impedance $(Z_E)_n$ caused by a change in the liquid height from h_o to h_n is given by

$$(Z_E)_n = \frac{v_o}{i_o} - \frac{v_n}{i_n} = \frac{v_o}{i_o} \left(1 - \frac{v_n}{v_o} \frac{i_o}{i_n} \right) \quad 4.2$$

where i is the current drive to the transducer and v is the voltage from the signal channel. The first part of the measurement gives

$$\frac{v_o}{i_o} = M e^{j\phi} \quad 4.3$$

and the succeeding measurements give

$$\frac{i_o}{i_n} \frac{v_n}{v_o} = \frac{P_n}{P_o} \exp(j \sum \theta_n) = P e^{j\theta} \quad 4.4$$

Dropping the suffix n , it follows from equations 4.2, 4.3 and 4.4

$$\text{that } \frac{h}{(Z_E)_n} = \frac{h}{\Delta Z_E} = \frac{h}{M} e^{-j\phi} \frac{1 - P \cos \theta + j P \sin \theta}{1 + P^2 - 2 P \cos \theta} \quad 4.5$$

where $h = h_n - h_o$

Separating equation 4.5 into real and imaginary parts gives

$$\begin{aligned} \text{Re } \frac{h}{\Delta Z_E} &= \frac{\cos \phi (1 - P \cos \theta) + P \sin \theta \sin \phi}{1 + P^2 - 2 P \cos \theta} \cdot \frac{h}{M} \\ \text{Im } \frac{h}{\Delta Z_E} &= \frac{P \sin \theta \cos \phi - \sin \phi (1 - P \cos \theta)}{1 + P^2 - 2 P \cos \theta} \cdot \frac{h}{M} \end{aligned} \quad 4.6$$

The quantities on the right hand side of equations 4.6 may then be calculated directly from the experimental measurements and plotted

graphically against h . The slopes and intercepts of these straight line graphs are then used to obtain the values of $|z|$ and $\angle z$ where z is the torsional impedance per unit height of the cylindrical system. It is at this point in the calculation that the calibration constant of the apparatus K^2 is required. Having obtained z , it is then necessary to find the corresponding values of G' and G'' as shown in appendix A. First, quantities $\text{mod } Y$ and $\arg Y$ are calculated:

$$\text{mod } Y = \frac{a f \rho}{z}, \quad \arg Y = -\angle z$$

where a is a constant, f is the measuring frequency and ρ is the density of the test liquid. The table in appendix B may then be used with suitable interpolation, to obtain values for the quantities MOD and ARG. These are related to G' and G'' by

$$G = \sqrt{G'^2 + G''^2} = \frac{b \rho f^2}{\text{MOD}} \quad \angle G = \tan^{-1} \frac{G''}{G'} = \text{ARG}$$

where b is a constant. The values for G' and G'' at the particular frequency f can be thus obtained.

The advantage of this graphical technique is that some estimate of the errors in the experiment may be determined from the scatter of points on the curve. Also, any spurious effects would be manifest as non-linearity of the curve.

4.6 Typical calculation

Test liquid:	Silicone fluid MS 200/30K
Temperature:	30°C

Density, ρ : 0.967 gms/cc.

Frequency, f : 60 c/s.

$$M = -60.1 \text{ db} \equiv 9.86 \times 10^{-4} \quad \phi = 0.7791^\circ$$

i	h_i cm.	h cm.	P_i	θ_i^c	P	θ^c	$\text{Re}\left(\frac{h}{\Delta Z_e}\right) \cdot 10^3$	$\text{Im}\left(\frac{h}{\Delta Z_e}\right) \cdot 10^3$
0	11.830	0	.3420	0	1	0	-	-
1	11.172	0.658	.3764	.0229	1.1006	.0229	-3.345	+5.510
2	10.514	1.316	.4210	.0349	1.2310	.0578	-2.620	+4.910
3	9.856	1.974	.4760	.0581	1.3977	.1159	-1.840	+4.387
4	9.198	2.632	.5547	.0880	1.6219	.2039	-1.104	+3.800
5	8.540	3.290	.6580	.1376	1.9240	.3415	-0.390	+3.193

The figures in the last two columns calculated from equation 4.6 are shown plotted against h in Figure 4.10. The slopes and intercepts found are:

$$S_1 = 1.128 \cdot 10^3 \Omega^{-1} \quad I_1 = -4.087 \cdot 10^3 \text{ cm}/\Omega$$

$$S_2 = -0.878 \cdot 10^3 \Omega^{-1} \quad I_2 = 6.081 \cdot 10^3 \text{ cm}/\Omega$$

From equations C.2 and C.3,

$$\tan \beta = -\frac{0.878}{1.128} = -0.778, \text{ giving } \beta = -0.658^\circ$$

$$\tan (2\beta + \alpha) = \frac{6.081}{-4.087} = -1.489, \text{ giving } (2\beta + \alpha) = -0.979^\circ$$

Therefore $\alpha = \arg Y = 0.337^\circ$

From equation C.4,

$$|z| = \frac{K^2(1.128^2 + 0.878^2)}{\sqrt{4.087^2 + 6.081^2}} \cdot 10^3 = 277.3 K^2$$

Inserting 174 for K^2 gives $|z| = 48,200$ dyne-secs.

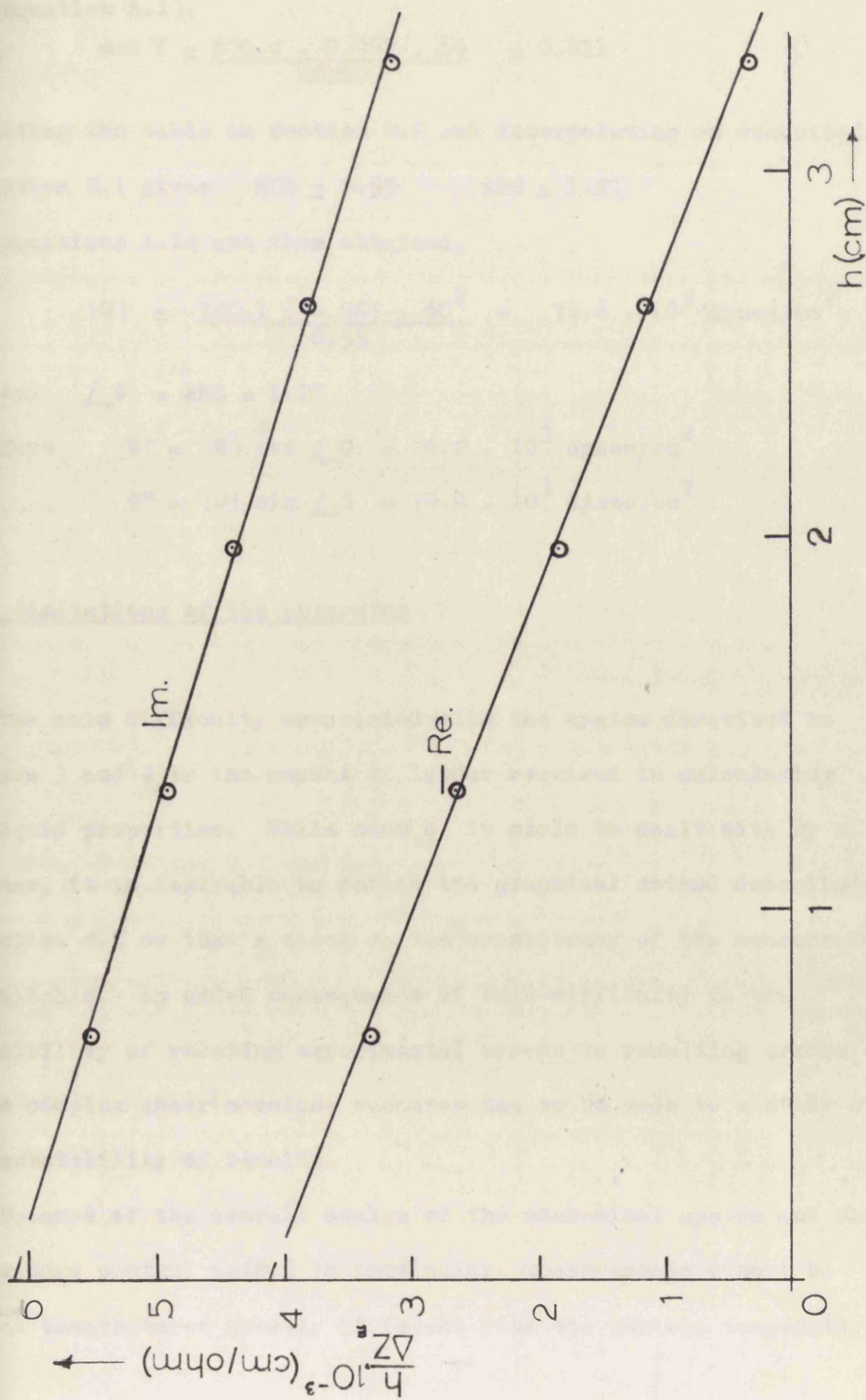


Fig. 4.10 Graph of Experimental Results

From equation A.13,

$$\text{mod } Y = \frac{680.4 \cdot 0.967 \cdot 60}{48200} = 0.821$$

Consulting the table in Section B.2 and interpolating as described in Section B.1 gives $\text{MOD} = 6.55$ $\text{ARG} = 1.21$

From equations A.14 are then obtained,

$$|G| = \frac{140.1 \cdot 0.967 \cdot 60^2}{6.55} = 74.6 \cdot 10^3 \text{ dynes/cm}^2$$

$$\text{and } \angle G = \text{ARG} = 1.21$$

$$\text{Therefore } G' = |G| \cos \angle G = 26.2 \cdot 10^3 \text{ dynes/cm}^2$$

$$G'' = |G| \sin \angle G = 70.0 \cdot 10^3 \text{ dynes/cm}^2$$

4.7 Limitations of the apparatus

The main difficulty associated with the system described in Chapters 3 and 4 is the amount of labour required in calculating the liquid properties. While much of it could be dealt with by a computer, it is desirable to retain the graphical method described in Section 4.5 so that a check on the consistency of the measurement is available. An added consequence of this difficulty is the impossibility of relating experimental errors to resulting errors in the complex shear modulus: recourse has to be made to a study of the repeatability of results.

Because of the overall design of the mechanical system and the temperature control method in particular, measurements cannot be made at temperatures greatly different from the ambient temperature.

At low temperatures the heat dissipated in the electromagnet coils becomes important and the bulk of the apparatus is such that total immersion in a low temperature bath is impracticable. At high temperatures the mechanical properties of the 'Araldite' cup would deteriorate and moreover the performance of the spring steel strips would be impaired.

The limitations on frequency range are determined by the electronic measuring system at low frequencies and the mechanical system at high frequencies. At low frequencies where the forward gain of the high gain amplifier becomes reduced, the gain stability suffers and the precision of the measuring system is thereby reduced. Also, with the present design of phasemeter, phase measurements are hampered by the lack of a sufficiently long time constant in the measuring potentiometer circuit. Although this could be improved by increasing the time constant, the measuring time required would be proportionately increased.

At frequencies above 1.5 Kc/s resonances in the oscillating cup were observed and this effect results in the graphs of $h/\Delta Z_E$ vs. h deviating appreciably from straight lines. By using a vibration meter probe it was found that the mode of resonance in the cup was radial decreasing in amplitude in a downwards direction. By using a material with greater stiffness i.e. glass, these modes could reasonably be expected to occur at higher frequencies.

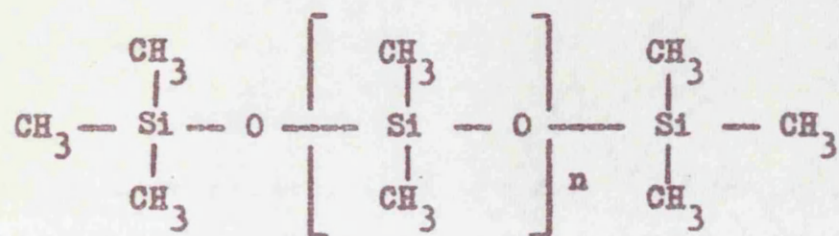
CHAPTER 5

EXPERIMENTAL RESULTS

5.1 Description of the siloxanes

Six polydimethyl siloxanes have been supplied by Midland Silicones Ltd. of which the viscoelastic properties of four have been determined by the author. The static properties of all six however have been included since they are relevant to the discussion in Chapter 6 in which reference is made to viscoelastic measurements taken at higher frequencies. The siloxane liquids are commercial samples of the MS 200 series with viscosity grades 100, 350, 12500, 30000 and 100000 cS (centistokes). The viscosity grade signifies the nominal kinematic viscosity at 25°C which is within 5% of the actual values.

The chemical structure of the fluids is of the form shown below



where the bracket suffix denotes n monomer units. The polymerisation process only determines an average chain length and the final material is not fractionated except for the removal of the very low molecular weight components. The polymer is consequently polydisperse and the molecular weight distribution is broad.

5.2 Density

The densities of the MS 200 fluids have been measured using a 25 cc. volumetric flask to an accuracy of 0.25% at a temperature of $30^{\circ}\text{C} \pm 0.1^{\circ}\text{C}$. The results are shown in Table 5.1.

Table 5.1

Densities at 30°C of the siloxanes

Viscosity grade (cS)	100	350	1000	12500	30000	100000
Density (gm/cc)	0.959	0.964	0.965	0.968	0.967	0.966

5.3 Static viscosity

The viscosities of the six fluids were measured at $30^{\circ}\text{C} \pm 0.1^{\circ}\text{C}$ using suspended level viscometers immersed in a constant temperature bath. Flow times were measured to one part in 200 or better and three results were averaged to determine the viscosity using the equation

$$\text{Viscosity (poise)} = c \rho t$$

where c is a calibration constant, ρ the density and t is the flow time. The values of the viscosity are estimated to be accurate to within 0.5%. Table 5.2 shows the values obtained.

Table 5.2Viscosities at 30°C of the siloxanes

Viscosity grade (cS)	100	350	1000	12500	30000	100000
Viscosity (poise)	0.893	3.15	8.96	108.5	287	944

5.4 Dynamic measurements

Measurements of the real and imaginary parts of the shear modulus were taken on four of the siloxanes using the apparatus described in Chapters 3 and 4. A single temperature of 30°C controlled within 0.1°C was used and measurements were taken in the frequency range 20 - 1300 c/s. On the basis of repeatability, it was found that the estimated accuracy decreased at the higher frequencies and also at low frequencies due to the low absolute magnitude of G in some cases. Table 5.3 shows the estimated accuracies of the measurements at the low and high frequency ends of the range (which are the worst cases) for two of the fluids.

Table 5.3Estimated accuracy of measurements

Viscosity grade (cS)	at L.F.	at H.F.
1000	$\pm 10\%$	$\pm 8\%$
100000	$\pm 3\%$	$\pm 10\%$

It should be noted that the accuracy is improved at frequencies between the two limits.

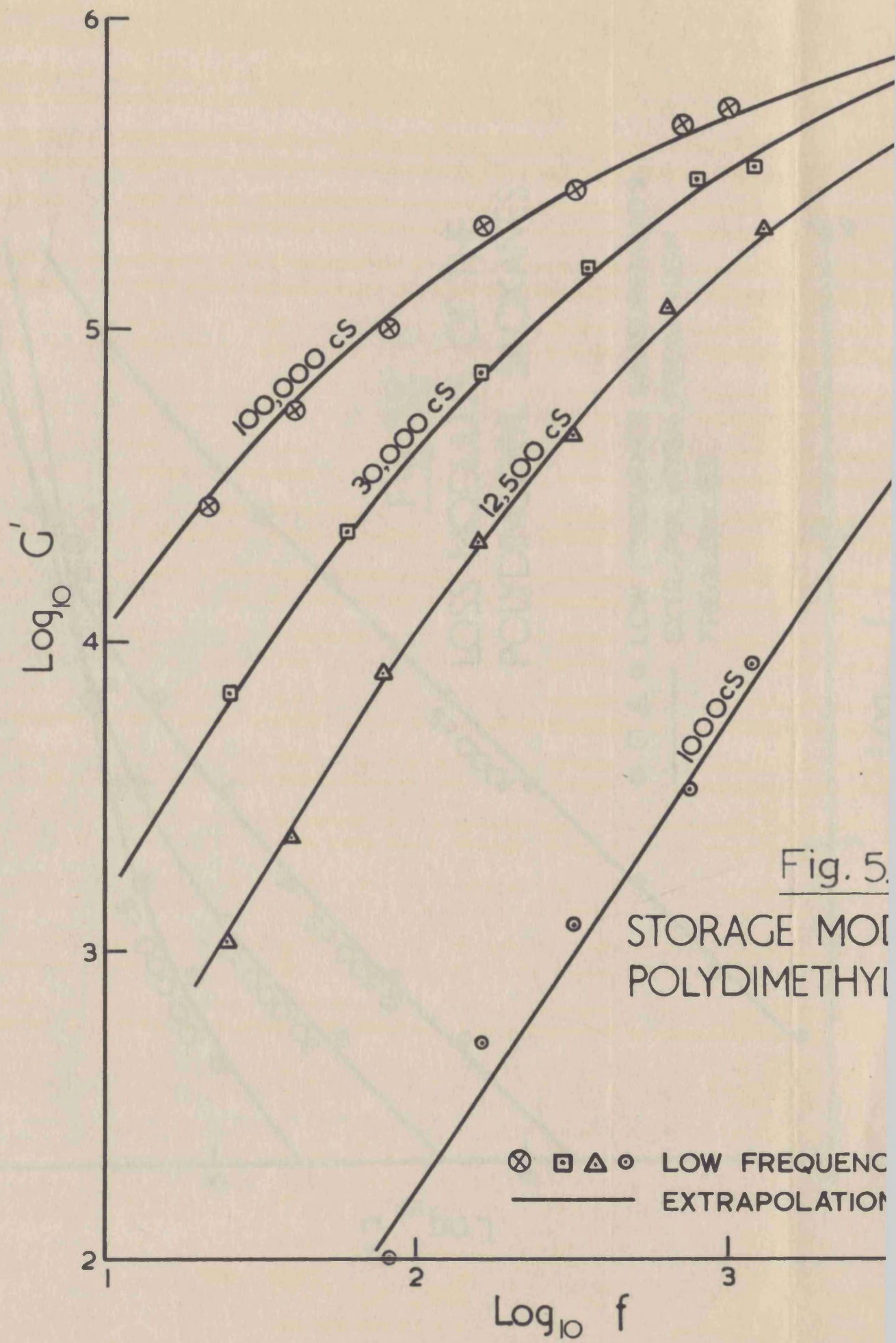
The results shown in Table 5.4 were those obtained for the 1000, 12500, 30000 and 100000 cS viscosity grade siloxanes.

Table 5.4

Dynamic moduli of the siloxanes

	Frequency (c/s)	$G' \times 10^{-3}$ (dynes/cm ²)	$G'' \times 10^{-3}$ (dynes/cm ²)	η_d (poise)
<u>1000cS</u>	25	-	1.3	8.3
	40	-	2.4	9.53
	80	0.1	4.6	9.15
	160	0.5	9.2	9.2
	320	1.2	17.5	8.72
	740	3.4	42	9.03
	1200	8.2	60	7.96
<u>12500cS</u>	25	1.1	16	102
	40	2.35	26	103
	80	7.9	58	115
	160	10.9	90	90
	320	46	150	74.5
	640	118	240	59.5
	1300	205	370	45.3
<u>30000cS</u>	25	6.8	39	248
	60	26.2	70	246
	80	29.5	121	240
	160	72	170	160
	350	155	220	100
	800	300	260	51.8
	1200	330	315	41.8
<u>100000cS</u>	21	27	95	720
	40	55	115	457
	80	100	170	338
	160	210	200	200
	320	275	250	124
	700	420	310	70.5
	1000	500	275	43.8

The results of Table 5.4 are shown plotted in Figures 5.1, 5.2 and 5.3 on a log-log scale. The continuous lines in these graphs are not the best smooth curves fitting the points but are predicted on the basis of a theory discussed in Chapter 6.



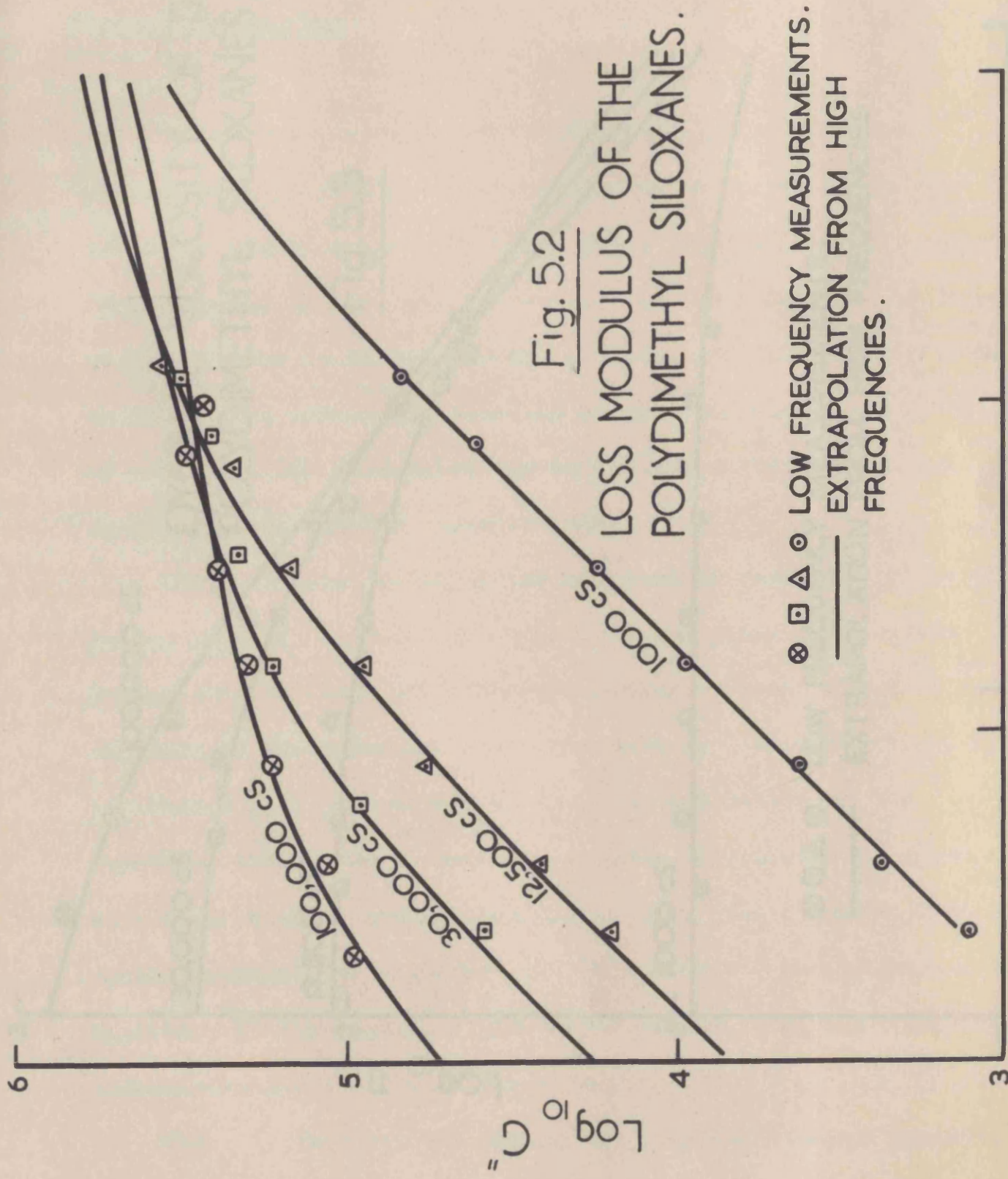
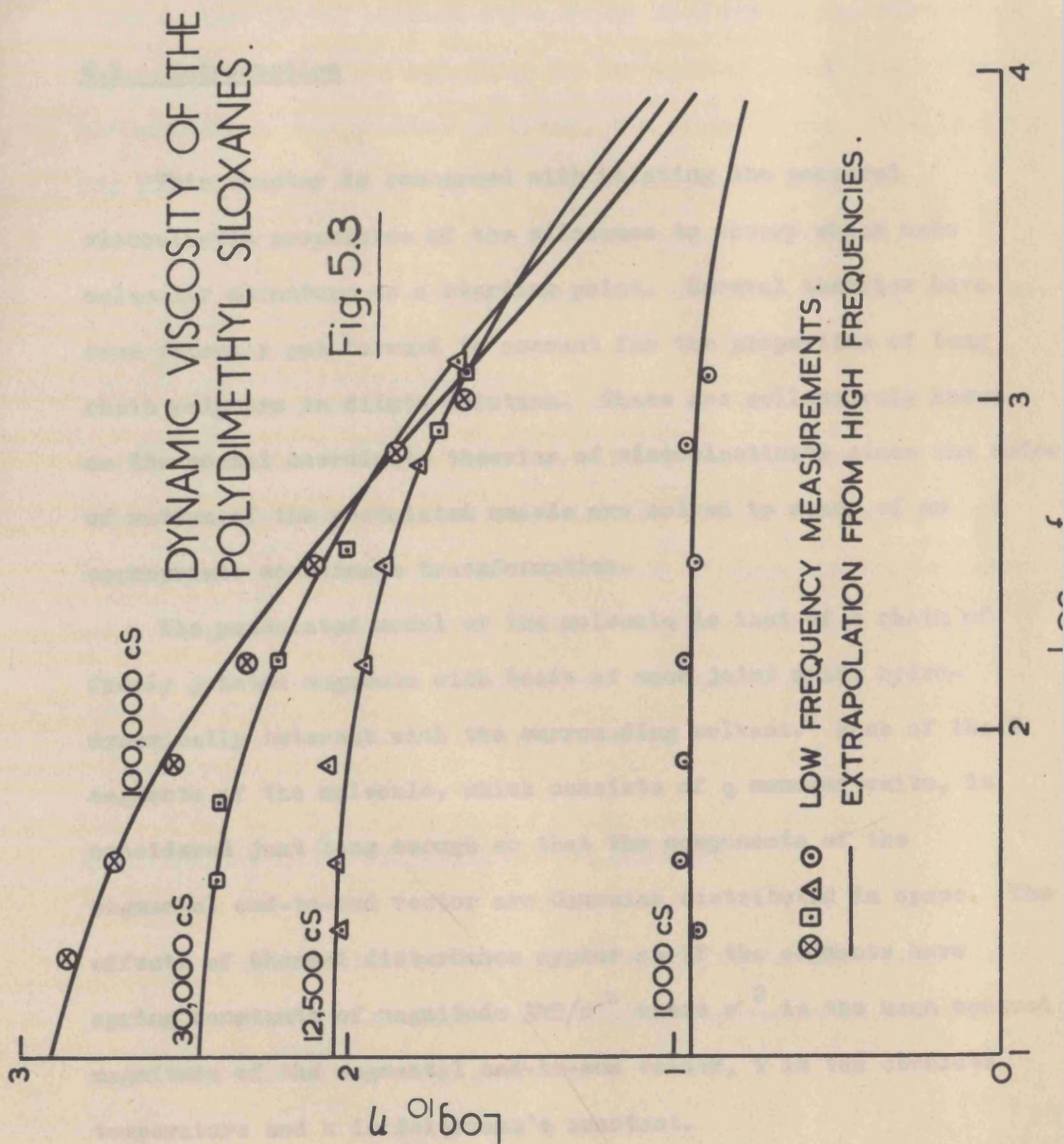


Fig. 5.2
LOSS MODULUS OF THE
POLYDIMETHYL SILOXANES.



CHAPTER 6

INTERPRETATION OF EXPERIMENTAL RESULTS

6.1 Introduction

This chapter is concerned with relating the measured viscoelastic properties of the siloxanes to theory which uses molecular structure as a starting point. Several theories have been recently put forward to account for the properties of long chain polymers in dilute solution. These are collectively known as the normal coordinate theories of viscoelasticity since the modes of motion of the postulated models are solved by means of an appropriate coordinate transformation.

The postulated model of the molecule is that of a chain of freely jointed segments with beads at each joint which hydrodynamically interact with the surrounding solvent. Each of the N segments of the molecule, which consists of q monomer units, is considered just long enough so that the components of the segmental end-to-end vector are Gaussian distributed in space. The effects of thermal disturbance appear as if the segments have spring constants of magnitude $3kT/\sigma^2$ where σ^2 is the mean squared magnitude of the segmental end-to-end vector, T is the absolute temperature and k is Boltzmann's constant.

The theories diverge in the consideration of the interaction between a molecule and the surrounding solvent. Rouse (1953)

assumes no interaction i.e. the velocity profile of the fluid is not affected by the presence of a polymer molecule, (free draining case). Zimm (1956) assumes interaction of a particular form which allows solution of the equations in two special cases, one of which corresponds to the results of Rouse, the other to what is termed the non free draining case. More recently, Tschoegl(1963) has calculated results for the general Zimm theory which predict behaviour in which the free draining and non free draining situations are limiting cases.

In applying any of these theories to the siloxanes allowance must be made for the fact that the polymer is undiluted and also that the molecular weight is distributed, i.e. not monodisperse as assumed in the theory. The discussion of this chapter is based on the arguments presented by Barlow, Harrison and Lamb (1964) which refer to the Rouse theory., but contains a more critical assessment of the theoretical limitations.

6.2 The Rouse theory and undiluted polymers

For a dilute solution of monodisperse polymer the Rouse theory predicts a number N of discrete relaxation processes all having a high frequency modulus G_{∞} given by

$$G_{\infty p} = n k T \quad 6.1$$

where p is the p^{th} process and n is the number of polymer molecules per cubic centimetre. The relaxation time τ_p of each process which

is related to the p^{th} mode of motion of the polymer molecule is

given by
$$\tau_p = \frac{q^2 a^2 x_0}{24 kT \sin^2 \left(\frac{\pi p/2}{N+1} \right)} \quad 6.2$$

where a^2 is the mean squared end to end distance of a monomer unit. x_0 is the monomeric friction coefficient and corresponds to the viscous resistance experienced by the beads. It may be observed that equations 6.1 and 6.2 satisfy the two postulates of the time temperature superposition principle described in Chapter 2. Since n and k are evidently independent of temperature it follows that the high frequency modulus is proportional to the absolute temperature for all relaxation processes. The only quantities that could vary with temperature in equation 6.2 are a^2 and x_0 . Since these are both properties of a monomer unit their temperature dependence cannot be affected by the mode number p . It is therefore apparent that all the relaxation times τ_p have a similar temperature dependence. If the number of segments N in the molecule is sufficiently large so that $N \gg 1$ and only lower order modes are considered so that $N \gg p\pi$ then equation 6.2 may be written

$$\tau_p \approx \frac{N^2 q^2 a^2 x_0}{6\pi^2 p^2 kT} \quad 6.3$$

which may be considered a sufficiently accurate representation if the number of modes included is such that $p \leq N/5$. Substituting equations 6.1 and 6.3 into equation 2.12 we obtain for the complex modulus as a function of frequency

$$G(j\omega) = nkT \sum_{p=1}^N \frac{j\omega N^2 q^2 a^2 x_0}{6\pi^2 p^2 kT + j\omega N^2 q^2 a^2 x_0} + j\omega \eta_s \quad 6.4$$

The complex modulus G in equation 6.4 is taken to be that due to the polymer contribution and that due to the solvent also. The solvent contributes an amount $j\omega \eta_s$ where η_s is the solvent viscosity with which there is no relaxation associated. Ferry, Landel and Williams (1955) suggest that in the case of undiluted polymers equation 6.4 may be expected to apply with $\eta_s = 0$. This may be imagined as being equivalent to the solvent and solution viscosity being the same. We therefore have for the modulus of an undiluted polymer

$$G(j\omega) = nkT \sum_{p=1}^N \frac{j\omega N^2 q^2 a^2 x_0}{6\pi^2 p^2 kT + j\omega N^2 q^2 a^2 x_0} \quad 6.5$$

The steady flow viscosity is consequently given by

$$\eta = \frac{nkTN^2 q^2 a^2 x_0}{6\pi^2 kT} \cdot \sum_{p=1}^N \frac{1}{p}$$

If N is sufficiently large the summation tends to the value $\pi^2/6$ (Peirce, 1950, p.99). Hence we have

$$\eta = \frac{1}{36} nN^2 q^2 a^2 x_0 \quad 6.6$$

Combining equations 6.6 and 6.3 we obtain

$$\tau_p = \frac{6\eta}{\pi^2 p^2 nkT} \quad 6.7$$

Hence the values of τ_p are given in terms of quantities that are either known or capable of experimental determination. The corresponding result for the complex modulus is

$$G(j\omega) = 6\eta nkT \sum_{p=1}^N \frac{j\omega}{\tau_p^2 p^2 nkT + 6j\omega\eta}$$

6.8

which concerns monodisperse undiluted polymers.

6.3 Generalisation to polydisperse polymers

We first observe that for a polydisperse system the number of molecules per cc. n , for a given species of molecular weight M_1 can be expressed in terms of the weight fraction w_1 of the species by

$$n = \frac{w_1 \rho R}{k M_1} \quad 6.9$$

as a consequence of the definitions. Since all species are divided into the same number of segments N it follows that for the i^{th} species the number of monomer units per segment is given by

$$q_i = \frac{M_i}{mN} \quad 6.10$$

where m is the 'molecular weight' of a monomer unit. We can therefore write for the contribution to the static viscosity of the i^{th} species from equation 6.6

$$\eta_i = \frac{1}{36} \frac{a^2 x_0 M_i w_i \rho R}{k m^2}$$

The static viscosity of the polydisperse liquid is therefore given by

$$\eta = \sum_i \eta_i = \frac{a^2 x_0 \rho R}{36 k m^2} \sum_i w_i M_i = \frac{a^2 x_0 \rho R}{36 k m^2} \bar{M}_w \quad 6.11$$

where $\bar{M}_w = \sum_i w_i M_i$ and is the weight average molecular weight. From equation 6.3 we may write for the relaxation times of the i^{th} species using equation 6.10:

$$\tau_{pi} = \frac{a^2 x_o}{6\pi p^2 kT} \frac{M_i^2}{m^2} \quad 6.12$$

Equations 6.11 and 6.12 may be combined to obtain

$$\tau_{pi} = \frac{6\eta}{r^2 \rho RT} \frac{M_i^2}{\bar{M}_w} \frac{1}{p^2} \quad 6.13$$

It will be observed that equations 6.11 and 6.13 have been derived on the assumption that the quantity $a^2 x_o$ is independent of chain length. This will only be the case if the molecular weights of all the species in the polydisperse system are high enough for the defined Gaussian distribution to obtain. The high frequency modulus $G_{\infty i}$ of the i^{th} species is given by

$$G_{\infty i} = \rho RT \frac{w_i}{\bar{M}_i} \quad 6.14$$

which is obtained from equations 6.9 and 6.1. The overall complex shear modulus is therefore

$$\begin{aligned} G(j\omega) &= \sum_i \sum_p \frac{\rho RT w_i}{r^2 \rho RT \bar{M}_w p^2 + j\omega 6\eta M_i^2} \quad 6.15 \\ &= 6\eta \rho RT \sum_i \sum_p \frac{j\omega w_i M_i}{r^2 \rho RT \bar{M}_w p^2 + 6j\omega \eta M_i^2} \end{aligned}$$

from equations 6.13 and 2.12.

The treatment so far concerns a discrete molecular weight distribution. For a continuous distribution resulting from a condensation polymerisation process Bueche (1962) gives

$$W(M) = \frac{u}{M_n} e^{-u} \quad 6.16$$

$W(M)dM$ is the weight fraction of molecules with molecular weights between M and $M + dM$, and $\mu = M/\bar{M}_n$ where \bar{M}_n is the number average molecular weight. It follows from equation 6.16 that $\bar{M}_w = 2 \bar{M}_n$.

For the discrete system $\mu = M_1/\bar{M}_n$ and substituting this into equation 6.15 and putting $\bar{M}_w = 2 \bar{M}_n$ we obtain

$$G(j\omega) = \rho RT \sum_i \sum_p \frac{j\omega w_1 / \mu_1^2 \tau_1}{p^2 + j\omega \mu_1^2 \tau_1} \quad 6.17$$

where τ_1 is defined as
$$\tau_1 = \frac{3 \eta \bar{M}_n}{\pi^2 \rho RT} \quad 6.18$$

In the case of a continuous distribution the summation with respect to i in equation 6.17 becomes an integral; and using equation 6.16 we obtain

$$G(j\omega) = \frac{\rho RT}{\bar{M}_n} \sum_p \int_0^\infty \frac{j\omega \mu^2 \tau_1 e^{-\mu}}{p^2 + j\omega \mu^2 \tau_1} d\mu \quad 6.19$$

6.4 Comparison with experiment

In order to compare this theoretical result with the experimental measurements a knowledge of the molecular weights of the siloxanes is required. Barlow et al. (1964) have collected such information from the literature and this is presented in Table 6.1 in a kinematic viscosity/number average molecular weight form assuming the distribution defined above.

Table 6.1

Viscosity grade (cS)	\bar{M}_n	τ_1 (secs)
100	6.3×10^3	7.09×10^{-8}
350	1.58×10^4	6.25×10^{-7}
1000	2.1×10^4	2.36×10^{-6}
12500	4.0×10^4	5.43×10^{-5}
30000	5.0×10^4	1.80×10^{-4}
100000	6.8×10^4	8.00×10^{-4}

Figures 6.1 and 6.2 show the real and imaginary parts of the shear modulus plotted against frequency. Both these quantities are normalised in the manner indicated in the graph to effect comparison between the experimental results and the theory. The continuous line corresponding to the theoretical predictions was obtained from equation 6.19 by integrating and summing p up to a value of 175 (i.e. $N = 175$). Agreement between theory and experiment is good especially at the lower frequencies. Not only does the normalising process bring the experimental results of the different siloxanes on to the same smooth curve but this smooth curve also corresponds very well with that predicted by equation 6.19.

6.4.1 The plateau region

The divergence from theory of the experimental results at high frequencies appears more significant when the higher frequency normalised experimental results of Harrison (1964) (continuous lines)

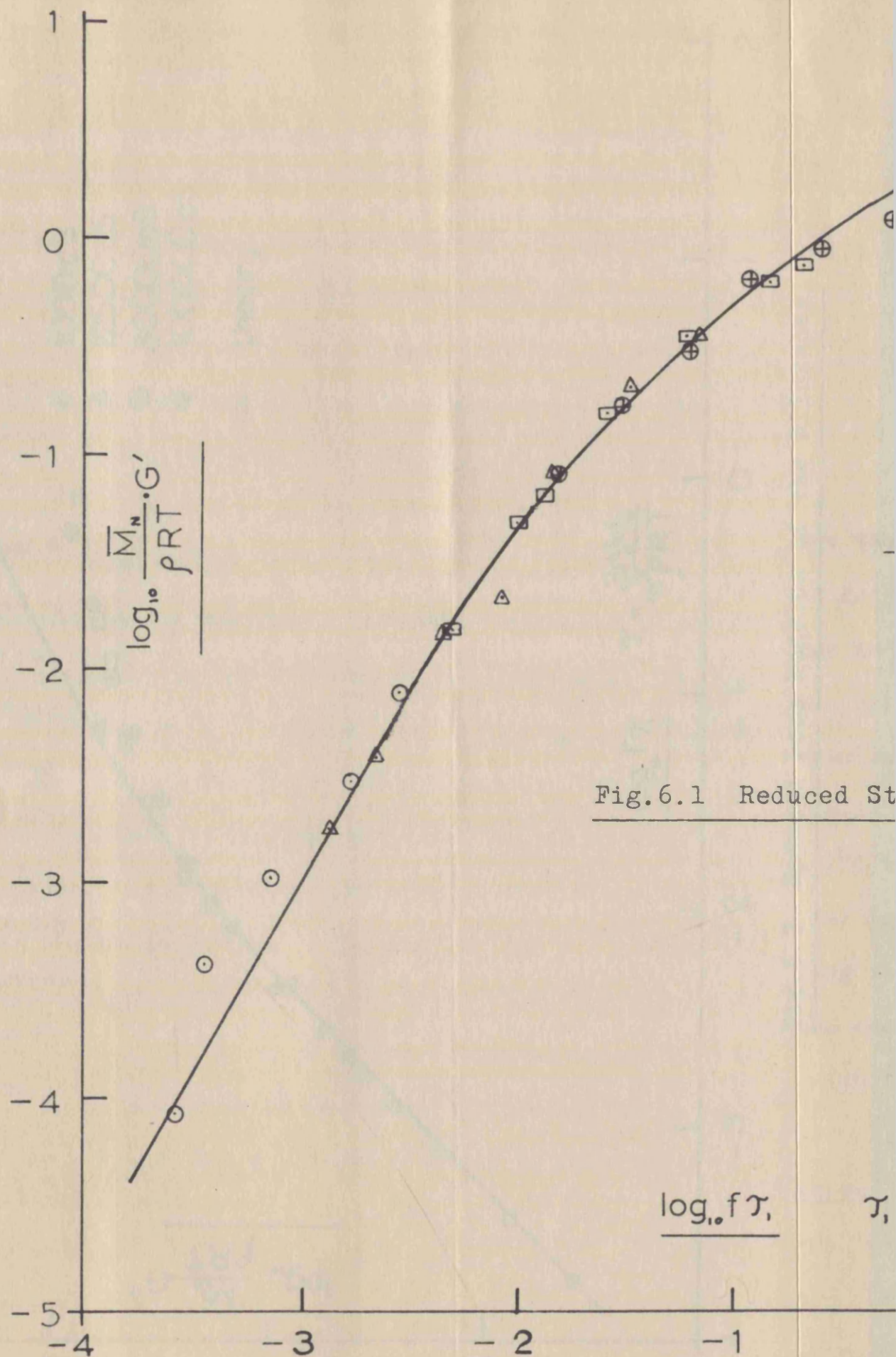


Fig.6.1 Reduced St

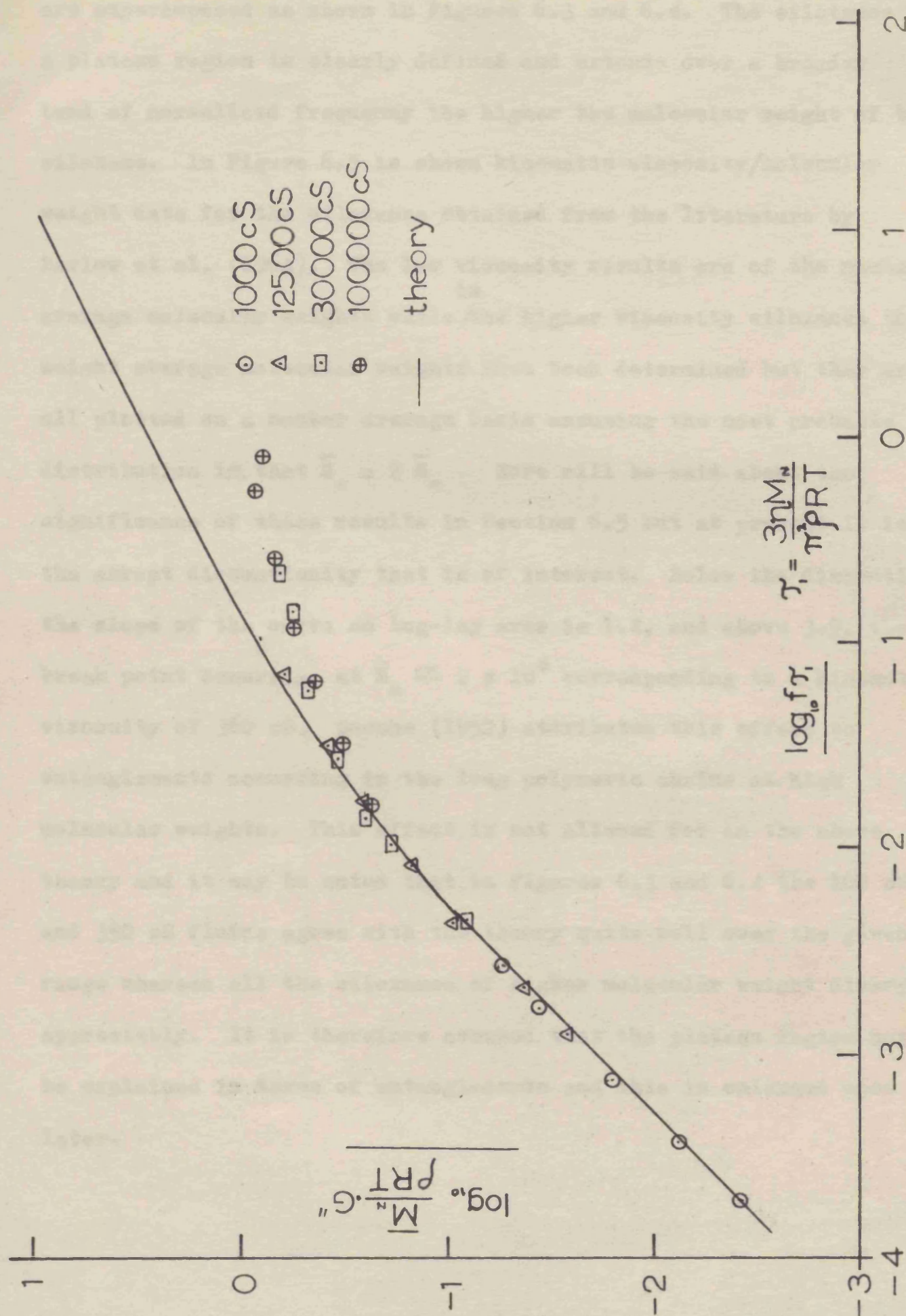
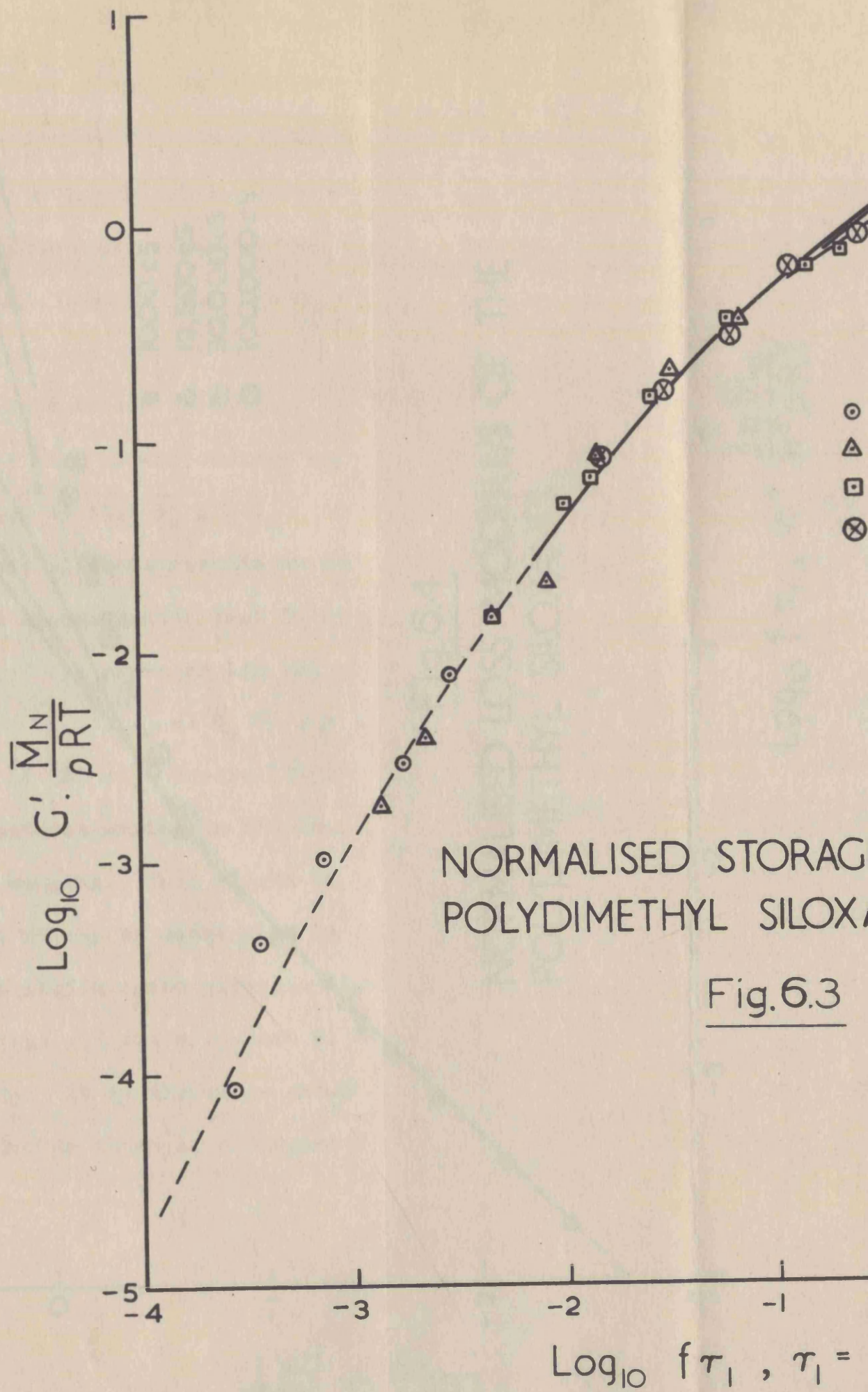


Fig. 6.2 Reduced Loss Modulus of the Siloxanes

are superimposed as shown in Figures 6.3 and 6.4. The existence of a plateau region is clearly defined and extends over a broader band of normalised frequency the higher the molecular weight of the siloxane. In Figure 6.5 is shown kinematic viscosity/molecular weight data for the siloxanes obtained from the literature by Barlow et al. (1964). The low viscosity results are of the number in average molecular weights while the higher viscosity siloxanes the weight average molecular weights have been determined but they are all plotted on a number average basis assuming the most probable distribution i.e. that $\bar{M}_w = 2 \bar{M}_n$. More will be said about the significance of these results in Section 6.5 but at present it is the abrupt discontinuity that is of interest. Below the discontinuity, the slope of the curve on log-log axes is 1.4, and above 3.9, the break point occurring at $\bar{M}_n \simeq 2 \times 10^4$ corresponding to a kinematic viscosity of 360 cS. Bueche (1952) attributes this effect to entanglements occurring in the long polymeric chains at high molecular weights. This effect is not allowed for in the above theory and it may be noted that in Figures 6.3 and 6.4 the 100 cS and 350 cS fluids agree with the theory quite well over the given range whereas all the siloxanes of higher molecular weight diverge appreciably. It is therefore assumed that the plateau region may be explained in terms of entanglements and this is enlarged upon later.



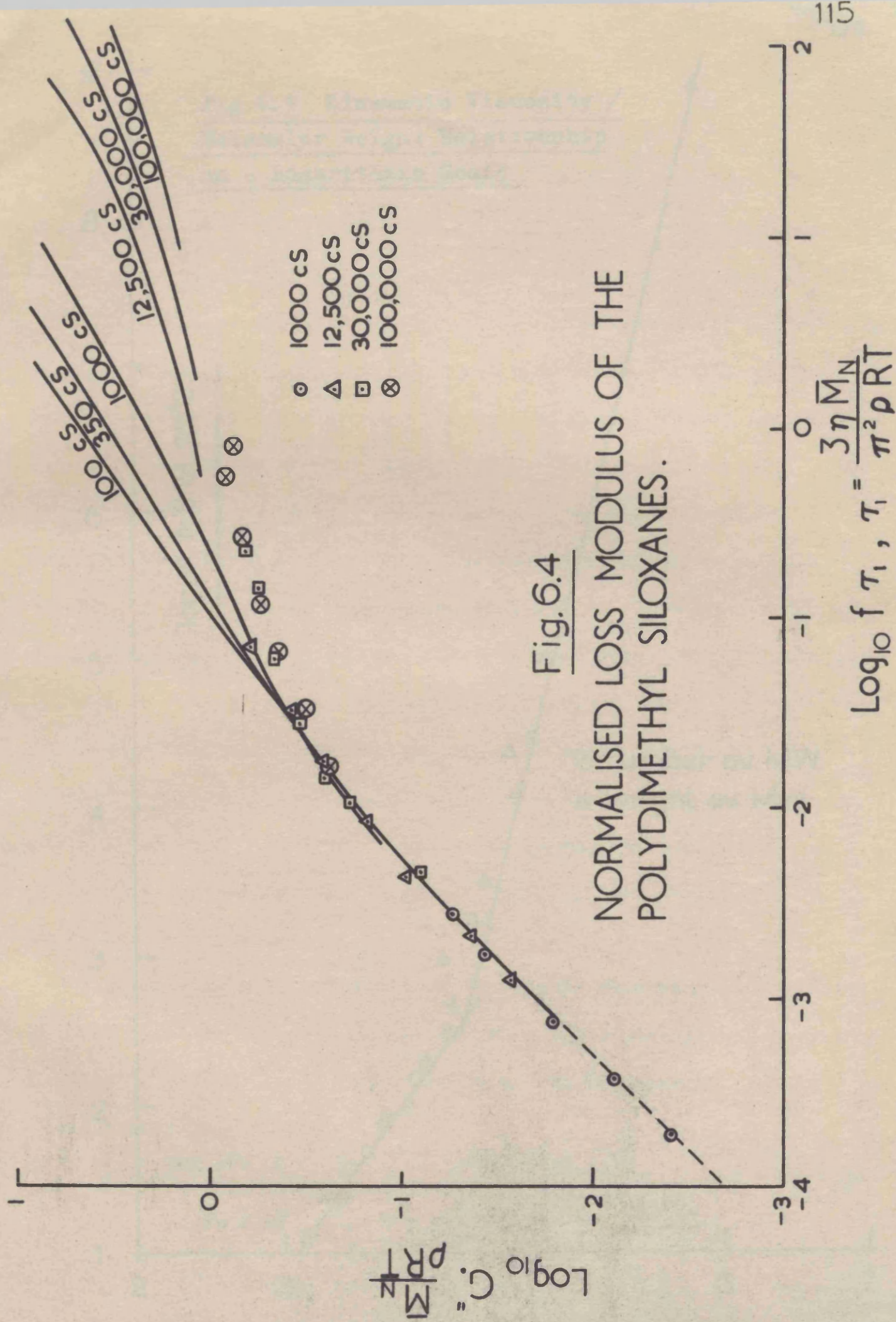
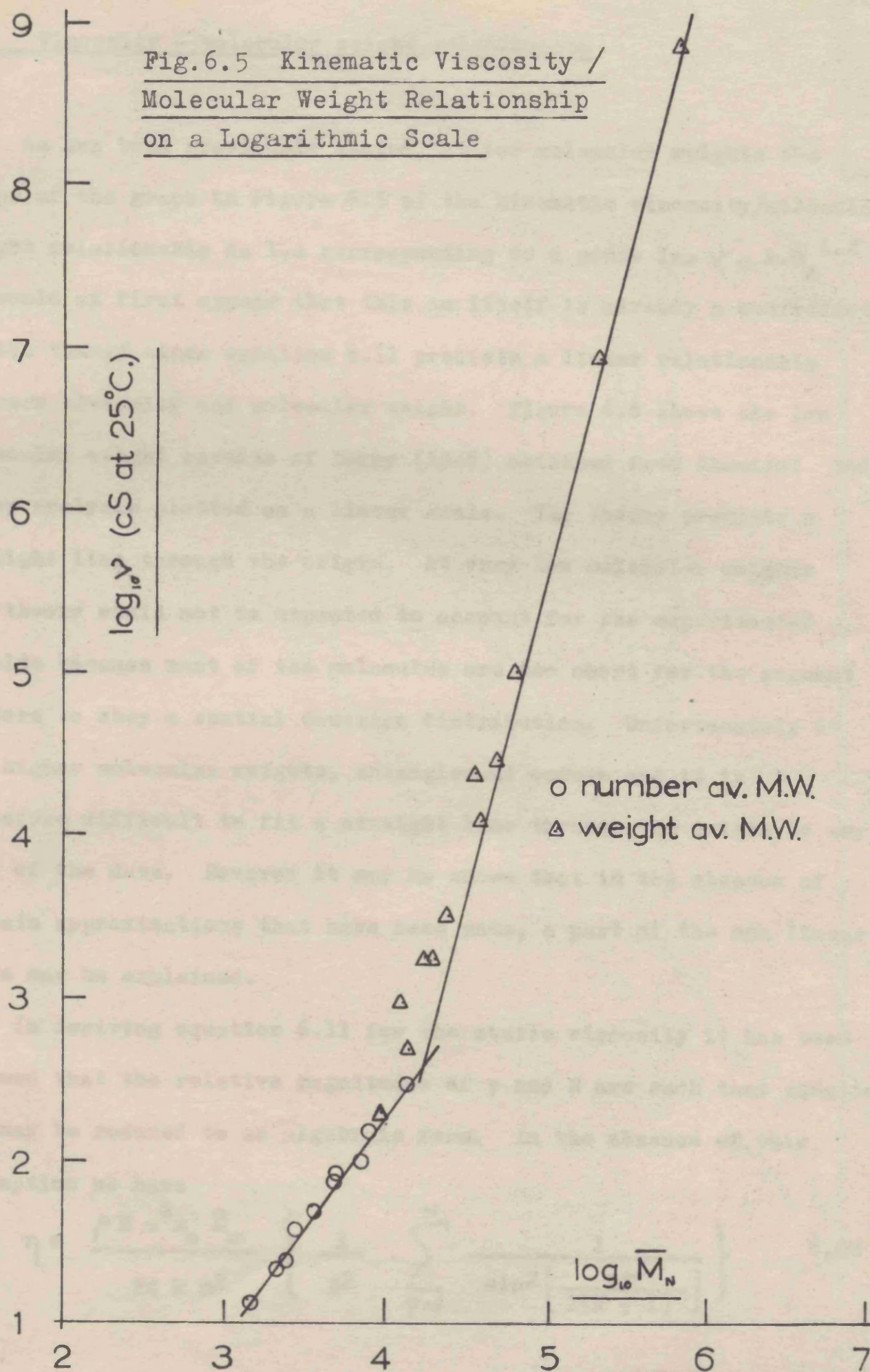


Fig.6.5 Kinematic Viscosity /
Molecular Weight Relationship
on a Logarithmic Scale

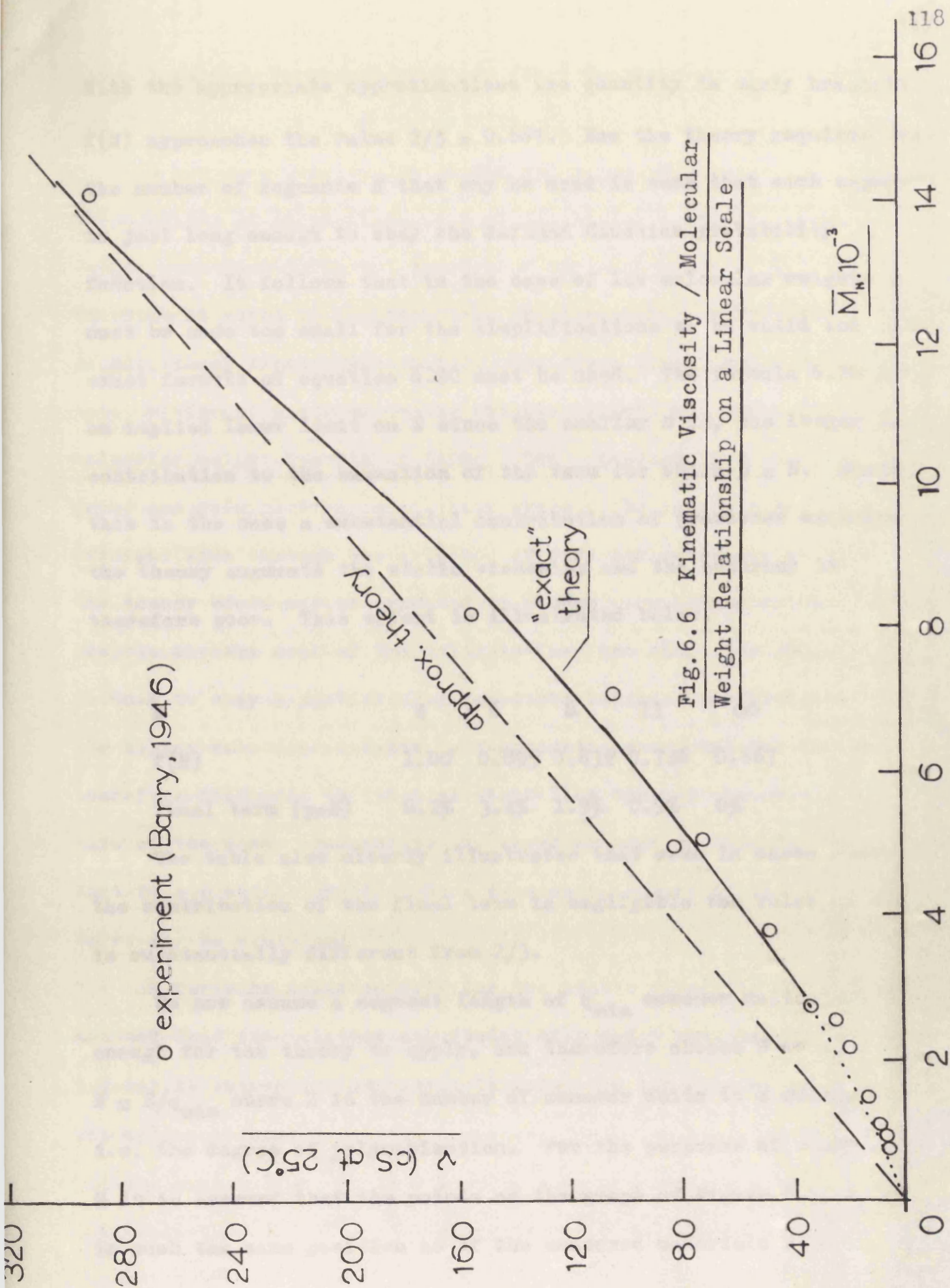


6.5 Viscosity - molecular weight relationship

As has been previously stated, at low molecular weights the slope of the graph in Figure 6.5 of the kinematic viscosity/molecular weight relationship is 1.4 corresponding to a power law $\nu = k \bar{M}_n^{1.4}$. It would at first appear that this in itself is already a contradiction of the theory since equation 6.11 predicts a linear relationship between viscosity and molecular weight. Figure 6.6 shows the low molecular weight results of Barry (1946) obtained from chemical end group analysis plotted on a linear scale. The theory predicts a straight line through the origin. At very low molecular weights the theory would not be expected to account for the experimental results because most of the molecules are too short for the segment vectors to obey a spatial Gaussian distribution. Unfortunately at the higher molecular weights, entanglement occurs and it is therefore difficult to fit a straight line through the origin to any part of the data. However it may be shown that in the absence of certain approximations that have been made, a part of the non linear curve may be explained.

In deriving equation 6.11 for the static viscosity it has been assumed that the relative magnitudes of p and N are such that equation 6.2 may be reduced to an algebraic form. In the absence of this assumption we have

$$\eta = \frac{\rho R a^2 x_0 \bar{M}_w}{24 k m^2} \left\{ \frac{1}{N^2} \cdot \sum_{p=1}^N \frac{1}{\sin^2 \left[\frac{p\pi}{2(N+1)} \right]} \right\} \quad 6.20$$



With the appropriate approximations the quantity in curly brackets $f(N)$ approaches the value $2/3 = 0.667$. Now the theory requires that the number of segments N that may be used is such that each segment is just long enough to obey the defined Gaussian probability function. It follows that in the case of low molecular weights N must be made too small for the simplifications to be valid and the exact formula of equation 6.20 must be used. The formula 6.20 imposes an implied lower limit on N since the smaller N is, the larger the contribution to the summation of the term for which $p = N$. Where this is the case a substantial contribution of processes excluded by the theory augments the static viscosity and the accuracy is therefore poor. This effect is illustrated below.

N	4	6	8	11	∞
$f(N)$	1.00	0.895	0.832	0.746	0.667
final term ($p=N$)	6.2%	3.4%	1.9%	0.9%	0%

The table also clearly illustrates that even in cases where the contribution of the final term is negligible the value of $f(N)$ is substantially different from $2/3$.

We now assume a segment length of q_{\min} monomer units just long enough for the theory to apply, and therefore choose N so that $N = Z/q_{\min}$ where Z is the number of monomer units in a molecule i.e. the degree of polymerisation. For the purposes of calculating Z it is assumed that the points on the graph of Figure 6.6 would be in much the same position as if the measured materials were

monodisperse. We then have $Z = \bar{M}_n/74$. We may rewrite equation 6.20 as

$$\begin{aligned} \frac{\eta}{\rho} &= \psi = k.f(N) \cdot \bar{M}_n \\ &= k.f(\bar{M}_n/74 q_{\min}) \cdot \bar{M}_n \end{aligned} \quad 6.21$$

By choosing an appropriate pair of values for k and q_{\min} (which gives rise to a different value of N for each value of \bar{M}_n) the continuous curve in Figure 6.6 is obtained which follows the experimental points quite well. The curve shown uses a value for q_{\min} of 12 and the value of k corresponds to a monomeric friction coefficient of $\tau_0 = 8.88 \times 10^{-9}$. The figure of 12 monomer units per segment agrees well with the figure of 10 obtained by Barlow et al. (1964) on the basis of the deviation from theory in high frequency viscoelastic measurements. The broken line in Figure 6.6 represents the results predicted by the approximate formula using 8.88×10^{-9} dynes/cm² for the monomeric friction coefficient; and by definition, the approximate and exact curves coalesce at higher molecular weights. It appears that siloxanes with kinematic viscosities above 350 cS may be predicted by means of the approximate formulae but Barlow et al. (1964) have also used the approximate formula to explain the behaviour of the 100 cS siloxane using a different value of monomeric friction coefficient.

There is no theoretical justification for this procedure since the chain length is adequately long for the premises of the theory to hold and consequently the monomeric friction coefficient remains at the same value. A corollary to this argument in connection with the behaviour of the 100 cS fluid is given in Section 6.7. The other

liquids investigated have molecular weights high enough for the approximation to be successfully used.

6.6 Modification of the theory for entanglements

6.6.1 The nature of entanglements

The sharp change in the kinematic viscosity/molecular weight curve of Figure 6.5 is attributed by Bueche (1952) to entanglements occurring in uncross-linked polymers. Although the exact nature of this molecular coupling is not fully understood, Mark and Tobolsky (1950, Chapter 10) suggest that even in uncross linked polymers transient networks may be formed by the adherence of individual molecules at widely separated points along the chain. These links break and reform at a rate dependent on the temperature and have the effect of substantially increasing the static viscosity. If M_e is the molecular weight between entanglements Ferry (1961, p.190) suggests that for molecular weights such that $M > 2 M_e$ there are on average two entanglement points per molecule and by analogy with the theory of cross linking in gels (Flory, 1953, Chapter 9) the network may be considered to extend throughout the system. Because the formation of these links is temporary and not permanent as in the case of cross linking the material does not possess a low frequency limiting rigidity i.e. the material is still fluid although with an increased viscosity which may be regarded as a consequence of the disentanglement process.

Figures 6.1 and 6.2 show that even in the case of entangled liquids (the 1000, 30000 and 100000 cS siloxanes) the theory successfully predicts the low frequency behaviour. The low frequency disturbance causes cooperative motion of portions of the chain on average much longer than the distance between entanglement points, and since this effect manifests itself in the static viscosity used in equation 6.18, the theory may possibly be expected to apply. Since the theory fits well for entangled liquids at low frequencies it follows that the Rouse model may be used at low frequencies subject to an enhanced monomeric friction coefficient, α , which allows for the increased friction due to entanglements.

6.6.2 Formulation

Ferry, Landel and Williams (1955) suggest that for a monodisperse polymer the relaxation times predicted by the theory should be divided into two blocks. The block of longer times corresponds to cooperative modes of motion involving chain lengths longer than the distance between entanglement points and is governed by the magnified monomeric friction coefficient α ($= Q \cdot \alpha_0$) where α_0 is the monomeric friction coefficient in the absence of entanglement and Q is a magnification factor. The block of shorter times involving chain lengths shorter than $2 M_e$ are determined by α_0 .

From the viscosity/molecular weight curve of Figure 6.5 it may be seen that for the siloxanes the critical molecular weight at which entanglements become important is $(M_n)_c = 1.6 \times 10^4$.

The nearest integer to $\bar{M}_n/(\bar{M}_n)_c$ represents the number average of entanglement points per molecule for a siloxane of number average molecular weight \bar{M}_n . The p_e^{th} mode, where p_e is the highest integer $> \bar{M}_n/(\bar{M}_n)_c$, represents the shortest relaxation time in the block of longer times to be affected by the presence of entanglements. Modes of motion corresponding to $p > p_e$ are unaffected by the entanglement points and are governed by the monomeric friction coefficient τ_0 .

We therefore have for equation 6.18

$$\tau_p = \frac{\tau_1}{p^2} = \frac{3\eta \bar{M}_n}{p^2 \pi^2 \rho RT} \quad \text{for } p \leq p_e$$

or

$$\tau_p = \frac{\tau_1}{p^2} = \frac{3\eta \bar{M}_n}{p^2 \pi^2 \rho RT} \cdot \frac{1}{Q} \quad \text{for } p > p_e \quad 6.22$$

The value of Q , the monomeric friction coefficient magnification factor, may be found from the graph of Figure 6.5. In accordance with the considerations of Section 6.5 it may be assumed that in the absence of entanglements the kinematic viscosity of the higher molecular weight siloxanes may be deduced by extrapolating from the discontinuity at unit slope on the log-log plot. This corresponds to a linear relation which is predicted by the theory (equation 6.11) at high molecular weights. For a given number average molecular weight, \bar{M}_n , a kinematic viscosity ν_x is obtained by means of this extrapolation which is lower than the experimental value ν . The value of the magnification factor Q is therefore given by $Q = \nu/\nu_x$ which may be used in the calculation of equation 6.22.

Harrison (1964) has calculated the results for the 100000 cS

siloxane for which: $\bar{M}_n = 6.8 \times 10^4$

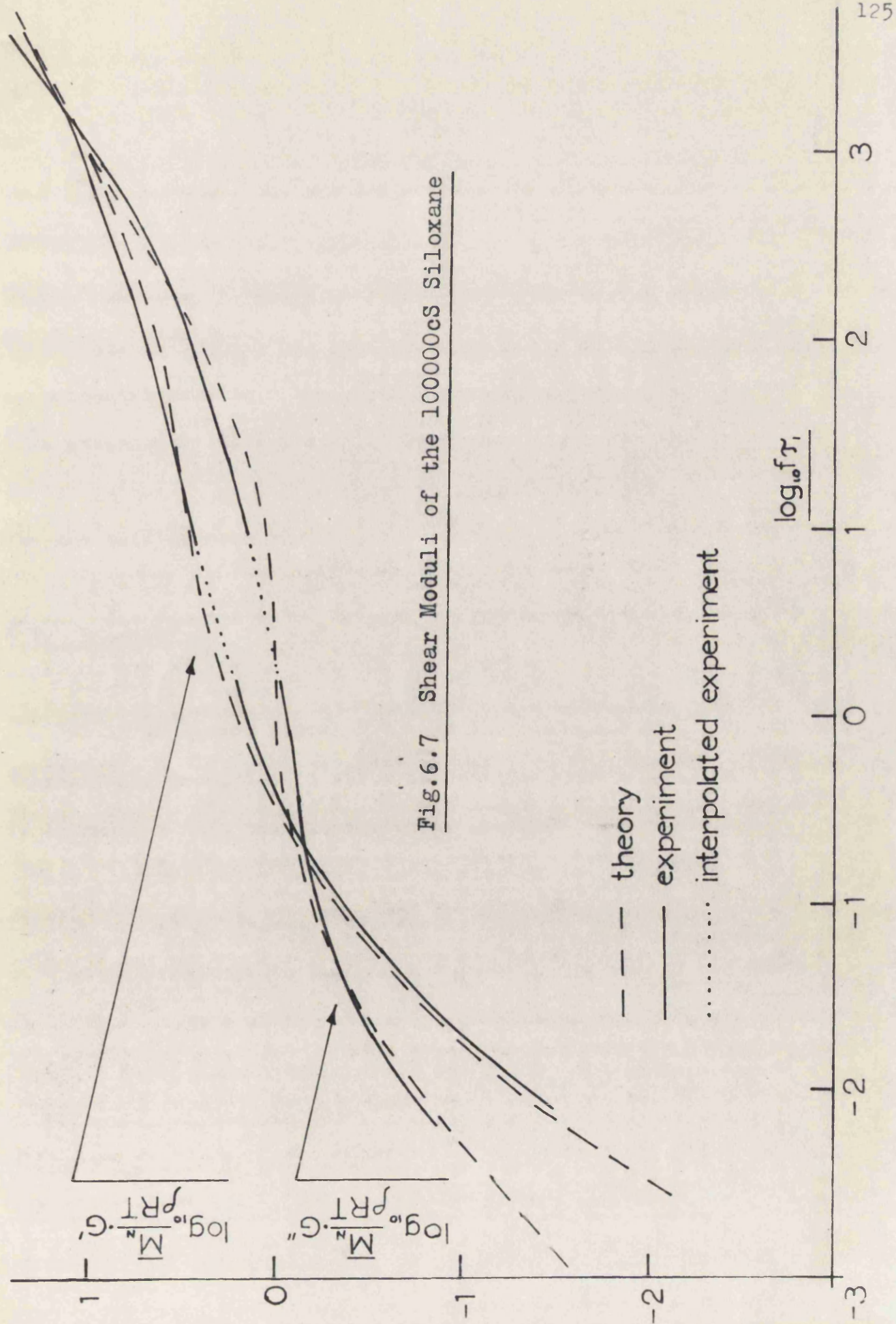
$$p_e = \frac{6.8 \times 10^4}{1.6 \times 10^4} \approx 4$$

$$Q = \nu/\nu_x = 66$$

A graph of the real and imaginary parts of the rigidity modulus versus frequency is shown in Figure 6.7. The broken line corresponding to the theory can be seen to agree quite well with the experimental results. The upper frequency experimental results have been obtained by Barlow et al. (1964) and the lower frequency results by the author. The dotted curve represents interpolation between the two sets of results.

6.7 Discussion

It is seen from Figure 6.7 that the plateau region is successfully predicted in spite of certain gross assumptions. It is improbable that the discontinuity assigned to the spectrum at $\tau_p = \tau_{pe}$ is realistic especially in view of the fact that the chain lengths are polydisperse. The theory implies the absence of any relaxation processes in the range $\tau_{pe} \rightarrow \tau_{pe+1}$, and in view of the statistical nature of the entanglement process this can only be regarded as an approximation. However the theoretical and experimental curves suggest that this approximation is valid. The calculation has not been performed on the siloxanes of lower molecular weight, since for a reasonable accuracy, the number of



relaxation mechanisms in the first block for which $p \leq p_0$ must contribute to the majority of the static viscosity. If this were not so, the value of the static viscosity in equations 6.22 would have to be reduced by an amount depending on the contribution from the second block of relaxation times. Since this quantity is unknown the calculation is necessarily limited to the higher molecular weight siloxanes.

For the unentangled liquids at low frequencies the experimental results are in good agreement with theory. Harrison (1964) has used plots similar to those in Figures 6.3 and 6.4 to extrapolate his high frequency results to low frequencies, on the basis that the curves for all the siloxanes appear to converge to a single curve. The results of these extrapolations are shown as continuous lines on the graphs in Figures 5.1, 5.2 and 5.3. It appears that the experimental results satisfactorily confirm the validity of this procedure. A difficulty however arises when considering the 100 cS fluid. From Figure 6.6 it can be seen that the chain length is too short for the approximations of the theory to be valid, but the experimental results nevertheless support the approximate theory (Figures 6.1 and 6.2). This may be explained by observing that the calculations of the relaxation times (equation 6.18) are all ultimately referred to the static viscosity. This in itself ensures the correct asymptotic behaviour at low frequencies though some deviation at higher frequencies might be expected. Barlow et al. (1964) have observed such a deviation though they attribute it to an appreciable contribution of processes excluded by the Rouse theory.

While this is inevitably true at even higher frequencies, the theory might agree over a more extended range with experiment if the numerical approximations of Section 6.2 were not used.

Further work is therefore required to resolve this difficulty. The foregoing discussion on the effect of certain approximations needs to be extended to embrace polydisperse systems; and a more systematic approach to the relative contributions of the various species within a polydisperse system at any given frequency is required to validate the simplifying assumptions made. Further low frequency measurements on low molecular weight fluids or higher frequency measurements on higher molecular weight fluids would also assist in this respect. Unfortunately it is not possible to obtain an approach to a monodisperse polydimethyl siloxane and consequently other polymers might be more suitable for this purpose e.g. polystyrene in solution.

CHAPTER 7

A THEORY OF STEADY SHEAR FLOW FOR VISCOELASTIC LIQUIDS

7.1 Introduction

The similarity between the apparent static viscosity/shear rate and dynamic viscosity/angular frequency relationships in many materials has led several authors (e.g. Philipoff, 1954) to suppose that a correlation necessarily exists between the two. At the heart of the problem is the determination of a sufficiently accurate equation of state and then to apply this to the coordinate system (the laboratory frame) pertinent to the experimental effect being examined. Oldroyd (1950) has suggested a procedure for formulating general equations of state on the basis that they must have the appropriate invariance properties under a transformation and that they fit the results of limited experiments already performed. It is shown that unfortunately when transformed to the laboratory frame an infinite number of such equations exist and the appropriate one may only be deduced as more experimental evidence becomes available.

Also this author (Oldroyd, 1958) has concentrated attention on the simplest possible equations of state which predict non-Newtonian steady shear behaviour and the Weissenberg (1947) climbing effect. While this approach is interesting from a theoretical point

of view it is doubtful whether a real fluid can be characterised by the three parameters of the Oldroyd model. These are a static

viscosity, a retardation and a relaxation time. More recently Oldroyd (1961) has developed a more general equation of state involving eight parameters and has investigated the properties of fluids in three special cases when five of the parameters may be eliminated. Dyson (1965) however has shown that on the basis of available experimental evidence five of Oldroyd's parameters may be eliminated but they do not correspond to any one of the special cases.

Roscoe (1964) uses a generalised form of Oldroyd's constitutive equation having n retardation and n relaxation times together with two additional parameters. A simple consequence of these derivations is that the functions $\eta_s(\alpha K)$ and $\eta_d(\omega)$ are equivalent where η_s is the steady shearing viscosity at shear rate K and η_d is the dynamic viscosity at angular frequency ω . α is a constant for a given material and shows that the apparent viscosities in the two experiments are equivalent if ω is assumed equivalent to α times the shear rate. Also a formal equivalence is established between the dynamic modulus and the normal stresses in steady shear which give rise to the Weissenberg effect. Onogi, Hamana and Hirai (1958) obtain good agreement with this result for concentrated solutions of polyvinyl alcohol with $\alpha \approx 1$ while for mineral oils Dyson finds $\alpha \approx 10^3$ at atmospheric pressure.

Other theories in this connection are those of de Witt (1955) who uses a two parameter constitutive equation, and Pao (1957) whose formulation allows of a discrete spectrum of relaxation times. The

latter theory however does not predict the appearance of normal stresses in steady shear. Boyd (1958) has investigated the shear rate dependence and dynamic properties of polymer melts and compared them with the Pao theory. Although the agreement is claimed to be good the method of creep recovery which is used to determine the relaxation spectrum is very inaccurate for the purpose (see Section 2.4) and consequently the results cannot be regarded as conclusive especially as no normal stress measurements were made. The correlation between ω and αK was first observed by Padden and de Witt (1954) for a solution of polyisobutylene in the case of η_s and η_d and the equivalence between the normal stress differences and the dynamic modulus for $\omega = \alpha K$ was shown by Markovitz and Williamson (1957).

7.2 Equations of state and coordinate systems

Ideally an equation of state or constitutive equation is one which, in the present context, describes the relationship between stress and deformation in a way which is independent of any particular coordinate system. The equation is thus uniquely relevant to the material it describes and its form does not depend on the vagaries of the laboratory or material frames of reference. There are three methods by which this may be achieved.

1) Oldroyd (1958) and Roscoe (1964) favour the method in which the equation is formulated in a Cartesian system fixed in space. Although this method allows easier interpretation of the equation in

the laboratory frame, the time derivatives of the various tensor quantities are rather complicated. In fact the so-called material derivative is used which may be interpreted as that tensor whose components referred to a Cartesian frame rotating with the particles of the liquid are equal to the partial derivatives of the corresponding components of the underived tensor. This may be regarded as the Eulerian approach.

2) De Witt (1955) and Pao (1957) use the Lagrangian method in which the equation of state is related to a coordinate system which rotates and connects with the particles of the fluid. The time derivative in this case is a simple total differential. Since the equation of state given in equation 2.22 does not imply any rotation or convection a Lagrangian approach is used in the following theory.

3) Lodge (1964) in his more restricted work on uniform strain rates uses an embedded vector method which in concept is similar to (2). The more general tensor treatment however is required for the investigation of non-uniform strain rates and inhomogeneous flow.

7.3 Theory

We first define a laboratory coordinate system for simple shear flow which has become standard in the literature as shown in Figure 7.1.

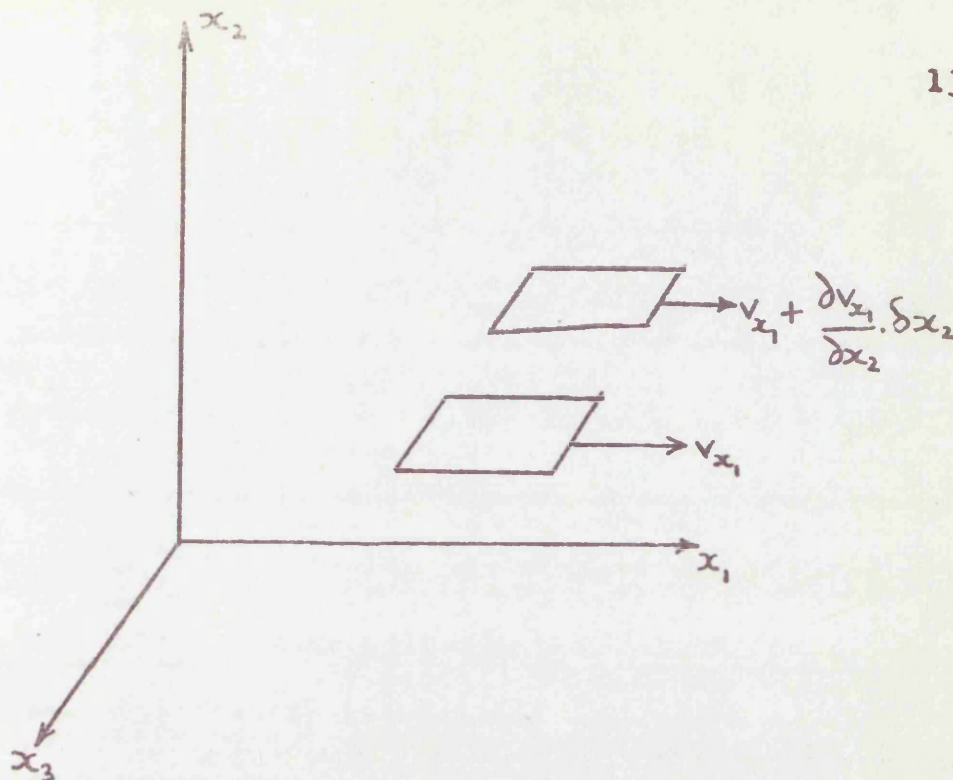


Figure 7.1

The 1 direction corresponds with the direction of flow and the 2 direction is the direction of the shear planes which are at right angles to the 1 direction. The 3 direction is at right angles to the 2 and 1 directions so as to form a right handed Cartesian frame. The vorticity of the shear field may be expressed as

$$\omega = \frac{1}{2} \left(\frac{\partial v_{x1}}{\partial x_2} - \frac{\partial v_{x2}}{\partial x_1} \right) = \frac{1}{2} \frac{\partial v_{x1}}{\partial x_2} \quad 7.1$$

where v is a velocity and the suffix indicates the direction and where evidently for simple shear flow

$$\frac{\partial v_{x2}}{\partial x_1} = 0.$$

Also we have that

$$\frac{\partial v_{x1}}{\partial x_2} = \frac{d}{dt} \left(\frac{\partial u_{x1}}{\partial x_2} \right) = \frac{\partial e_{x1}}{\partial t} = K$$

where u_{x1} is the displacement in the x_1 direction, e_{x1} the corresponding

strain and K is the shear rate. It can therefore be seen that

$$\omega = \frac{1}{2} K \quad 7.3$$

or that the vorticity which is in a clockwise direction in Figure 7.1 is equal to half the shear rate.

Any particle in the shear flow rotates with angular velocity as it convects in the x_1 direction and it is now assumed that the constitutive equation 2.22 holds in the Y coordinate system which rotates with clockwise angular velocity ω in the X frame. It is further assumed that the flow is homogeneous and there is therefore no need to make allowance for the particle convection. The coordinates in the two frames are related by the equations

$$\begin{aligned} x_1 &= y_1 \cos \phi + y_2 \sin \phi \\ x_2 &= -y_1 \sin \phi + y_2 \cos \phi \\ x_3 &= y_3 \end{aligned} \quad 7.4$$

where ϕ is the instantaneous angle between the two frames. We now consider a symmetric 2nd order tensor which will later be related to the stress and strain tensors. A second order tensor in the X frame has components which may be referred to the Y frame as follows.

$$Y_{ab} = X_{ij} \frac{\partial x_i}{\partial y_a} \cdot \frac{\partial x_j}{\partial y_b} \quad 7.5$$

by the usual transformation formula for a 2nd order tensor. It follows from equations 7.5 and 7.4 that the various components are related by

$$\begin{aligned} Y_{11} &= X_{11} \cos^2 \phi - X_{12} \sin 2\phi + X_{22} \sin^2 \phi \\ Y_{21} &= Y_{12} = \frac{1}{2} (X_{11} - X_{22}) \sin 2\phi + X_{12} \cos 2\phi \end{aligned}$$

$$Y_{22} = X_{11} \sin^2 \phi + X_{12} \sin 2\phi + X_{22} \cos^2 \phi$$

$$Y_{31} = Y_{13} = X_{13} \cos \phi - X_{23} \sin \phi$$

$$Y_{32} = Y_{23} = X_{13} \sin \phi + X_{23} \cos \phi$$

$$Y_{33} = X_{33}$$

7.6

For the use of the constitutive equation the deviatoric components of the tensor in the rotating Y frame must be used. For a deviatoric

$$\text{component: } Y'_{ij} = Y_{ij} - \frac{1}{3} \delta_{ij} Y_{kk} \quad 7.7$$

where the prime denotes a deviatoric component and δ_{ij} is the Kronecher delta. Thus only the principal diagonal elements of the deviatoric tensor are different from the corresponding elements of the original tensor. They are

$$Y'_{11} = \frac{2}{3} Y_{11} - \frac{1}{3} (Y_{22} + Y_{33})$$

$$= \frac{2}{3} X_{11} - \frac{1}{3} (X_{22} + X_{33}) - X_{11} \sin^2 \phi - X_{12} \sin 2\phi + X_{22} \sin^2 \phi$$

$$Y'_{22} = \frac{2}{3} Y_{22} - \frac{1}{3} (Y_{11} + Y_{33})$$

$$= \frac{2}{3} X_{22} - \frac{1}{3} (X_{11} + X_{33}) + X_{11} \sin^2 \phi + X_{12} \sin 2\phi - X_{22} \sin^2 \phi$$

$$Y'_{33} = \frac{2}{3} Y_{33} - \frac{1}{3} (Y_{11} + Y_{22}) = \frac{2}{3} X_{33} - \frac{1}{3} (X_{11} + X_{22}) \quad 7.8$$

We may now rewrite the equation of state for convenience

$$\sigma'_{ab}{}^Y = \sum_n \int_{-\infty}^t k_r \exp(-s_r[t-\tau]) \frac{d\sigma'_{ab}{}^Y}{d\tau} d\tau \quad 7.9$$

The superscript Y is included to emphasise the fact that the equation holds in the rotating Y frame only.

7.3.1 The strain tensor components

We first evaluate the total derivatives of the strain components as required by equation 7.9. By the chain rule of differentiation

$$\frac{de^Y}{d\tau} = \frac{\partial e^Y}{\partial \tau} + \frac{\partial e^Y}{\partial \phi} \frac{d\phi}{d\tau}$$

which has the physical significance that the total rate of change of strain in the Y frame is made up of the deformation in the Y frame alone and also that due to the rotation of the Y frame in the X frame.

Since the vorticity ω is constant in time and throughout the fluid

$$\phi = \omega\tau \quad \text{and so} \quad \frac{de^Y}{d\tau} = \frac{\partial e^Y}{\partial \tau} + \omega \frac{\partial e^Y}{\partial \phi} \quad 7.10$$

Before performing the differentiations it is first noted that certain simplifications can be made to the X frame strain tensor. For

rectilinear homogeneous flow the only non-zero strain components are

e_{11}^X , e_{12}^X and e_{22}^X . i.e. the strain tensor is of the form

$$\begin{pmatrix} e_{11}^X & e_{12}^X & 0 \\ e_{12}^X & e_{22}^X & 0 \\ 0 & 0 & 0 \end{pmatrix}$$

In many experiments the apparatus walls constrain the fluid so that $e_{11} = 0$. i.e. the shearing surfaces are maintained at a constant distance apart. It is also assumed that $e_{22} = 0$ or that the fluid is prevented from elongating in the direction of flow. This will certainly be the case in the concentric cylinder type of apparatus but not necessarily in the cone and plate. The only non-zero partial derivative of the X frame strain tensor is therefore $\frac{\partial e_{12}^X}{\partial \tau} = K$

The total derivatives of the strain tensor in the Y frame are given by equation 7.10 and by using equations 7.6 and 7.8 we obtain subject to the above restrictions

$$\begin{aligned}
 \frac{de'_{11}}{d\tau} &= -K \sin 2\omega\tau - 2\omega e_{12}^x \cos 2\omega\tau \\
 \frac{de'_{21}}{d\tau} &= \frac{de'_{12}}{d\tau} = K \cos 2\omega\tau - 2\omega e_{12}^x \sin 2\omega\tau \\
 \frac{de'_{22}}{d\tau} &= K \sin 2\omega\tau + 2\omega e_{12}^x \cos 2\omega\tau \\
 \frac{de'_{33}}{d\tau} &= \frac{de'_{13}}{d\tau} = \frac{de'_{31}}{d\tau} = \frac{de'_{32}}{d\tau} = \frac{de'_{23}}{d\tau} = 0
 \end{aligned} \tag{7.11}$$

7.3.2 The stress tensor components

For the simple shear flow described the stress tensor in the X frame is of the form

$$\begin{pmatrix} \sigma_{11} & \sigma_{12} & 0 \\ \sigma_{12} & \sigma_{22} & 0 \\ 0 & 0 & \sigma_{33} \end{pmatrix}$$

The deviatoric components in the Y frame using equations 7.6 and 7.8 and simplifying algebraically are

$$\begin{aligned}
 \sigma'_{11} &= \frac{1}{6}(\sigma_{11}^x + \sigma_{22}^x - 2\sigma_{33}^x) + \frac{1}{2}(\sigma_{11}^x - \sigma_{22}^x) \cos 2\omega\tau - \sigma_{12}^x \sin 2\omega\tau \\
 \sigma'_{21} &= \sigma'_{12} = \frac{1}{2}(\sigma_{11}^x - \sigma_{22}^x) \sin 2\omega\tau + \sigma_{12}^x \cos 2\omega\tau \\
 \sigma'_{22} &= \frac{1}{6}(\sigma_{11}^x + \sigma_{22}^x - 2\sigma_{33}^x) - \frac{1}{2}(\sigma_{11}^x - \sigma_{22}^x) \cos 2\omega\tau + \sigma_{12}^x \sin 2\omega\tau \\
 \sigma'_{33} &= \frac{1}{3}(2\sigma_{33}^x - \sigma_{11}^x - \sigma_{22}^x)
 \end{aligned} \tag{7.12}$$

7.3.3 Substitution into the constitutive equation

As an example the first set of equations 7.11 and 7.12 are used for substitution into the constitutive equation. The other equations all give consistent results but they are all contained in each of the first three equations. Substituting therefore into equation 7.9 gives

$$\frac{1}{6}(\sigma_{11} + \sigma_{22} - 2\sigma_{33}) + \frac{1}{2}(\sigma_{11} - \sigma_{22})\cos 2\omega t - \sigma_{12}\sin 2\omega t =$$

$$\sum_n \int_{-\infty}^t k_r \exp(-s_r[t-\tau]) \{-K\sin 2\omega\tau - 2\omega e_{12}\cos 2\omega\tau\} d\tau \quad 7.13$$

The superscripts have now been dropped since all the tensor components now refer to the laboratory X frame only. Performing the integration on the right hand side and omitting the terms containing an exponential decay we obtain for the steady state:

$$\begin{aligned} & \frac{1}{6}(\sigma_{11} + \sigma_{22} - 2\sigma_{33}) + \frac{1}{2}(\sigma_{11} - \sigma_{22})\cos 2\omega t - \sigma_{12}\sin 2\omega t \\ &= \sum_n k_r \left\{ -K \cdot \frac{s_r \sin 2\omega t - 2\omega \cos 2\omega t}{s_r^2 + (2\omega)^2} - 2\omega e_{12} \frac{s_r \cos 2\omega t - 2\omega \sin 2\omega t}{s_r^2 + (2\omega)^2} \right\} \end{aligned} \quad 7.14$$

Equating coefficients of unity, $\cos 2\omega t$ and $\sin 2\omega t$ we obtain respectively

$$\sigma_{11} + \sigma_{22} - 2\sigma_{33} = 0$$

$$\frac{1}{2}(\sigma_{11} - \sigma_{22}) = \sum_n k_r \frac{2K\omega}{s_r^2 + (2\omega)^2} - e_{12} \sum_n \frac{k_r 2\omega s_r}{s_r^2 + (2\omega)^2}$$

$$\sigma_{12} = \sum_n \frac{k_r K s_r}{s_r^2 + (2\omega)^2} + e_{12} \sum_n \frac{k_r (2\omega)^2}{s_r^2 + (2\omega)^2} \quad 7.15$$

Remembering that $\omega = \frac{1}{2} K$ it can be seen that the summations on the

right hand sides of equations 7.15 are none other than the moduli G' and G'' defined in equations 2.13 with K the shear rate as the argument of the functions instead of ω the angular frequency. We may thus rewrite equations 7.15 as

$$\begin{aligned}\sigma_{11} - \sigma_{22} - 2\sigma_{33} &= 0 \\ \frac{1}{2}(\sigma_{11} - \sigma_{22}) &= G'(K) - e_{12}G''(K) \\ \sigma_{12} &= G''(K) + e_{12}G'(K)\end{aligned}$$

The last of equations 7.16 may be rewritten in terms of viscosity as

$$\eta_s(K) = \frac{\sigma_{12}}{K} = \eta_d(K) + e_{12}G'(K)/K \quad 7.17$$

where η_s and η_d are the steady flow and dynamic viscosities respectively.

7.4 Discussion of the theory

In equations 7.16, e_{12} represents the elastic shear strain in the viscoelastic fluid when being sheared at rate K . Unfortunately the measurement of shear recovery is difficult and has not been extensively undertaken so that the theory in its existing state cannot be thoroughly checked. However it may be interpreted that the kinematic indeterminacy of the elastic strain is a consequence of the equation of state used, and that this equation is too general to completely determine the behaviour of a viscoelastic fluid in steady shear flow. The theory does nevertheless show that subject to the restrictions on the stress and strain tensors, a material exhibiting dynamic moduli G' and G'' in oscillatory testing shows properties indicated in equations 7.16 in steady shear flow.

Pao (1957) has used a more restricted form for the stress tensor than has been used here with the result that the normal stress difference $\sigma_{11} - \sigma_{22}$ turns out to be zero. It is interesting to note that if $\sigma_{11} - \sigma_{22} = 0$ (which is not the case in the majority of polymer solutions, for instance) then e_{12} may be eliminated to give

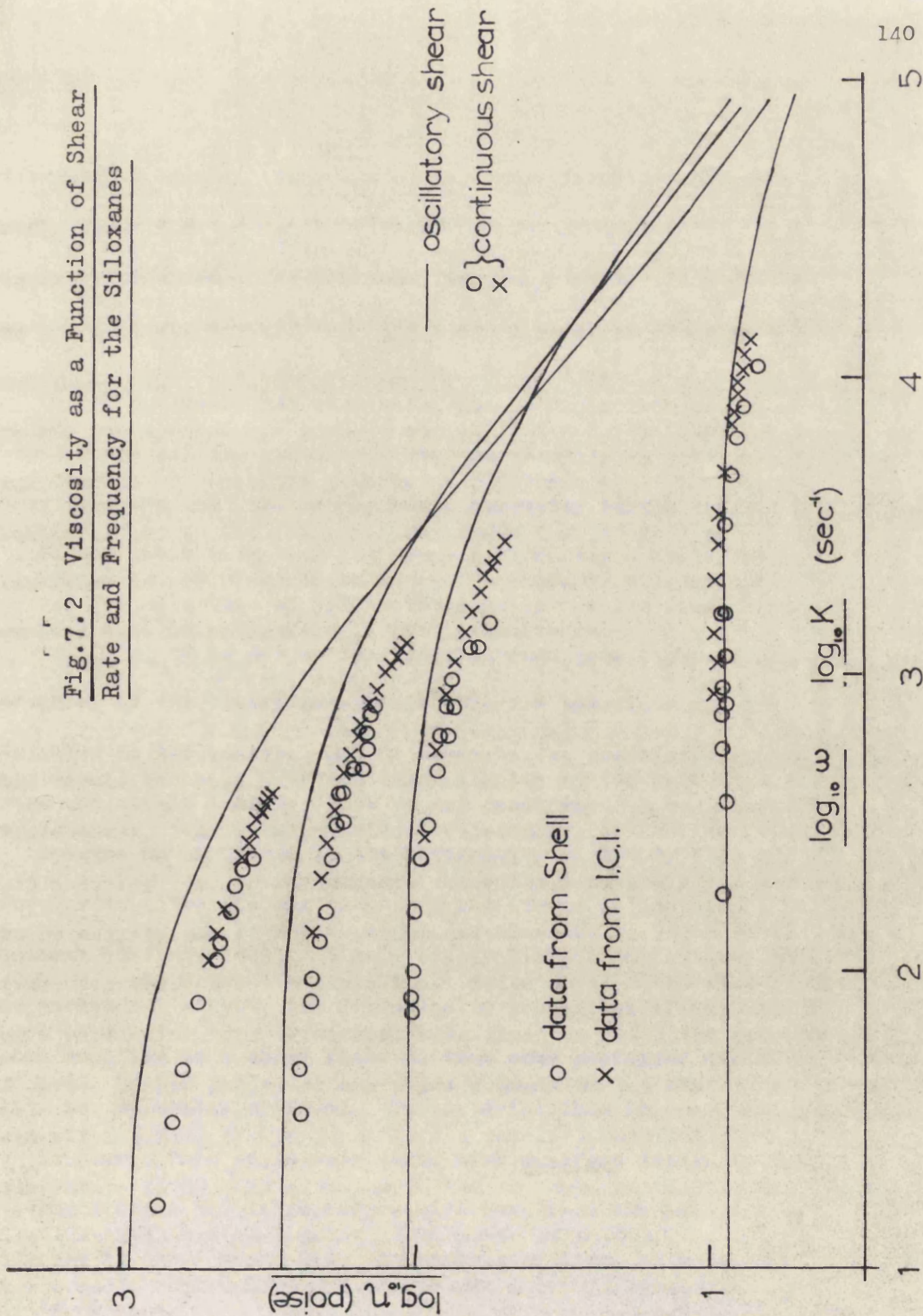
$$\sigma_{12} = G''(K) + \frac{G'^2(K)}{G''(K)} \quad \text{which is Pao's result.}$$

One of the important conclusions to be drawn from equation 7.17 is that since all the quantities must necessarily be positive, the theory predicts that the steady state viscosity begins to fall off at a higher shear rate than the dynamic viscosity. While this is observed for solutions of polyisobutylene in decalin (Padden and de Witt, 1954) it is not so for the silicones (see Figure 7.2). Inadequacy of the theory to explain observed behaviour may be attributed to two causes. One of these is the restrictions on the stress and strain tensors; this is not considered to be important

because no anomalies in the homogeneity of steady flow in viscoelastic materials has been reported except in incipient fracture phenomena (Hutton, 1963). A more likely limitation is that, due to some structural effect, the viscoelastic properties of the material become modified in a shear field so that some preferred direction exists for molecular movement. The material thus becomes anisotropic

in flow. This anisotropy would also manifest itself in the rotating Y frame and is therefore different from the anisotropy occurring in the X frame with the restricted class of materials considered here.

Fig.7.2 Viscosity as a Function of Shear Rate and Frequency for the Siloxanes



7.5 An extension of the theory

The data normally available for viscoelastic materials in steady shear flow is confined to the shear stress and the normal stress differences as functions of the shear rate. In addition the shear moduli G' and G'' as functions of angular frequency are available. With this information equations 7.16 can only be checked for consistency in the absence of any further information regarding the recoverable elastic shear strain e_{12} . The viscoelastic liquid so far described may however be endowed with further properties in order to obtain another relation involving e_{12} . An equation that often appears in the literature is

$$\frac{\sigma_{11} - \sigma_{22}}{2 \sigma_{12}} = e_{12} \quad 7.18$$

This result has been obtained theoretically by two authors (Weissenberg, 1947., Lodge 1964). Weissenberg derived equation 7.18 assuming that in any state of flow for a viscoelastic liquid the principal axes of shear stress and elastically recoverable shear strain are coincident in direction. Lodge obtains the same result for a particular type of viscoelastic fluid in which the component of normal stress acting on any plane depends on the history of separation ratios of the plane from a parallel material plane. Weissenberg (1949) has also shown that the same result applies if planes exhibit the same normal components of stress if they have undergone the same normal displacements per unit area from their

neighbouring parallel planes. It would appear that this may be regarded as a special case of Lodge's assumption. It is also stated by Roscoe (1964) that equation 7.18 applies to any material exhibiting fading memory at low rates of shear.

Since these assumptions do not in any way contradict the equation of state used here, the theory may be extended by incorporating equation 7.18 in equations 7.16. We then obtain

$$\frac{G' - \sigma_{12} G''}{G'' + \sigma_{12} G'} = \sigma_{12}$$

which gives
$$\sigma_{12} = \frac{-G'' + \sqrt{G'^2 + G''^2}}{G'} \quad 7.19$$

Substitution of equation 7.19 into the last of equations 7.16 gives the interesting relation

$$\sigma_{12} = \sqrt{G'^2 + G''^2} \quad 7.20$$

Instead of moduli G' and G'' the real and imaginary viscosities η' and η'' may be used in which case equation 7.20 becomes

$$\eta_s = \frac{\sigma_{12}}{K} = \sqrt{\eta'^2 + \eta''^2} \quad 7.21$$

or the steady shear viscosity is the modulus of the complex dynamic viscosity. Such a relationship was postulated empirically by Cox and Merz (1958) and shows good agreement with their experimental results on molten polyethylene and polystyrene (1959).

Equation 7.19 may also be used to find an expression for the normal stresses. Substituting this equation into the second of equations 7.16 gives

$$\frac{1}{2}(\sigma_{11} - \sigma_{22}) = G' + \frac{G''^2}{G'} \left\{ 1 - \sqrt{1 + \left(\frac{G'}{G''}\right)^2} \right\} \quad 7.22$$

At low rates of shear or frequency where $G' \ll G''$, the square root may be expanded to give the limiting result $\sigma_{11} - \sigma_{22} \rightarrow G'$ which agrees with a result given by Coleman and Markovitz (1964).

7.6 Comparison with experiment

Although much information has been published on the dynamic and steady flow properties of a wide variety of materials, very few papers deal with steady flow and dynamic measurements on the same material. For the purposes of checking the theory, shear and normal stresses as a function of shear rate are required as well as the real and imaginary parts of the dynamic shear modulus as a function of frequency. A further check of the theory would be available if the recoverable shear strain as a function of shear rate were also known. The most complete set of data for these purposes known to the author are those of den Otter (1965) who has measured the properties of two concentrations (1.03% and 2%) of high molecular weight polyisobutylene in a low molecular weight solvent of the same material.

Both dynamic and steady shear experiments were performed on a cone and plate instrument. The experimental results for the dynamic shear moduli are shown in Figure 7.3. Figures 7.4 and 7.5 show the shear and normal stresses as a function of shear rate for the two solutions compared with the predictions based on equations 7.20 and

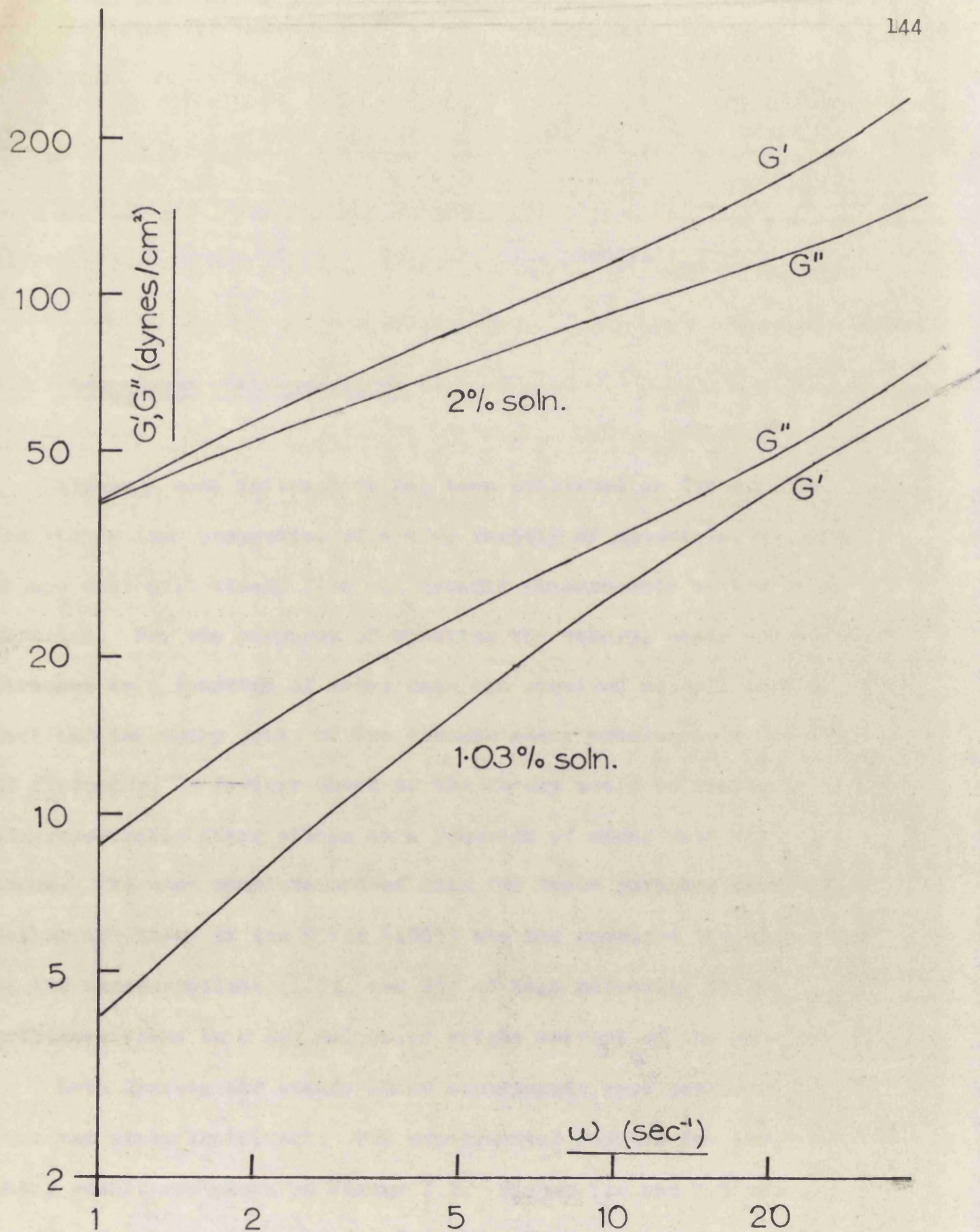


Fig.7.3 Dynamic Shear Moduli of Polyisobutylene
Solutions

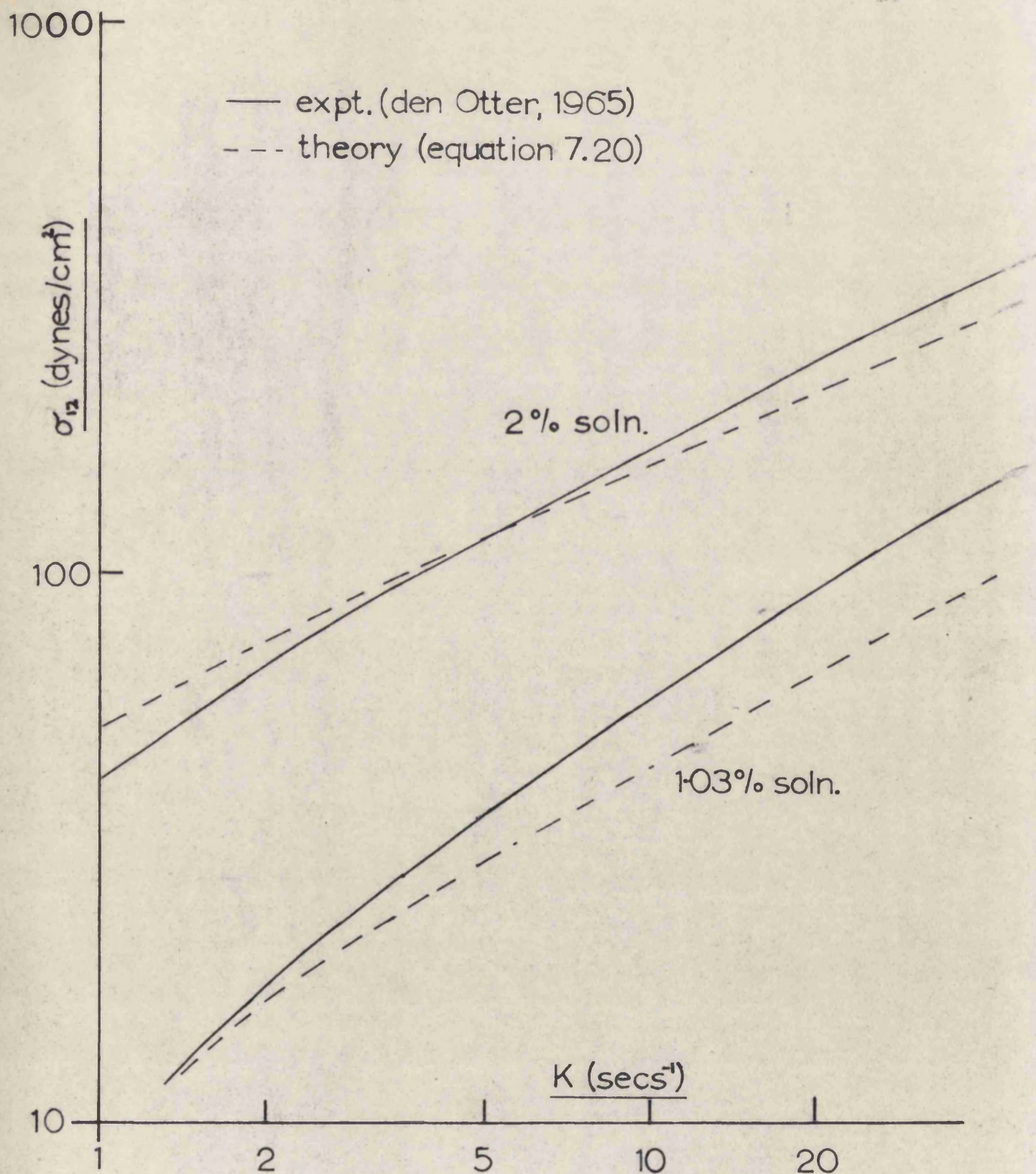


Fig.7.4 Comparison of Experimental and Theoretical
Shear Stresses

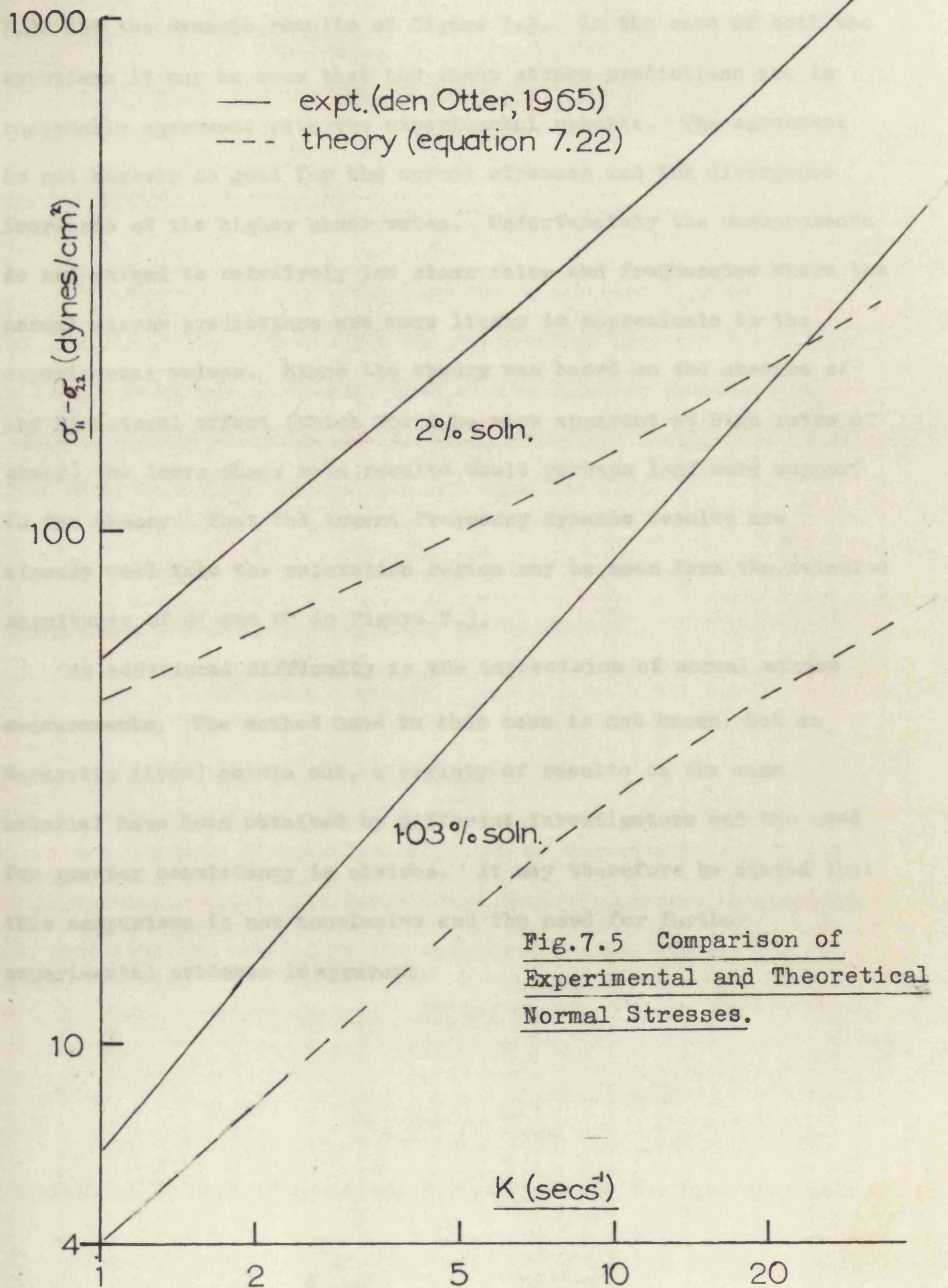


Fig.7.5 Comparison of
Experimental and Theoretical
Normal Stresses.

7.22 and the dynamic results of figure 7.3. In the case of both the solutions it may be seen that the shear stress predictions are in reasonable agreement with the experimental results. The agreement is not however so good for the normal stresses and the divergence increases at the higher shear rates. Unfortunately the measurements do not extend to relatively low shear rates and frequencies where the normal stress predictions are more likely to approximate to the experimental values. Since the theory was based on the absence of any structural effect (which would be more apparent at high rates of shear) the lower shear rate results would perhaps lend more support to the theory. That the lowest frequency dynamic results are already well into the relaxation region may be seen from the relative magnitudes of G' and G'' in Figure 7.3.

An additional difficulty is the imprecision of normal stress measurements. The method used in this case is not known, but as Markovitz (1960) points out, a variety of results on the same material have been obtained by different investigators and the need for greater consistency is obvious. It may therefore be stated that this comparison is not conclusive and the need for further experimental evidence is apparent.

CHAPTER 8

AUTOMATIC COMPUTATION OF RELAXATION SPECTRA

8.1 Nature of the problem

In Chapter 2 it was shown that the viscoelastic properties of a material may be described by a relaxation spectrum $N(s)$ where s is the frequency or inverse time of a relaxation process. The complex elastic shear modulus as an experimental function of angular frequency ω is given by the integral equation 2.15.

$$G(j\omega) = \int_0^{\infty} N(s) \frac{j\omega}{s + j\omega} ds \quad 8.1$$

Separating into real and imaginary parts gives,

$$\begin{aligned} G'(j\omega) &= \int_0^{\infty} N(s) \frac{\omega^2}{s^2 + \omega^2} ds \\ G''(j\omega) &= \int_0^{\infty} N(s) \frac{\omega s}{s^2 + \omega^2} ds \end{aligned} \quad 8.2$$

Now the pair of equations 8.2 must be consistent in that the experimentally determined functions G' and G'' are not independent. In fact they are related by the equations (Gross, 1953):

$$\begin{aligned} G'(\omega) &= \frac{2\omega^2}{\pi} \int_0^{\infty} \frac{G''(s)}{s(\omega^2 - s^2)} ds \\ G''(\omega) &= \frac{2\omega}{\pi} \int_0^{\infty} \frac{G'(s)}{s^2 - \omega^2} ds \end{aligned}$$

Therefore, if both of equations 8.2 are soluble for $N(s)$ then only

one of the experimental functions need be used. The other may be used as a check if desired. In the majority of experimental determinations G' and G'' are not measured explicitly but are derived from an impedance function $Z_L = R_L + jX_L$ which is related to the modulus G by the equations (Barlow and Lamb, 1959)

$$\begin{aligned} G' &= \frac{R_L^2 - X_L^2}{\rho} \\ G'' &= \frac{2 R_L X_L}{\rho} \end{aligned} \quad 8.3$$

where ρ is the density. Now G' is a monotonically increasing function while G'' has a maximum in the middle of the relaxation region and tails off to zero on either side. Since R_L and X_L are usually accompanied by absolute as well as relative errors the values of G' and G'' are likely to be least accurate where their amplitudes are smallest. For this reason, when calculating relaxation spectra, the function G' is usually used and the inaccuracies are then concentrated at lower values of ω only. In the following analyses, therefore, the first of equations 8.2 is used only, although the second equation is also amenable to a similar treatment.

The problem is then to determine the function $N(s)$ from $G'(\omega)$ when the two are related by the equation

$$G'(\omega) = \int_0^{\infty} N(s) \frac{\omega^2}{s^2 + \omega^2} ds \quad 8.4$$

Since the range of the variables s and ω in equation 8.4 is very large, it is more normal to use logarithmic variables defined by

$$x = \ln \omega \quad \text{and} \quad y = \ln s$$

whence,

$$g(x) = \int_{-\infty}^{\infty} n(y) \frac{1}{1 + e^{-2(x-y)}} dy \quad 8.5$$

where $g(x) = G^0(e^x)$ and $n(y) = e^y N(e^y)$. It is interesting to note that by means of this substitution the integral equation has been reduced to one of the convolution type. However it should be observed that this has no physical significance since the convolution integrals appearing in the mathematics of linear systems involve 'memory' functions of time, whereas the arguments of the functions appearing in equation 8.5 are logarithms of frequency.

Linear integral equations of the first kind (Lovitt, 1950) of the type in equation 8.5 may in principle be solved operationally by a method due to van der Pol and Bremmer (1955, p.300). If equation 8.5 is rewritten in the form

$$g(x) = \int_{-\infty}^{\infty} n(y) \cdot K(x-y) dy$$

and the Laplace transform of both sides is taken, we obtain

$$\bar{g}(p) = \bar{n}(p) \cdot \bar{K}(p)$$

which may be rearranged to give

$$\bar{n}(p) = \frac{1}{\bar{K}(p)} \cdot \bar{g}(p) \quad 8.6$$

where K is referred to as the kernel function and a superscript bar denotes a Laplace transform. The inverse transform of equation 8.6 can be taken to give another convolution integral but with a different kernel function defined by

$$K^* = \mathcal{L}^{-1} \frac{1}{\bar{K}(p)}$$

which is referred to as a reciprocal kernel. Unfortunately the kernel function

$$[1 + e^{-2(x-y)}]^{-1}$$

has no reciprocal since its Laplace transform is the reciprocal of a sine function and a sine function has no inverse transform. By the same token it may be shown that the function n cannot be described in terms of an integral equation of the second kind either, viz.

$$n(x) = g(x) - \int_{-\infty}^{\infty} K(x-y) \cdot g(y) dy$$

For these reasons recourse is made to approximate numerical methods which have the advantage that the effect of 'noise' on the data can be assessed as the calculation proceeds.

8.2 Numerical methods

A variety of methods have been discussed in the literature to determine spectra from storage modulus data. They usually depend on some iterative scheme which is terminated when the recalculated function g approximates to the experimental results with appropriate accuracy. Williams and Ferry (1953) suggest a method which requires the numerical derivatives of g and n ; and starting with an arbitrary spectrum, a formula for a better approximation is given. Methods are also available which require higher derivatives of g such as that of Fujita (1958) or Schwarzl and Staverman (1953) which require second and third derivatives respectively. Because the experimental function g is subject to errors, the process of taking derivatives higher than the first is hazardous and must usually be accompanied by some form of smoothing. For these reasons the above methods are most suitably performed graphically.

Methods based on Fourier series have been developed by Roesler and Pearson (1954) and Roesler (1955); and a simple iteration method is discussed by Roesler and Twyman (1955). They have the advantage that the limiting resolution of the process becomes apparent during the calculation. Unfortunately, a common feature shared by all these methods is the amount of labour involved in the calculations, and a means of calculating spectra automatically by means of a computer is therefore desirable. Direct programming of the methods previously mentioned suffers from the difficulty that the smoothing processes required at various stages of the calculation are not easily defined. In addition there is the problem of deciding upon a suitable criterion as to when to terminate iteration procedures. For these reasons certain simpler procedures are suggested which perhaps lack the sophistication of the other methods but which are more amenable to simple programming.

8.3 First method

The two methods to be described assume that the continuous spectrum may be approximated by a line spectrum if the spacing of the lines is sufficiently close. This has already been discussed in Section 2.4.1. For simplicity it is further arranged that the line spacings are equal on a logarithmic basis so that a constant factor m relates one relaxation frequency to its neighbour. For a discrete spectrum

we have

$$G'(\omega) = \sum_{p=0}^n G_p \frac{\omega^2}{\omega^2 + s_p^2}$$

where G_p is the intensity of the p^{th} line and s_p its relaxation frequency. In terms of m this may be written

$$\begin{aligned} G^i(\omega) &= \sum_n G_p \frac{\omega^2}{\omega^2 + m^2 s_o^2} \\ &= \sum_n G_p \frac{(\omega/s_o)^2}{(\omega/s_o)^2 + m^2} \end{aligned} \quad 8.7$$

where s_o may be considered as some reference relaxation frequency. We now consider the values of the function $G^i(\omega)$ for $\omega = \omega_o, m\omega_o, m^2\omega_o, \dots, m^n\omega_o$, and refer to the q^{th} value of the function g_q so that

$$g_q = G^i(m^q \omega_o)$$

If it is then arbitrarily arranged that $\omega_o = s_o$, equation 8.7 may be written

$$\begin{aligned} g_q &= \sum_{p=0}^n G_p \frac{m^{2q}}{m^{2q} + m^{2p}} \\ &= \sum_{p=0}^n \frac{G_p}{1 + m^{2(p-q)}} \end{aligned} \quad 8.8$$

Equation 8.8 is a set of linear simultaneous equations and if it is further arranged to use n values of g , the set is soluble. The equations are,

$$\begin{aligned} g_0 &= \frac{1}{2} G_0 + \frac{1}{1+m^2} G_1 + \frac{1}{1+m^4} G_2 + \dots + \frac{1}{1+m^{2n}} G_n \\ g_1 &= \frac{1}{1+m^{-2}} G_0 + \frac{1}{2} G_1 + \frac{1}{1+m^2} G_2 + \dots + \frac{1}{1+m^{2(n-2)}} G_n \\ g_n &= \frac{1}{1+m^{-2n}} G_0 + \frac{1}{1+m^{-2(n-1)}} G_1 + \dots + \frac{1}{2} G_n \end{aligned} \quad 8.9$$

The values of $g_0 \dots g_n$ are known and it is required to find the values $G_0 \dots G_n$. If it is arranged that $m > 1$ so that $g_{q+1} > g_q$ since g is a monotonically increasing function, then the coefficients in equation 8.9 decrease from left to right, increase from top to bottom and are all positive.

Although the matrix of coefficients, M , is non-singular, its inverse indicates extreme ill-conditioning. This may be demonstrated by observing the inverse matrix in table 8.1 for which $m = 1.5849$ corresponding to logarithmic increments of 0.2 decades. This interval is used because it represents a value consistent with the resolution of average data. For this matrix $n = 38$ corresponding to a total frequency range of 7.6 decades. The inverse matrix was calculated on a computer and checked by multiplying it by the original matrix. The resultant matrix differed from the unit matrix by not more than one figure in the fourth place. The values for the spectrum may theoretically be obtained by pre-multiplying the vector of g values by the matrix of table 8.1. The alternately large positive and negative values along a row of the matrix indicate that an accuracy of at least 0.1% is required on the values of g in order to obtain meaningful results. In practice this is an impossible requirement and the inverse matrix method is not feasible although a modified version of it provides the basis for a second method to be discussed later.

An alternative means of solving the equations is by some numerical method of which there are many described in the literature. The method chosen here is the Gauss-Seidel procedure (Redish, 1961, p.19) which is the easiest to programme. The method involves writing equations

8.9 in the form

$$G_0 = \begin{matrix} \cdot & \cdot & \cdot & \cdot \end{matrix}$$

$$G_1 = \begin{matrix} \cdot & \cdot & \cdot & \cdot \\ & & \vdots & \end{matrix}$$

$$G_2 = \begin{matrix} \cdot & \cdot & \cdot & \cdot \end{matrix}$$

etc.

A trial guess is first made, typically zero, for the values $G_1 \cdot \cdot \cdot G_n$ and each equation is used sequentially to obtain better values for G . At each stage the most up to date values of the unknowns are used and the cycle is continued until convergence results. Owing to the ill-conditioning in this set of equations a large scatter is obtained in the results for G even though the corresponding values for g are within experimental error. To overcome this difficulty a criterion of 'smoothness' is applied to the G values, so that the G_p must not only satisfy the equations but also have continuity.

The means of smoothing used is that discussed by Lanczos (1957, p, 331). A Fourier analysis is performed on the G_p values to find the n coefficients required for description by a Fourier series. The series is then truncated at some arbitrary term l ($l < n$) and the smoothed values of G_p are then obtained by using the truncated series. In this way the higher 'frequency' components are eliminated. In mathematical terms, g is considered to be a continuous function of some variable x expandable in a sine series, i.e.

$$g(x) = b_1 \sin \frac{\pi x}{L} + b_2 \sin \frac{2\pi x}{L} + \cdot \cdot \cdot + b_n \sin \frac{n\pi x}{L}$$

where L is the range of x and the b_q are the Fourier coefficients which are given by

$$b_q \approx \frac{2}{n} \sum_{x=x_0}^{x_{q-1}} g(x) \sin \frac{q\pi x}{L}$$

The values b_q are computed only up to $q = l$ and the smoothed version of $g(x)$, $\bar{g}(x)$, is obtained from the truncated series

$$\bar{g}(x) = \sum_{q=1}^l b_q \sin \frac{q\pi x}{L}$$

It should be noted that the smoothing is performed on a logarithmic scale so that x is equivalent to $\log(\text{frequency})$. The overall procedure is to perform one Gauss-Seidel iteration followed by smoothing, and then to use the smoothed values for the next iteration. The process is terminated when successive smoothed values of G_p do not differ by more than a certain amount. This does not however ensure that the corresponding values for g are within experimental error; it will depend on how much smoothing has been applied. In practice it is arranged that the maximum amount of smoothing is used consistent with the g values being within experimental error. For programming the main advantage of the Fourier method of smoothing is that only one parameter $\overset{e}{\wedge}$ is necessary to determine the amount of smoothing, viz. l , the number of Fourier components used for the description of g .

Ideally the programme should select an appropriate smoothing parameter based on the progress of the calculation, but since this would take an excessive time the amount of smoothing is predetermined. Calculations in Section 8.4 suggest that with data that is accurate to about three significant figures little more information is given about the spectrum than 1.5 Fourier components per decade. The value of l is therefore the nearest integer to 1.5 times the frequency range in decades. A flow diagram of the computation is shown in Figure 8.1.

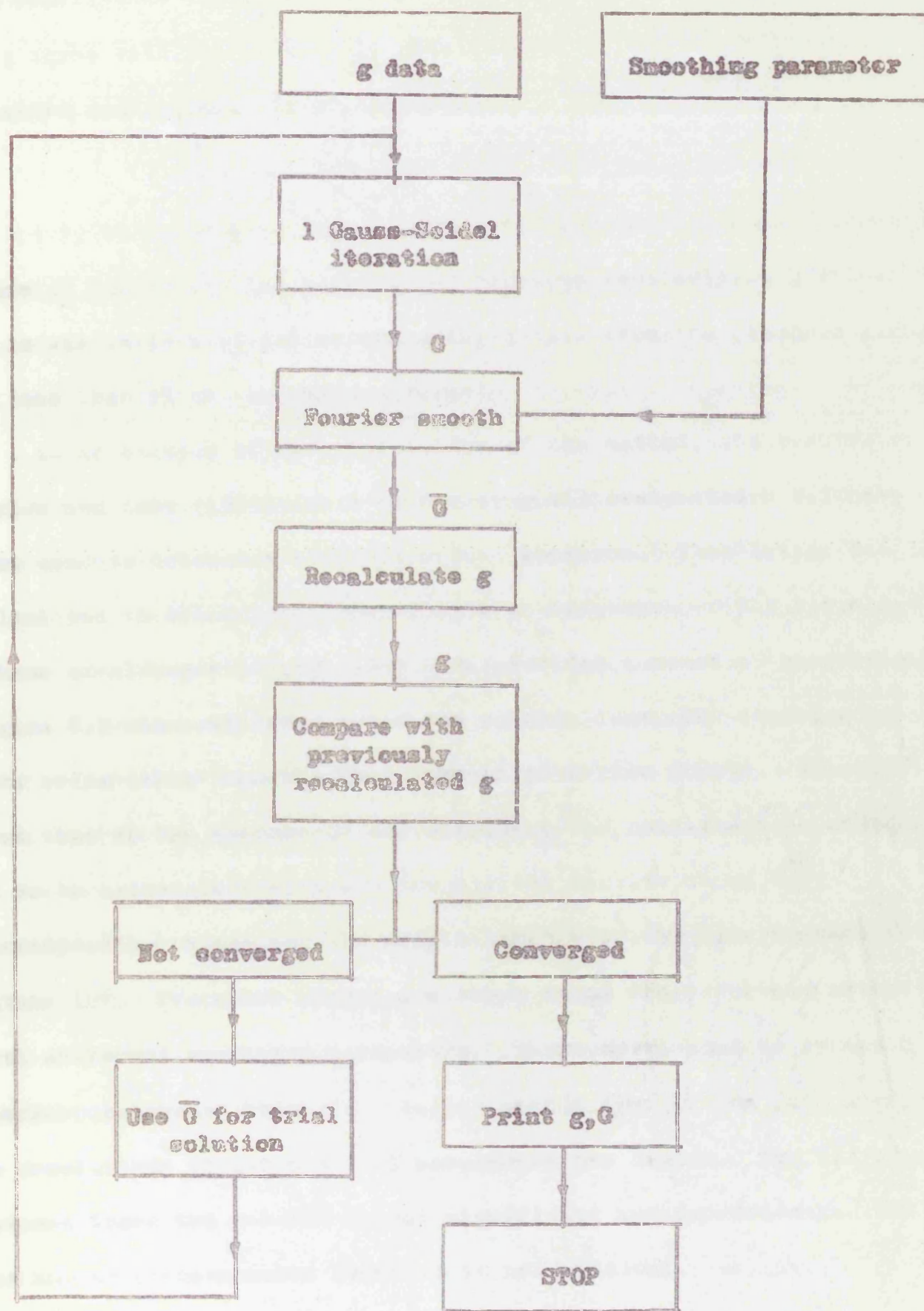


Fig.8.1 Flow Diagram of First Method.

The convergence condition used is that the current recalculated values of g agree with the previously recalculated values according to a relative mean squared error criterion:

$$\sqrt{\frac{1}{n} \sum_{p=1}^n (g_p' - g_p'')^2} < 0.01 g_n$$

where g' and g'' are the current and previous recalculated g values and g_n is the largest of the experimental data. Thus the standard error must be less than 1% of the maximum value.

As an example of the application of the method, the results of Barlow and Lamb (1959) for a lubricating oil designated M.V.I have been used to determine the relaxation spectrum. This latter was also calculated in the original paper by a method based on the iterative scheme of Alfrey and Doty (1945) and provides a means of comparison. Figure 8.2 shows the results of the calculations, the experimental data being taken from the Ph.D. thesis of Barlow (1959). It can be seen that in the absence of any smoothing the points are so scattered as to be meaningless although for all the results shown the corresponding values for the moduli agree with the experimental values within 10%. Two other curves are shown using the described method with different smoothing parameters. These correspond to 12 and 8 Fourier components which for the 7.6 decade span of the data give rise to resolutions of 1.6 and 1.05 components per decade. The difference between these two results is not significant and demonstrates that the number of components required is not critical.

It would appear that on the basis of these results the

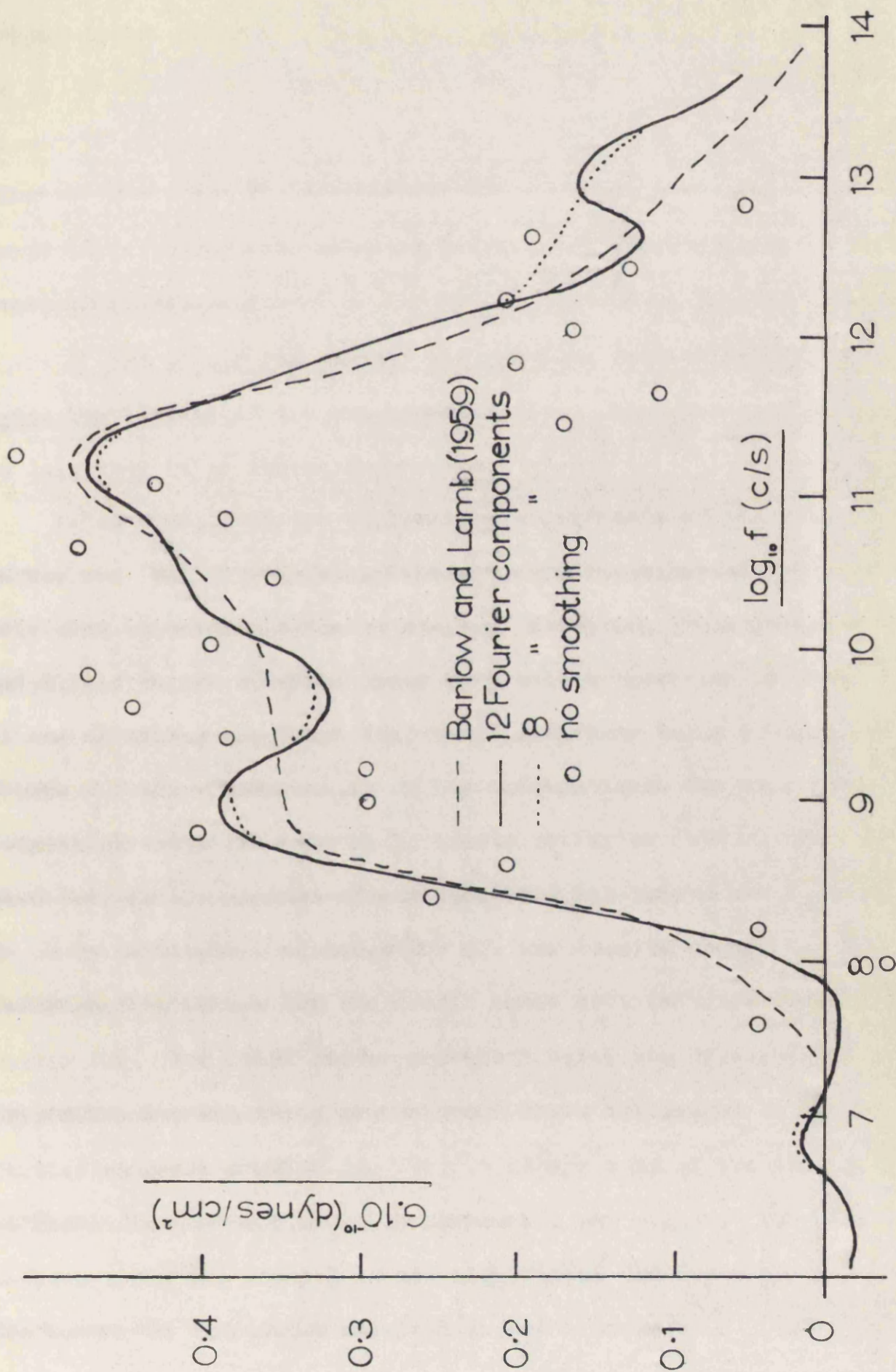


Fig.8.2 First Method applied to MVI Lubricating Oil

graphical smoothing of Barlow and Lamb tends to be rather too severe as can be seen especially on the left hand peak of the spectrum. It should be emphasised that the diagram of Figure 8.2 represents a discrete spectrum of lines spaced at 0.2 decade intervals. A smooth curve drawn through the points represents an approximation to the continuous spectrum.

8.4 Second method

The second method to be described uses the same discrete spectrum formulation but depends on matrix properties. Equations 8.9 may be rewritten in matrix form as $g = M G$ where g and G are column vectors and M is a matrix of which the $p q$ element is given by $1/(1+m^{2(q-p)})$. It has already been stated that the formulation $G = M^{-1} g$ is unsatisfactory because of the ill-conditioning of the matrix M .

However, by means of a device, it is possible to find a matrix P_r which is an r^{th} approximation to M^{-1} and for which $\lim_{r \rightarrow \infty} P_r = M^{-1}$.

We first note that for any arbitrary non-singular matrix D the following identity holds: $= (DM)^{-1} D$

$$M^{-1} \equiv M^{-1} D^{-1} D = (DM)^{-1} D$$

The matrix product $(DM)^{-1}$ may be written

$$(DM)^{-1} = (I - [I - DM])^{-1}$$

which may be expanded in a power series

$$(DM)^{-1} = I + (I - DM) + (I - DM)^2 + \dots \quad 8.10$$

where I is the unit matrix.

The series 8.10 is not necessarily convergent but may be made so by appropriate choice of the matrix D . Indeed it can be seen that the closer D is to the inverse of M , the more rapid the convergence, and D can be regarded as a first approximation to the inverse. An r^{th} approximation to M^{-1} can then be defined:

$$P_r = [I + (I - DM) + (I - DM)^2 + \dots + (I - DM)^{r-1}] \cdot D \quad 8.11$$

which is a truncated version of the series 8.10.

In order to find a suitable form for D an analogy is drawn with the properties of the continuous spectrum. From equation 8.2 one has

$$G'(\omega) = \int_0^\infty N(s) \frac{\omega^2}{\omega^2 + s^2} ds$$

The form of the kernel function is a gradual step decreasing in the direction of increasing ω and centred at $\omega = s$. As a first approximation in accordance with the method of Alfrey and Doty (1945) the kernel function may be replaced by a step function in which case the integral simplifies to

$$G'(\omega) \simeq \int_0^s N(s) ds$$

from which it can be seen that

$$N(s) \simeq \left. \frac{dG'(\omega)}{d\omega} \right|_{\omega = s}$$

is a first approximation to the spectrum. Since the discrete spectrum must approximate to the continuous one, the same type of first approximation may be used. In the present context this amounts to finding the matrix D which numerically differentiates a post-multiplied vector column.

The matrix is constructed from a method described by Lanczos

(1957, p. 321) for the differentiation of an empirical function. It is assumed that the values of a function $y(x)$ are available at equispaced intervals and a parabola is fitted to five adjacent points on a least squares basis. The value of the derivative at the centre point $y_0 = y(x_0)$ is then given by the formula

$$\left. \frac{dy}{dx} \right|_{x=x_0} = -0.2 y_{-2} - 0.1 y_{-1} + 0.1 y_1 + 0.2 y_2$$

For the first and last two ordinates, this formula obviously cannot be used and Lanczos gives a four point asymmetric formula for these cases. The process for all the ordinates may be condensed into a matrix multiplication for which the differential matrix D becomes

-1.05	0.65	0.85	0.45	0	0	0	0
-0.55	0.15	0.35	0.05	0	0	0	0
-0.2	-0.1	0	0.1	0.2	0	0	0
0	-0.2	-0.1	0	0.1	0.2	0
0	0
.
.	.	.	-0.2	-0.1	0	0.1	0.2	0
.	.	.	0	-0.2	-0.1	0	0.1	0.2
.	.	.	0	0	-0.05	-0.35	-0.15	0.55
0	0	0	.	.	.	0	0	0.45	-0.85	-0.65	1.05	.

The matrix can evidently be constructed for any size equal to or exceeding 5×5 . The effect of premultiplying a vector by the matrix D is to combine a numerical differentiation with a smoothing process since continuity of the curve is ensured by fitting a parabola through

two more points than the minimum necessary.

A programme to calculate the r^{th} approximation to M^{-1} according to equation 8.11 only requires two input parameters. These are the size of the matrix determined by the number of ordinates used, and also the ordinate spacing in decades d where $m = \text{antilog}(d)$. This programme is not shown since it only involves standard matrix operations. The result for the third approximation P_3 for which the matrix size is 38×38 and the ordinate spacing is 0.2 decades is shown in Table 8.2. This matrix may be compared with the exact inverse of Table 8.1. It can be seen that the third approximation puts far lesser stringent demands on the accuracy of the data and in addition its structure is tending to that of a band matrix. The latter property indicates that by means of this procedure the value of the spectrum at a certain point does not depend on too many neighbouring values of the storage modulus curve. In this case approximately six neighbours on either side of a given point give non-negligible contributions to the spectrum at the centre point.

In order to check the resolving power of this method, calculations have been performed on single relaxation time data rounded off to three figures. This test puts a realistic amount of 'noise' on the data and at the same time the ultimate shape of the spectrum is known. The difference between the single line spectrum from which the data is deduced, and the spectrum calculated according to the method gives an idea of the resolving power. Figure 8.3 shows the spectra calculated using three different approximations, P_2 , P_3 and P_5 . The ordinate

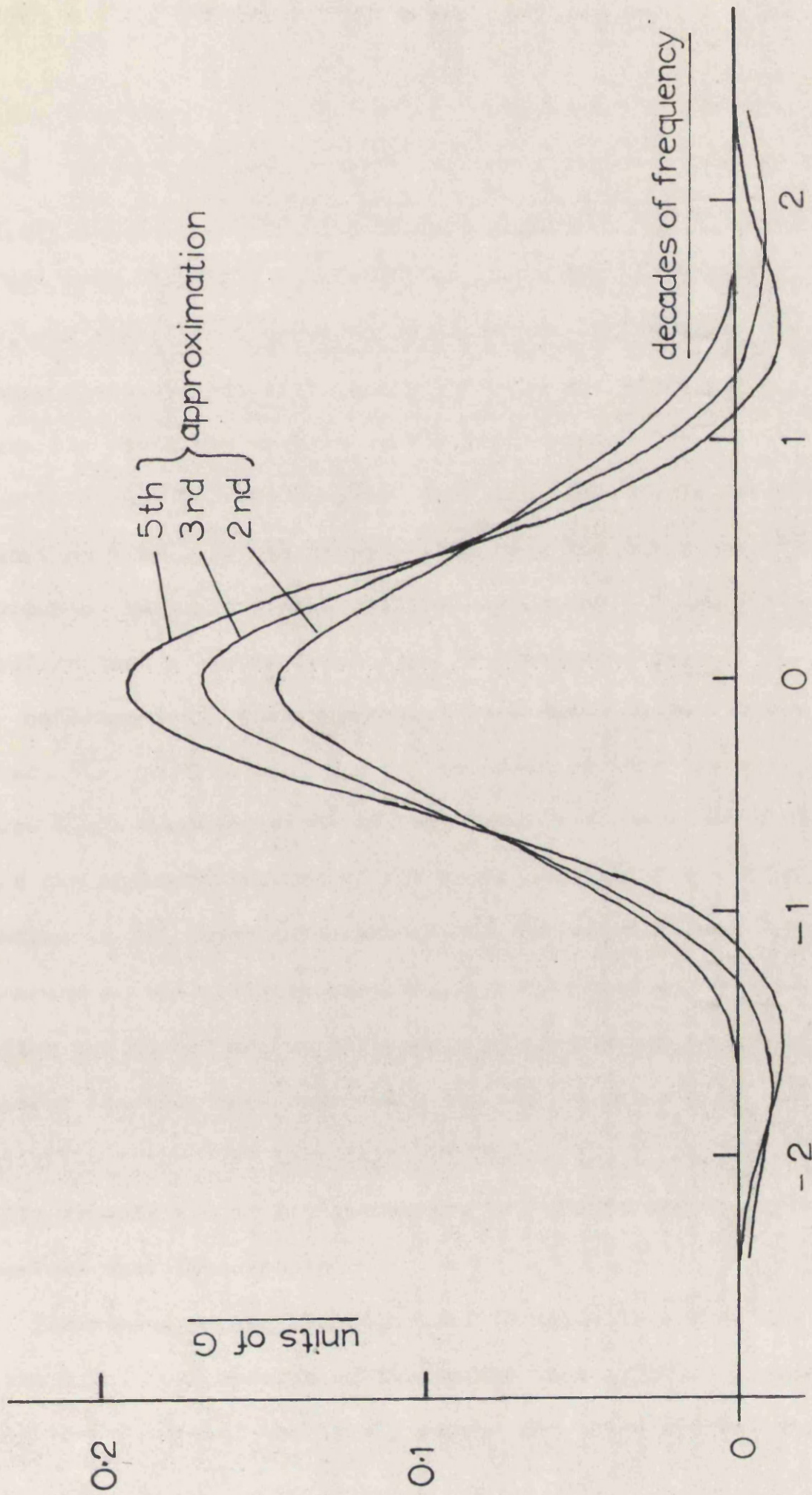


Fig.8.3 Approximations to a Single Relaxation Time Spectrum

spacing used was 0.1 decades and the data covers 2.8 decades. Although it may be seen that each successive approximation improves the spectrum, they are all very different from a single point of one unit intensity. In fact even the fifth approximation has a maximum intensity of only 0.19, and significant negative portions are beginning to develop. Although it would at first appear that the method is unsatisfactory Figure 8.4 shows the modulus curves recalculated from the three spectra shown in Figure 8.3 and compared with the exact curve for a single relaxation time. It can be seen that even the third approximation reproduces the curve with negligible error and the conclusion is therefore that a higher resolution is unnecessary.

Unfortunately, this means that with data limited to the accuracy stated, the spectrum can be no better defined than those shown in Figure 8.3. However, since in real materials the spectra are relatively broad the apparent failure of the method to describe a single line spectrum is not important although the curves of Figure 8.3 do give a measure of the ultimate resolving power. This may be assessed by finding the number of Fourier components necessary to describe the broadest spectrum that reproduces the single relaxation time data with negligible error. By inspection of Figure 8.3 it may be seen that this hardly exceeds 1.0 to 1.5 components per decade and the first method therefore uses this result.

The second method has been used to again determine the spectrum of the M.V.I. oil results of Barlow and Lamb (1959). Figure 8.5 shows the results of the first, second and third approximations

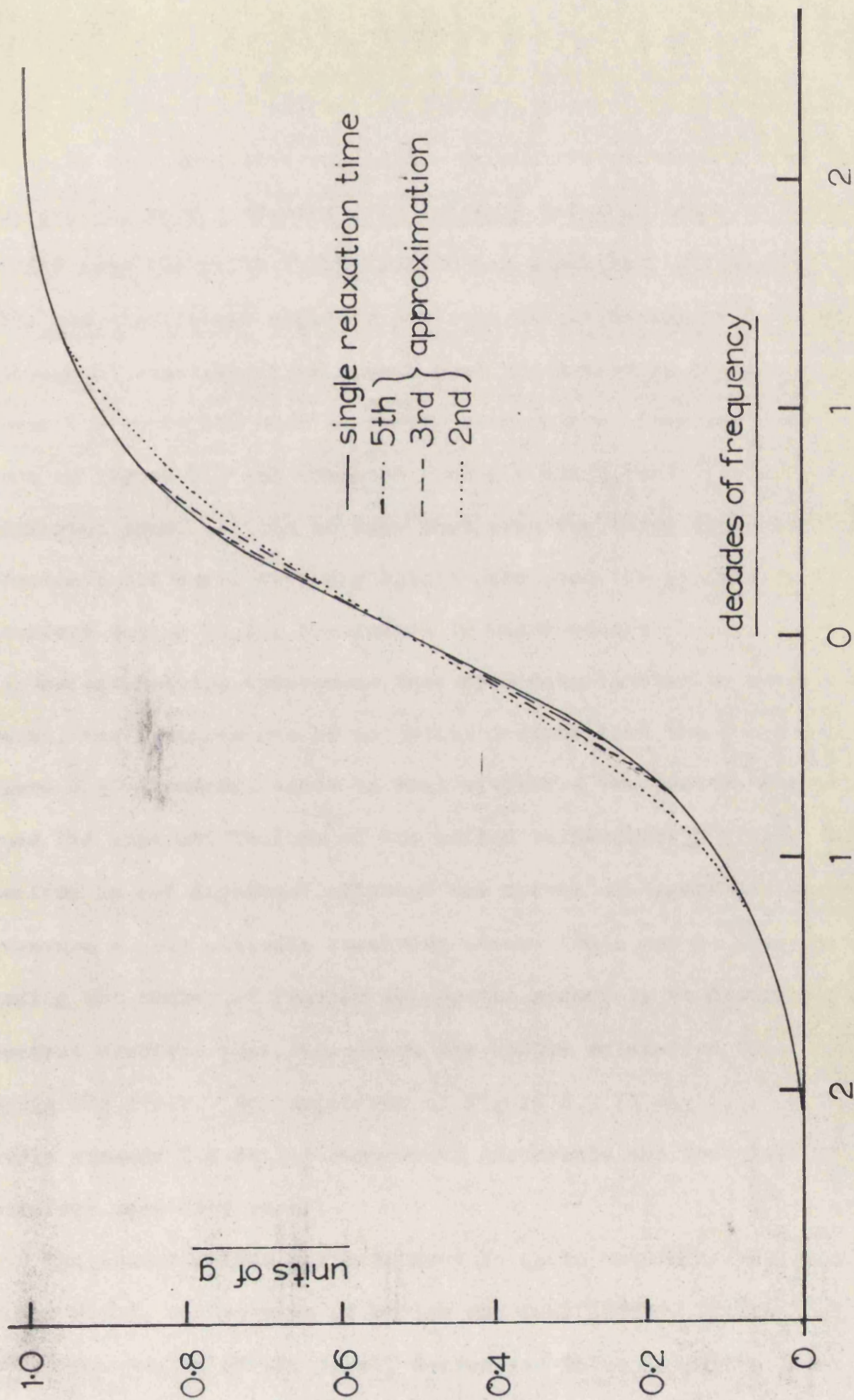


Fig.8.4 Approximations to the Storage Modulus for a Single Relaxation Time

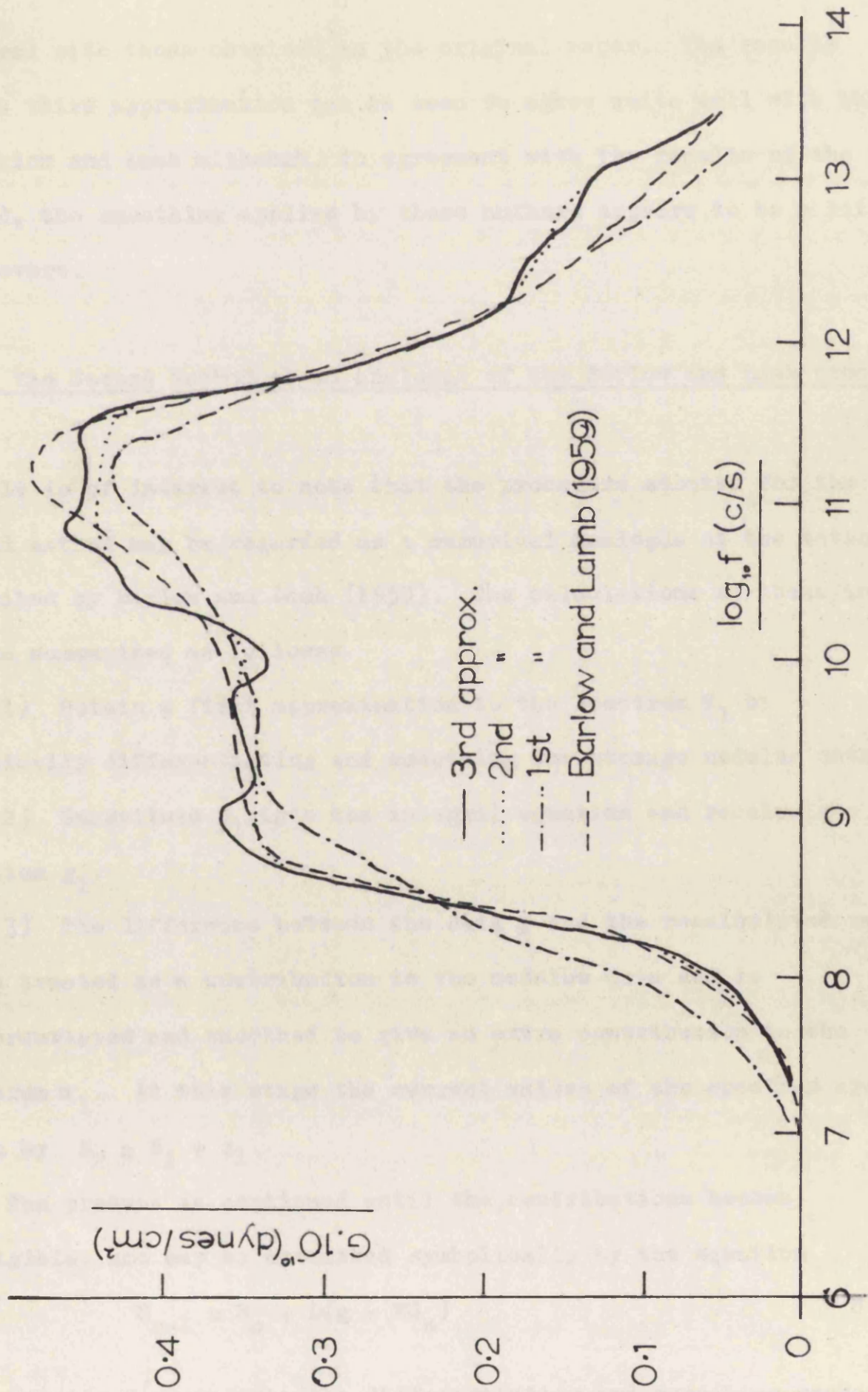


Fig. 8.5 Second Method applied to MVI Lubricating Oil

compared with those obtained in the original paper. The results of the third approximation can be seen to agree quite well with those of Barlow and Lamb although, in agreement with the results of the first method, the smoothing applied by these authors appears to be a little too severe.

8.5 The Second Method as an analogue of the Barlow and Lamb procedure.

It is of interest to note that the procedure adopted for the second method may be regarded as a numerical analogue of the method described by Barlow and Lamb (1959). The calculations of these authors may be summarised as follows:

- 1) Obtain a first approximation to the spectrum S_1 by graphically differentiating and smoothing the storage modulus data g .
- 2) Substitute S_1 into the integral equation and recalculate the function g_1 .
- 3) The difference between the data g and the recalculated values g_1 is treated as a contribution to the modulus data and is differentiated and smoothed to give an extra contribution to the spectrum s_1 . At this stage the current values of the spectrum are given by $S_2 = S_1 + s_1$.

The process is continued until the contributions become negligible, and may be described symbolically by the equation

$$S_{n-1} = S_n + D(g - MS_n) \quad 8.12$$

The operator D represents the differentiating and smoothing process while M represents the integration. The suffices refer to the order

of approximation. Rearranging and noting that Dg represents the first approximation to the spectrum, S_1 , we obtain

$$S_{n+1} = (I - DM)S_n + S_1$$

where I is an identity operator. By induction it can be seen that

$$S_r = [I + (I - DM) + (I - DM)^2 + \dots + (I - DM)^{r-1}] \cdot S_1.$$

Since $S_1 = Dg$ a formal equivalence is established between this process and equation 8.11

8.6 Discussion

The two methods described both enable spectra to be satisfactorily obtained from storage modulus data in ways suitable for programming. Although the two methods give slightly different results, for example in the case of the M.V.I. lubricating oil, the differences cannot be said to be important since the recalculated values of the data are all sufficiently close. Indeed, this only serves to illustrate the lack of precision with which the spectrum may be determined.

Of the two methods, perhaps the second is easier to apply since once the approximating matrix has been calculated automatically, the result may be obtained by simply performing a matrix-vector multiplication. A number of approximating matrices could be calculated using different ordinate spacings and ranges, and the appropriate one used to solve any particular set of data. The spectrum is then obtained by multiplying the vector of experimental quantities by the appropriate square matrix. This process could

reasonably be carried out by hand and would take approximately one and a half hours for the 38 ordinate system using an electric calculating machine. Using a KDF 9 computer with a medium speed compiler ("Kidsgrove intermediate") the 38×38 third approximation matrix required approximately ten minutes before punching was completed. For the first method, using KDF 9, each iteration on a 38 ordinate system took approximately 2.5 minutes. It appeared that in general seven or eight iterations were necessary giving a total time of 15 - 20 minutes for the complete spectrum calculation. The times given above should be reduced by approximately a factor of ten when the latest version of the compiler ("Kidsgrove optimised") becomes available.

APPENDIX AAnalysis of shear wave propagation in cylindrical coordinates

Consider an infinitesimal cylindrical annulus of viscoelastic fluid of width δr and unit height at radius r under conditions of oscillatory shear. The torque at radius r is equal to $2\pi r \cdot G \cdot r \frac{d\theta}{dr}$ where G is the shear modulus (which is complex) and θ is the angular displacement. The nett torque on the annulus is therefore

$$\frac{d}{dr} \left(2\pi r^3 G \frac{d\theta}{dr} \right) \delta r = 2\pi G \left\{ r^3 \frac{d^2\theta}{dr^2} + 3r^3 \frac{d\theta}{dr} \right\} \delta r$$

which is balanced by the inertial torque of the accelerating fluid:

$$- 2\pi r \delta r \rho r^2 \omega^2 \theta = - 2\pi r^3 \rho \omega^2 \theta \delta r$$

where ω is the radian frequency of oscillation and ρ is the density.

The equation of motion is therefore

$$\frac{d^2\theta}{dr^2} + \frac{3}{r} \frac{d\theta}{dr} + \frac{\omega^2 \rho}{G} \theta = 0 \quad A.1$$

An equation of similar form is derived by Markovitz (1952) and is of the Bessel type. The solution of this equation (McLachlan, 1934) is:

$$\theta = \frac{1}{r} \left[A J_1(\omega r \sqrt{\rho/G}) + B Y_1(\omega r \sqrt{\rho/G}) \right] \quad A.2$$

where J_1 and Y_1 are first order Bessel functions of the first and second kinds. At the inner fixed boundary of the system $\theta = 0$ and $r = R$ which gives

$$A J_1(\omega R \sqrt{\rho/G}) + B Y_1(\omega R \sqrt{\rho/G}) = 0 \quad A.3$$

The measured quantity z is the torsional impedance per unit height presented to the oscillating boundary at radius r , defined as

$$z = \frac{\text{torque/unit height}}{\text{angular velocity}} = \frac{2\pi r^3 G}{j\omega \theta} \frac{d\theta}{dr} \quad A.4$$

Differentiating equation A.2:

$$\frac{d\theta}{dr} = \frac{1}{r} [AJ_1' + BY_1'] - \frac{1}{r^2} [AJ_1 + BY_1]$$

whence

$$\frac{1}{\theta} \frac{d\theta}{dr} = \frac{AJ_1' + BY_1'}{AJ_1 + BY_1} - \frac{1}{r}$$

where the arguments of the Bessel functions are understood. Inserting the initial conditions of equation A.3 and substituting into equation A.4, we obtain

$$z = \frac{2\pi r^3 \omega \rho}{j \Gamma^2} \left\{ \frac{Y_1(\Gamma r) J_1'(\Gamma r) - J_1(\Gamma r) Y_1'(\Gamma r)}{Y_1(\Gamma r) J_1(\Gamma r) - J_1(\Gamma r) Y_1(\Gamma r)} - \frac{1}{r} \right\} \quad A.5$$

where Γ , the propagation constant, $= \omega \sqrt{\rho/G}$. Equations of the form of equation A.5 occur in many boundary value problems with cylindrical symmetry. Oliner (1948) obtains a similar equation in connection with slow wave electromagnetic propagation in cylindrical waveguides. The present situation however is more difficult from a computational standpoint, because the propagation constant is in this case complex. Also, it will be observed that z is the measured quantity and Γ which is buried in the argument of the Bessel functions, is to be calculated from it. For computational purposes, a recursion property of Bessel functions (McLachlan, 1934 p.158) enables equation A.5 to be written in the form

$$z = \frac{2\pi \omega \rho r^3}{j \Gamma} \left\{ \frac{Y_1(\Gamma r) J_0(\Gamma r) - J_1(\Gamma r) Y_0(\Gamma r)}{Y_1(\Gamma r) J_1(\Gamma r) - J_1(\Gamma r) Y_1(\Gamma r)} - \frac{2}{\Gamma r} \right\} \quad A.6$$

Unfortunately equation A.6 is not in a suitable form for tabulation of corresponding complex values of z and Γ . This arises because for the range of values of practical interest both the numerator and the denominator of the fraction involving Bessel functions, tend

to zero. A very high degree of precision is therefore required on all the calculations in order to assume the desired end accuracy. In addition, after performing the calculation no check on the end accuracy is available. For these reasons the closed form solution of equation A.6 was not used for calculation purposes.

In order to avoid these difficulties, recourse was made to the differential equations, which were solved numerically by a step by step method in which accuracy checks were incorporated. Instead of solving the second order linear differential equation of A.1, a first order non linear equation is first obtained by combining equations A.1 and A.4.

We first define a torsional admittance $y = \frac{1}{z}$.

From equation A.4 we obtain,

$$y \frac{d\theta}{dr} = \frac{j\omega\theta}{2\pi r^3 G} \quad A.7$$

Differentiating with respect to r:

$$y \frac{d^2\theta}{dr^2} + \frac{dy}{dr} \frac{d\theta}{dr} = \frac{j\omega}{2\pi G} \left(-\frac{3\theta}{r^4} + \frac{1}{r^3} \frac{d\theta}{dr} \right)$$

$$\text{or, } \frac{d^2\theta}{dr^2} = -\frac{1}{y} \frac{dy}{dr} \frac{d\theta}{dr} + \frac{j\omega}{2\pi G r^3 y} \left(-\frac{3\theta}{r} + \frac{d\theta}{dr} \right)$$

Substituting into equation A.1 and using A.7

$$\frac{dy}{dr} - \frac{j\omega}{2\pi G r^3} + j\omega 2\pi r^3 y^2 = 0 \quad A.8$$

We now introduce the dimensionless variables s and Y as follows

$$Y = 2\pi\omega r^4 (s+1)^3 y$$

$$s = (r/R) - 1 \quad A.9$$

Equation A.8 then becomes

$$\frac{dY}{ds} - \frac{3Y}{s+1} - \frac{j\omega^2 \rho R^2}{G} + jY^2 = 0 \quad A.10$$

Quantities a and ψ are then introduced such that

$$a = \frac{\omega^2 \rho R^2}{|G|} \quad \text{and} \quad \psi = \angle G \quad A.11$$

Equation A.10 then becomes

$$\frac{dY}{ds} - \frac{3Y}{s+1} - ja(\cos \psi - j \sin \psi) + jY^2 = 0$$

Y is a complex number and this equation may be separated into real and imaginary parts to give the pair of equations:

$$\begin{aligned} \frac{dY_1}{ds} &= \frac{3Y_1}{s+1} + 2Y_1Y_2 + a \sin \psi \\ \frac{dY_2}{ds} &= \frac{3Y_2}{s+1} + Y_2^2 - Y_1^2 + a \cos \psi \end{aligned} \quad A.12$$

For the purposes of numerical computation described in Appendix B the variables are named differently,

$$\text{MOD} \equiv a; \quad \text{ARG} \equiv \psi; \quad \text{mod } Y \equiv |Y| \quad \text{arg } Y \equiv \angle Y$$

The important equations are now summarised for convenience:

$$\begin{aligned} \text{mod } Y &= \frac{2\pi\omega\rho R^4(s+1)^3}{|z|} \quad \text{from equation A.9} \\ \text{arg } Y &= -\angle z \\ \text{MOD} &= \frac{\omega^2 \rho R^2}{|G|} \\ \text{ARG} &= \angle G \end{aligned} \quad A.13$$

where $s = (r/R) - 1$ which may be termed the 'relative gap'.

In the present apparatus, with the dimensions given in Figure 3.5
¹²
 equations A.12 may be simplified to:

$$\left. \begin{aligned} \text{mod } Y &= 680.4 \frac{\rho f}{|z|} \\ \text{arg } Y &= -\angle z \end{aligned} \right\} \quad \text{A.13}$$

$$\left. \begin{aligned} \text{MOD} &= 140.1 \frac{\rho f^2}{|G|} \\ \text{ARG} &= \angle G \end{aligned} \right\} \quad \text{A.14}$$

The equations A.12 are thus required to be integrated from the fixed boundary ($s=0$) where $Y=0$ (since the boundary presents zero admittance) to the oscillating boundary where $s=\bar{s}$. The purpose of using equations involving admittance functions rather than impedance functions is so that the initial conditions are zero rather than infinite.

APPENDIX B.Numerical integration of propagation equationsB.1 Description of the integration process

The equations A.11 were integrated automatically using a KDF 9 machine. A four stage Runge-Kutta process was used (Collatz, 1960, p.61) and the integration out to the boundary was performed 430 times in order to cover a reasonable range of possible viscoelastic properties. The independent variable s has a value of 0.11 at the measuring boundary in the present apparatus and the initial step length used for the integration was 0.01. To ensure a certain accuracy in the calculated values at the boundary the following procedure was used.

One step of the integration was first performed and then again using the half steps. The two results were then compared and if different by more than 0.01%, the step length was halved. This was repeated until the desired step accuracy was achieved, and the relevant values were stored. The next step was then integrated in the same way and so on until the boundary was reached. To speed the calculation up where possible, it was arranged that a trial step length was always made double the previously chosen step length.

After reaching the boundary the whole integration was repeated halving each step length chosen in the previous calculation. The values obtained at the boundary this time were compared with the previous values and if differing by more than 0.1%, the process

was repeated until this accuracy was reached. In this way the accuracy of the overall calculation may be guaranteed to 0.1% and the method is not prone to instability as when fixed step lengths are used.

The following pages contain the results of these integrations and the table consists of four parts: a main table, a sub-table and an interpolation table for each. The sub-table is used in the range $\text{MOD} = 50$ to $\text{MOD} = 5000$ where the values change more rapidly and interpolation accuracy is likely to be poor. It is found in practice that for adjacent entries in the table, interpolating for $\arg Y$, ARG and $\text{mod } Y$, MOD may be performed separately with satisfactory accuracy. The angles are given in radians and may be interpolated linearly. The interpolation for MOD and $\text{mod } Y$ however is slightly more complicated. It is found that over a small range MOD and $\text{mod } y$ are related by a power law, thus

$$\frac{\text{MOD}_2}{\text{MOD}_1} = \left\{ \frac{(\text{mod } Y)_2}{(\text{mod } Y)_1} \right\}^k$$

for a given angle, ARG , where k is an interpolating coefficient. In the interpolating tables, for each value of ARG , a value of the exponent k is given (referred to as Coeff.) for the range between adjacent MOD values.

Finally, to avoid transcription errors the table shown was photo-copied from the actual computer output.

B.2. Table of values for the integrated propagation equations

Main table

MOD		ARG		mod Y		arg Y	
1.0	x	-1	+1.57080	1.238	x	-2	-0.0004
1.0	x	-1	+1.48353	1.238	x	-2	+0.0869
1.0	x	-1	+1.39626	1.238	x	-2	+0.1742
1.0	x	-1	+1.30900	1.238	x	-2	+0.2614
1.0	x	-1	+1.22173	1.238	x	-2	+0.3486
1.0	x	-1	+1.13446	1.238	x	-2	+0.4361
1.0	x	-1	+1.04720	1.239	x	-2	+0.5231
1.0	x	-1	+0.95993	1.239	x	-2	+0.6103
1.0	x	-1	+0.87266	1.238	x	-2	+0.6978
1.0	x	-1	+0.78540	1.238	x	-2	+0.7851
2.0	x	-1	+1.57080	2.476	x	-2	-0.0009
2.0	x	-1	+1.48353	2.476	x	-2	+0.0864
2.0	x	-1	+1.39626	2.476	x	-2	+0.1737
2.0	x	-1	+1.30900	2.477	x	-2	+0.2609
2.0	x	-1	+1.22173	2.477	x	-2	+0.3483
2.0	x	-1	+1.13446	2.477	x	-2	+0.4355
2.0	x	-1	+1.04720	2.477	x	-2	+0.5229
2.0	x	-1	+0.95993	2.477	x	-2	+0.6104
2.0	x	-1	+0.87266	2.477	x	-2	+0.6974
2.0	x	-1	+0.78540	2.478	x	-2	+0.7848
5.0	x	-1	+1.57080	6.190	x	-2	-0.0022
5.0	x	-1	+1.48353	6.191	x	-2	+0.0851
5.0	x	-1	+1.39626	6.193	x	-2	+0.1723
5.0	x	-1	+1.30900	6.194	x	-2	+0.2596
5.0	x	-1	+1.22173	6.195	x	-2	+0.3470
5.0	x	-1	+1.13446	6.196	x	-2	+0.4343
5.0	x	-1	+1.04720	6.197	x	-2	+0.5216
5.0	x	-1	+0.95993	6.198	x	-2	+0.6090
5.0	x	-1	+0.87266	6.199	x	-2	+0.6965
5.0	x	-1	+0.78540	6.200	x	-2	+0.7838
1.0	x	+0	+1.57080	1.238	x	-1	-0.0044
1.0	x	+0	+1.48353	1.238	x	-1	+0.0829
1.0	x	+0	+1.39626	1.239	x	-1	+0.1702
1.0	x	+0	+1.30900	1.240	x	-1	+0.2575
1.0	x	+0	+1.22173	1.240	x	-1	+0.3449
1.0	x	+0	+1.13446	1.240	x	-1	+0.4324
1.0	x	+0	+1.04720	1.241	x	-1	+0.5198
1.0	x	+0	+0.95993	1.241	x	-1	+0.6074
1.0	x	+0	+0.87266	1.242	x	-1	+0.6947
1.0	x	+0	+0.78540	1.242	x	-1	+0.7823
2.0	x	+0	+1.57080	2.476	x	-1	-0.0088
2.0	x	+0	+1.48353	2.478	x	-1	+0.0785
2.0	x	+0	+1.39626	2.480	x	-1	+0.1658
2.0	x	+0	+1.30900	2.481	x	-1	+0.2533
2.0	x	+0	+1.22173	2.484	x	-1	+0.3407
2.0	x	+0	+1.13446	2.485	x	-1	+0.4282

MOD	ARG	mod Y	arg Y
2.0	n +0	+1.04720	2.487 n -1 +0.5160
2.0	n +0	+0.95993	2.489 n -1 +0.6037
2.0	n +0	+0.87266	2.490 n -1 +0.6916
2.0	n +0	+0.78540	2.492 n -1 +0.7792
5.0	n +0	+1.57080	6.188 n -1 -0.0219
5.0	n +0	+1.48353	6.200 n -1 +0.0654
5.0	n +0	+1.39626	6.212 n -1 +0.1528
5.0	n +0	+1.30900	6.224 n -1 +0.2404
5.0	n +0	+1.22173	6.235 n -1 +0.3282
5.0	n +0	+1.13446	6.246 n -1 +0.4162
5.0	n +0	+1.04720	6.258 n -1 +0.5043
5.0	n +0	+0.95993	6.268 n -1 +0.5926
5.0	n +0	+0.87266	6.278 n -1 +0.6809
5.0	n +0	+0.78540	6.288 n -1 +0.7695
1.0	n +1	+1.57080	1.236 n +0 -0.0439
1.0	n +1	+1.48353	1.241 n +0 +0.0434
1.0	n +1	+1.39626	1.246 n +0 +0.1310
1.0	n +1	+1.30900	1.251 n +0 +0.2188
1.0	n +1	+1.22173	1.256 n +0 +0.3069
1.0	n +1	+1.13446	1.260 n +0 +0.3955
1.0	n +1	+1.04720	1.265 n +0 +0.4845
1.0	n +1	+0.95993	1.269 n +0 +0.5736
1.0	n +1	+0.87266	1.273 n +0 +0.6633
1.0	n +1	+0.78540	1.277 n +0 +0.7530
2.0	n +1	+1.57080	2.463 n +0 -0.0874
2.0	n +1	+1.48353	2.482 n +0 -0.0007
2.0	n +1	+1.39626	2.501 n +0 +0.0867
2.0	n +1	+1.30900	2.521 n +0 +0.1747
2.0	n +1	+1.22173	2.541 n +0 +0.2635
2.0	n +1	+1.13446	2.560 n +0 +0.3530
2.0	n +1	+1.04720	2.579 n +0 +0.4432
2.0	n +1	+0.95993	2.599 n +0 +0.5341
2.0	n +1	+0.87266	2.616 n +0 +0.6255
2.0	n +1	+0.78540	2.634 n +0 +0.7180
5.0	n +1	+1.57080	6.000 n +0 -0.2138
5.0	n +1	+1.48353	6.109 n +0 -0.1312
5.0	n +1	+1.39626	6.226 n +0 -0.0471
5.0	n +1	+1.30900	6.350 n +0 +0.0386
5.0	n +1	+1.22173	6.479 n +0 +0.1261
5.0	n +1	+1.13446	6.615 n +0 +0.2154
5.0	n +1	+1.04720	6.755 n +0 +0.3066
5.0	n +1	+0.95993	6.899 n +0 +0.4001
5.0	n +1	+0.87266	7.045 n +0 +0.4959
5.0	n +1	+0.78540	7.190 n +0 +0.5939
1.0	n +2	+1.57080	1.105 n +1 -0.3984
1.0	n +2	+1.48353	1.139 n +1 -0.3278

MOD		ARG	mod Y		arg Y
1.0	x +2	+1.39626	1.175	x +1	-0.2562
1.0	x +2	+1.30900	1.217	x +1	-0.1827
1.0	x +2	+1.22173	1.264	x +1	-0.1073
1.0	x +2	+1.13446	1.317	x +1	-0.0293
1.0	x +2	+1.04720	1.378	x +1	+0.0520
1.0	x +2	+0.95993	1.442	x +1	+0.1363
1.0	x +2	+0.87266	1.516	x +1	+0.2256
1.0	x +2	+0.78540	1.599	x +1	+0.3204
2.0	x +2	+1.57080	1.763	x +1	-0.6445
2.0	x +2	+1.48353	1.820	x +1	-0.5978
2.0	x +2	+1.39626	1.885	x +1	-0.5523
2.0	x +2	+1.30900	1.960	x +1	-0.5077
2.0	x +2	+1.22173	2.046	x +1	-0.4646
2.0	x +2	+1.13446	2.149	x +1	-0.4353
2.0	x +2	+1.04720	2.275	x +1	-0.3983
2.0	x +2	+0.95993	2.426	x +1	-0.3629
2.0	x +2	+0.87266	2.610	x +1	-0.3299
2.0	x +2	+0.78540	2.839	x +1	-0.2992
5.0	x +2	+1.57080	2.501	x +1	-0.8488
5.0	x +2	+1.48353	2.513	x +1	-0.8214
5.0	x +2	+1.39626	2.525	x +1	-0.7972
5.0	x +2	+1.30900	2.544	x +1	-0.7810
5.0	x +2	+1.22173	2.538	x +1	-0.7598
5.0	x +2	+1.13446	2.540	x +1	-0.7478
5.0	x +2	+1.04720	2.535	x +1	-0.7413
5.0	x +2	+0.95993	2.525	x +1	-0.7414
5.0	x +2	+0.87266	2.507	x +1	-0.7484
5.0	x +2	+0.78540	2.479	x +1	-0.7651
1.0	x +3	+1.57080	3.254	x +1	-0.8337
1.0	x +3	+1.48353	3.233	x +1	-0.7946
1.0	x +3	+1.39626	3.207	x +1	-0.7554
1.0	x +3	+1.30900	3.176	x +1	-0.7159
1.0	x +3	+1.22173	3.135	x +1	-0.6751
1.0	x +3	+1.13446	3.088	x +1	-0.6335
1.0	x +3	+1.04720	3.028	x +1	-0.5898
1.0	x +3	+0.95993	2.953	x +1	-0.5434
1.0	x +3	+0.87266	2.862	x +1	-0.4929
1.0	x +3	+0.78540	2.748	x +1	-0.4374
2.0	x +3	+1.57080	4.559	x +1	-0.8056
2.0	x +3	+1.48353	4.554	x +1	-0.7616
2.0	x +3	+1.39626	4.551	x +1	-0.7171
2.0	x +3	+1.30900	4.549	x +1	-0.6720
2.0	x +3	+1.22173	4.550	x +1	-0.6271
2.0	x +3	+1.13446	4.557	x +1	-0.5807
2.0	x +3	+1.04720	4.573	x +1	-0.5338
2.0	x +3	+0.95993	4.602	x +1	-0.4861

MOD			ARG	mod Y			arg Y
2.0	n	+3	+0.87266	4.651	n	+1	-0.4379
2.0	n	+3	+0.78540	4.726	n	+1	-0.3857
5.0	n	+3	+1.57080	7.166	n	+1	-0.7991
5.0	n	+3	+1.48353	7.161	n	+1	-0.7561
5.0	n	+3	+1.39626	7.157	n	+1	-0.7129
5.0	n	+3	+1.30900	7.151	n	+1	-0.6698
5.0	n	+3	+1.22173	7.145	n	+1	-0.6266
5.0	n	+3	+1.13446	7.138	n	+1	-0.5832
5.0	n	+3	+1.04720	7.117	n	+1	-0.5398
5.0	n	+3	+0.95993	7.121	n	+1	-0.4954
5.0	n	+3	+0.87266	7.085	n	+1	-0.4508
5.0	n	+3	+0.78540	7.060	n	+1	-0.4044
1.0	n	+4	+1.57080	1.010	n	+2	-0.7954
1.0	n	+4	+1.48353	1.009	n	+2	-0.7518
1.0	n	+4	+1.39626	1.009	n	+2	-0.7086
1.0	n	+4	+1.30900	1.008	n	+2	-0.6654
1.0	n	+4	+1.22173	1.008	n	+2	-0.6221
1.0	n	+4	+1.13446	1.007	n	+2	-0.5789
1.0	n	+4	+1.04720	1.007	n	+2	-0.5356
1.0	n	+4	+0.95993	1.006	n	+2	-0.4921
1.0	n	+4	+0.87266	1.005	n	+2	-0.4487
1.0	n	+4	+0.78540	1.004	n	+2	-0.4048
2.0	n	+4	+1.57080	1.423	n	+2	-0.7922
2.0	n	+4	+1.48353	1.423	n	+2	-0.7491
2.0	n	+4	+1.39626	1.423	n	+2	-0.7058
2.0	n	+4	+1.30900	1.423	n	+2	-0.6622
2.0	n	+4	+1.22173	1.422	n	+2	-0.6192
2.0	n	+4	+1.13446	1.422	n	+2	-0.5755
2.0	n	+4	+1.04720	1.422	n	+2	-0.5322
2.0	n	+4	+0.95993	1.420	n	+2	-0.4886
2.0	n	+4	+0.87266	1.419	n	+2	-0.4453
2.0	n	+4	+0.78540	1.419	n	+2	-0.4017
5.0	n	+4	+1.57080	2.245	n	+2	-0.7895
5.0	n	+4	+1.48353	2.245	n	+2	-0.7463
5.0	n	+4	+1.39626	2.245	n	+2	-0.7028
5.0	n	+4	+1.30900	2.244	n	+2	-0.6594
5.0	n	+4	+1.22173	2.245	n	+2	-0.6161
5.0	n	+4	+1.13446	2.243	n	+2	-0.5723
5.0	n	+4	+1.04720	2.244	n	+2	-0.5289
5.0	n	+4	+0.95993	2.243	n	+2	-0.4846
5.0	n	+4	+0.87266	2.239	n	+2	-0.4416
5.0	n	+4	+0.78540	2.241	n	+2	-0.3971
1.0	n	+5	+1.57080	3.172	n	+2	-0.7885
1.0	n	+5	+1.48353	3.172	n	+2	-0.7448
1.0	n	+5	+1.39626	3.170	n	+2	-0.7012
1.0	n	+5	+1.30900	3.172	n	+2	-0.6593

MOD		ARG	mod Y		arg Y
1.0	n +5	+1.22173	3.186	n +2	-0.6130
1.0	n +5	+1.13446	3.171	n +2	-0.5708
1.0	n +5	+1.04720	3.169	n +2	-0.5263
1.0	n +5	+0.95993	3.167	n +2	-0.4830
1.0	n +5	+0.87266	3.163	n +2	-0.4413
1.0	n +5	+0.78540	3.167	n +2	-0.3965
2.0	n +5	+1.57080	4.478	n +2	-0.7846
2.0	n +5	+1.48353	4.481	n +2	-0.7440
2.0	n +5	+1.39626	4.481	n +2	-0.7004
2.0	n +5	+1.30900	4.473	n +2	-0.6578
2.0	n +5	+1.22173	4.487	n +2	-0.6148
2.0	n +5	+1.13446	4.478	n +2	-0.5680
2.0	n +5	+1.04720	4.468	n +2	-0.5283
2.0	n +5	+0.95993	4.478	n +2	-0.4825
2.0	n +5	+0.87266	4.478	n +2	-0.4392
2.0	n +5	+0.78540	4.476	n +2	-0.3881
5.0	n +5	+1.57080	7.077	n +2	-0.7865
5.0	n +5	+1.48353	7.087	n +2	-0.7429
5.0	n +5	+1.39626	7.079	n +2	-0.6997
5.0	n +5	+1.30900	7.077	n +2	-0.6551
5.0	n +5	+1.22173	7.096	n +2	-0.6122
5.0	n +5	+1.13446	7.076	n +2	-0.5686
5.0	n +5	+1.04720	7.080	n +2	-0.5256
5.0	n +5	+0.95993	7.077	n +2	-0.4814
5.0	n +5	+0.87266	7.078	n +2	-0.4388
5.0	n +5	+0.78540	7.077	n +2	-0.3945
1.0	n +6	+1.57080	1.000	n +3	-0.7877
1.0	n +6	+1.48353	1.001	n +3	-0.7428
1.0	n +6	+1.39626	9.997	n +2	-0.6988
1.0	n +6	+1.30900	1.001	n +3	-0.6555
1.0	n +6	+1.22173	1.001	n +3	-0.6123
1.0	n +6	+1.13446	1.001	n +3	-0.5685
1.0	n +6	+1.04720	1.001	n +3	-0.5247
1.0	n +6	+0.95993	1.001	n +3	-0.4812
1.0	n +6	+0.87266	9.914	n +2	-0.4436
1.0	n +6	+0.78540	1.001	n +3	-0.3940
2.0	n +6	+1.57080	1.415	n +3	-0.7859
2.0	n +6	+1.48353	1.415	n +3	-0.7423
2.0	n +6	+1.39626	1.415	n +3	-0.6991
2.0	n +6	+1.30900	1.415	n +3	-0.6551
2.0	n +6	+1.22173	1.414	n +3	-0.6125
2.0	n +6	+1.13446	1.415	n +3	-0.5680
2.0	n +6	+1.04720	1.415	n +3	-0.5244
2.0	n +6	+0.95993	1.417	n +3	-0.4801
2.0	n +6	+0.87266	1.415	n +3	-0.4373
2.0	n +6	+0.78540	1.416	n +3	-0.3950

MOD		ARG	mod Y		arg Y
5.0	x +6	+1.57080	2.237	x +3	-0.7857
5.0	x +6	+1.48353	2.247	x +3	-0.7413
5.0	x +6	+1.39626	2.236	x +3	-0.6990
5.0	x +6	+1.30900	2.237	x +3	-0.6551
5.0	x +6	+1.22173	2.236	x +3	-0.6118
5.0	x +6	+1.13446	2.241	x +3	-0.5676
5.0	x +6	+1.04720	2.234	x +3	-0.5199
5.0	x +6	+0.95993	2.236	x +3	-0.4809
5.0	x +6	+0.87266	2.229	x +3	-0.4362
5.0	x +6	+0.78540	2.237	x +3	-0.3934
1.0	x +7	+1.57080	3.163	x +3	-0.7856
1.0	x +7	+1.48353	3.154	x +3	-0.7405
1.0	x +7	+1.39626	3.164	x +3	-0.6986
1.0	x +7	+1.30900	3.164	x +3	-0.6549
1.0	x +7	+1.22173	3.163	x +3	-0.6119
1.0	x +7	+1.13446	3.163	x +3	-0.5677
1.0	x +7	+1.04720	3.160	x +3	-0.5251
1.0	x +7	+0.95993	3.164	x +3	-0.4800
1.0	x +7	+0.87266	3.158	x +3	-0.4445
1.0	x +7	+0.78540	3.144	x +3	-0.3947

Interpolation for main table

MOD range				ARG	Coeff	
1.0	n	-1	-> 2.0	n -1	+1.57080	+1.000
1.0	n	-1	-> 2.0	n -1	+1.48353	+0.999
1.0	n	-1	-> 2.0	n -1	+1.39626	+1.000
1.0	n	-1	-> 2.0	n -1	+1.30900	+1.000
1.0	n	-1	-> 2.0	n -1	+1.22173	+1.000
1.0	n	-1	-> 2.0	n -1	+1.13446	+0.999
1.0	n	-1	-> 2.0	n -1	+1.04720	+1.000
1.0	n	-1	-> 2.0	n -1	+0.95993	+1.000
1.0	n	-1	-> 2.0	n -1	+0.87266	+1.000
1.0	n	-1	-> 2.0	n -1	+0.78540	+1.000
2.0	n	-1	-> 5.0	n -1	+1.57080	+1.000
2.0	n	-1	-> 5.0	n -1	+1.48353	+1.000
2.0	n	-1	-> 5.0	n -1	+1.39626	+1.000
2.0	n	-1	-> 5.0	n -1	+1.30900	+1.000
2.0	n	-1	-> 5.0	n -1	+1.22173	+0.999
2.0	n	-1	-> 5.0	n -1	+1.13446	+0.999
2.0	n	-1	-> 5.0	n -1	+1.04720	+0.999
2.0	n	-1	-> 5.0	n -1	+0.95993	+0.999
2.0	n	-1	-> 5.0	n -1	+0.87266	+0.999
2.0	n	-1	-> 5.0	n -1	+0.78540	+0.999
5.0	n	-1	-> 1.0	n +0	+1.57080	+1.000
5.0	n	-1	-> 1.0	n +0	+1.48353	+1.000
5.0	n	-1	-> 1.0	n +0	+1.39626	+1.000
5.0	n	-1	-> 1.0	n +0	+1.30900	+0.999
5.0	n	-1	-> 1.0	n +0	+1.22173	+0.999
5.0	n	-1	-> 1.0	n +0	+1.13446	+0.999
5.0	n	-1	-> 1.0	n +0	+1.04720	+0.998
5.0	n	-1	-> 1.0	n +0	+0.95993	+0.999
5.0	n	-1	-> 1.0	n +0	+0.87266	+0.998
5.0	n	-1	-> 1.0	n +0	+0.78540	+0.998
1.0	n	+0	-> 2.0	n +0	+1.57080	+1.000
1.0	n	+0	-> 2.0	n +0	+1.48353	+0.999
1.0	n	+0	-> 2.0	n +0	+1.39626	+0.999
1.0	n	+0	-> 2.0	n +0	+1.30900	+0.999
1.0	n	+0	-> 2.0	n +0	+1.22173	+0.998
1.0	n	+0	-> 2.0	n +0	+1.13446	+0.997
1.0	n	+0	-> 2.0	n +0	+1.04720	+0.997
1.0	n	+0	-> 2.0	n +0	+0.95993	+0.996
1.0	n	+0	-> 2.0	n +0	+0.87266	+0.996
1.0	n	+0	-> 2.0	n +0	+0.78540	+0.995
2.0	n	+0	-> 5.0	n +0	+1.57080	+1.000
2.0	n	+0	-> 5.0	n +0	+1.48353	+0.999
2.0	n	+0	-> 5.0	n +0	+1.39626	+0.998
2.0	n	+0	-> 5.0	n +0	+1.30900	+0.996
2.0	n	+0	-> 5.0	n +0	+1.22173	+0.996
2.0	n	+0	-> 5.0	n +0	+1.13446	+0.994

MOD range				ARG		Coeff	
2.0	n	+0	-> 5.0	n	+0	+1.04720	+0.993
2.0	n	+0	-> 5.0	n	+0	+0.95993	+0.992
2.0	n	+0	-> 5.0	n	+0	+0.87266	+0.991
2.0	n	+0	-> 5.0	n	+0	+0.78540	+0.990
5.0	n	+0	-> 1.0	n	+1	+1.57080	+1.002
5.0	n	+0	-> 1.0	n	+1	+1.48353	+0.999
5.0	n	+0	-> 1.0	n	+1	+1.39626	+0.996
5.0	n	+0	-> 1.0	n	+1	+1.30900	+0.993
5.0	n	+0	-> 1.0	n	+1	+1.22173	+0.990
5.0	n	+0	-> 1.0	n	+1	+1.13446	+0.987
5.0	n	+0	-> 1.0	n	+1	+1.04720	+0.985
5.0	n	+0	-> 1.0	n	+1	+0.95993	+0.983
5.0	n	+0	-> 1.0	n	+1	+0.87266	+0.981
5.0	n	+0	-> 1.0	n	+1	+0.78540	+0.978
1.0	n	+1	-> 2.0	n	+1	+1.57080	+1.005
1.0	n	+1	-> 2.0	n	+1	+1.48353	+1.000
1.0	n	+1	-> 2.0	n	+1	+1.39626	+0.994
1.0	n	+1	-> 2.0	n	+1	+1.30900	+0.989
1.0	n	+1	-> 2.0	n	+1	+1.22173	+0.984
1.0	n	+1	-> 2.0	n	+1	+1.13446	+0.978
1.0	n	+1	-> 2.0	n	+1	+1.04720	+0.972
1.0	n	+1	-> 2.0	n	+1	+0.95993	+0.967
1.0	n	+1	-> 2.0	n	+1	+0.87266	+0.962
1.0	n	+1	-> 2.0	n	+1	+0.78540	+0.957
2.0	n	+1	-> 5.0	n	+1	+1.57080	+1.029
2.0	n	+1	-> 5.0	n	+1	+1.48353	+1.017
2.0	n	+1	-> 5.0	n	+1	+1.39626	+1.005
2.0	n	+1	-> 5.0	n	+1	+1.30900	+0.992
2.0	n	+1	-> 5.0	n	+1	+1.22173	+0.979
2.0	n	+1	-> 5.0	n	+1	+1.13446	+0.965
2.0	n	+1	-> 5.0	n	+1	+1.04720	+0.952
2.0	n	+1	-> 5.0	n	+1	+0.95993	+0.939
2.0	n	+1	-> 5.0	n	+1	+0.87266	+0.925
2.0	n	+1	-> 5.0	n	+1	+0.78540	+0.913
5.0	n	+1	-> 1.0	n	+2	+1.57080	+1.136
5.0	n	+1	-> 1.0	n	+2	+1.48353	+1.113
5.0	n	+1	-> 1.0	n	+2	+1.39626	+1.091
5.0	n	+1	-> 1.0	n	+2	+1.30900	+1.065
5.0	n	+1	-> 1.0	n	+2	+1.22173	+1.037
5.0	n	+1	-> 1.0	n	+2	+1.13446	+1.007
5.0	n	+1	-> 1.0	n	+2	+1.04720	+0.972
5.0	n	+1	-> 1.0	n	+2	+0.95993	+0.940
5.0	n	+1	-> 1.0	n	+2	+0.87266	+0.904
5.0	n	+1	-> 1.0	n	+2	+0.78540	+0.867
1.0	n	+2	-> 2.0	n	+2	+1.57080	+1.483
1.0	n	+2	-> 2.0	n	+2	+1.48353	+1.479

MOD range						ARG	Coeff	
1.0	n	+2	->	2.0	n	+2	+1.39626	+1.467
1.0	n	+2	->	2.0	n	+2	+1.30900	+1.455
1.0	n	+2	->	2.0	n	+2	+1.22173	+1.440
1.0	n	+2	->	2.0	n	+2	+1.13446	+1.414
1.0	n	+2	->	2.0	n	+2	+1.04720	+1.382
1.0	n	+2	->	2.0	n	+2	+0.95993	+1.333
1.0	n	+2	->	2.0	n	+2	+0.87266	+1.277
1.0	n	+2	->	2.0	n	+2	+0.78540	+1.208
2.0	n	+2	->	5.0	n	+2	+1.57080	+2.618
2.0	n	+2	->	5.0	n	+2	+1.48353	+2.837
2.0	n	+2	->	5.0	n	+2	+1.39626	+3.138
2.0	n	+2	->	5.0	n	+2	+1.30900	+3.514
2.0	n	+2	->	5.0	n	+2	+1.22173	+4.251
2.0	n	+2	->	5.0	n	+2	+1.13446	+5.494
2.0	n	+2	->	5.0	n	+2	+1.04720	+8.459
2.0	n	+2	->	5.0	n	+2	+0.95993	+22.988
2.0	n	+2	->	5.0	n	+2	+0.87266	-22.808
2.0	n	+2	->	5.0	n	+2	+0.78540	-6.753
5.0	n	+2	->	1.0	n	+3	+1.57080	+2.635
5.0	n	+2	->	1.0	n	+3	+1.48353	+2.752
5.0	n	+2	->	1.0	n	+3	+1.39626	+2.895
5.0	n	+2	->	1.0	n	+3	+1.30900	+3.127
5.0	n	+2	->	1.0	n	+3	+1.22173	+3.283
5.0	n	+2	->	1.0	n	+3	+1.13446	+3.544
5.0	n	+2	->	1.0	n	+3	+1.04720	+3.906
5.0	n	+2	->	1.0	n	+3	+0.95993	+4.420
5.0	n	+2	->	1.0	n	+3	+0.87266	+5.239
5.0	n	+2	->	1.0	n	+3	+0.78540	+6.733
1.0	n	+3	->	2.0	n	+3	+1.57080	+2.055
1.0	n	+3	->	2.0	n	+3	+1.48353	+2.023
1.0	n	+3	->	2.0	n	+3	+1.39626	+1.981
1.0	n	+3	->	2.0	n	+3	+1.30900	+1.928
1.0	n	+3	->	2.0	n	+3	+1.22173	+1.860
1.0	n	+3	->	2.0	n	+3	+1.13446	+1.781
1.0	n	+3	->	2.0	n	+3	+1.04720	+1.680
1.0	n	+3	->	2.0	n	+3	+0.95993	+1.563
1.0	n	+3	->	2.0	n	+3	+0.87266	+1.427
1.0	n	+3	->	2.0	n	+3	+0.78540	+1.278
2.0	n	+3	->	5.0	n	+3	+1.57080	+2.026
2.0	n	+3	->	5.0	n	+3	+1.48353	+2.025
2.0	n	+3	->	5.0	n	+3	+1.39626	+2.024
2.0	n	+3	->	5.0	n	+3	+1.30900	+2.026
2.0	n	+3	->	5.0	n	+3	+1.22173	+2.030
2.0	n	+3	->	5.0	n	+3	+1.13446	+2.031
2.0	n	+3	->	5.0	n	+3	+1.04720	+2.072
2.0	n	+3	->	5.0	n	+3	+0.95993	+2.099

MOD range				ARG	Coeff
2.0	n	+3	->	5.0 n +3	+0.87266 +2.177
2.0	n	+3	->	5.0 n +3	+0.78540 +2.283
5.0	n	+3	->	1.0 n +4	+1.57080 +2.019
5.0	n	+3	->	1.0 n +4	+1.48353 +2.021
5.0	n	+3	->	1.0 n +4	+1.39626 +2.020
5.0	n	+3	->	1.0 n +4	+1.30900 +2.018
5.0	n	+3	->	1.0 n +4	+1.22173 +2.016
5.0	n	+3	->	1.0 n +4	+1.13446 +2.028
5.0	n	+3	->	1.0 n +4	+1.04720 +2.000
5.0	n	+3	->	1.0 n +4	+0.95993 +2.006
5.0	n	+3	->	1.0 n +4	+0.87266 +1.981
5.0	n	+3	->	1.0 n +4	+0.78540 +1.966
1.0	n	+4	->	2.0 n +4	+1.57080 +2.023
1.0	n	+4	->	2.0 n +4	+1.48353 +2.017
1.0	n	+4	->	2.0 n +4	+1.39626 +2.014
1.0	n	+4	->	2.0 n +4	+1.30900 +2.012
1.0	n	+4	->	2.0 n +4	+1.22173 +2.012
1.0	n	+4	->	2.0 n +4	+1.13446 +2.009
1.0	n	+4	->	2.0 n +4	+1.04720 +2.008
1.0	n	+4	->	2.0 n +4	+0.95993 +2.010
1.0	n	+4	->	2.0 n +4	+0.87266 +2.009
1.0	n	+4	->	2.0 n +4	+0.78540 +2.006
2.0	n	+4	->	5.0 n +4	+1.57080 +2.009
2.0	n	+4	->	5.0 n +4	+1.48353 +2.010
2.0	n	+4	->	5.0 n +4	+1.39626 +2.010
2.0	n	+4	->	5.0 n +4	+1.30900 +2.010
2.0	n	+4	->	5.0 n +4	+1.22173 +2.007
2.0	n	+4	->	5.0 n +4	+1.13446 +2.010
2.0	n	+4	->	5.0 n +4	+1.04720 +2.008
2.0	n	+4	->	5.0 n +4	+0.95993 +2.004
2.0	n	+4	->	5.0 n +4	+0.87266 +2.011
2.0	n	+4	->	5.0 n +4	+0.78540 +2.004
5.0	n	+4	->	1.0 n +5	+1.57080 +2.005
5.0	n	+4	->	1.0 n +5	+1.48353 +2.005
5.0	n	+4	->	1.0 n +5	+1.39626 +2.009
5.0	n	+4	->	1.0 n +5	+1.30900 +2.004
5.0	n	+4	->	1.0 n +5	+1.22173 +1.979
5.0	n	+4	->	1.0 n +5	+1.13446 +2.004
5.0	n	+4	->	1.0 n +5	+1.04720 +2.007
5.0	n	+4	->	1.0 n +5	+0.95993 +2.009
5.0	n	+4	->	1.0 n +5	+0.87266 +2.006
5.0	n	+4	->	1.0 n +5	+0.78540 +2.006
1.0	n	+5	->	2.0 n +5	+1.57080 +2.010
1.0	n	+5	->	2.0 n +5	+1.48353 +2.006
1.0	n	+5	->	2.0 n +5	+1.39626 +2.003
1.0	n	+5	->	2.0 n +5	+1.30900 +2.016

MOD range						ARG	Coeff	
1.0	n	+5	->	2.0	n	+5	+1.22173	+2.025
1.0	n	+5	->	2.0	n	+5	+1.13446	+2.007
1.0	n	+5	->	2.0	n	+5	+1.04720	+2.018
1.0	n	+5	->	2.0	n	+5	+0.95993	+2.001
1.0	n	+5	->	2.0	n	+5	+0.87266	+1.994
1.0	n	+5	->	2.0	n	+5	+0.78540	+2.003
2.0	n	+5	->	5.0	n	+5	+1.57080	+2.002
2.0	n	+5	->	5.0	n	+5	+1.48353	+1.999
2.0	n	+5	->	5.0	n	+5	+1.39626	+2.003
2.0	n	+5	->	5.0	n	+5	+1.30900	+1.997
2.0	n	+5	->	5.0	n	+5	+1.22173	+1.999
2.0	n	+5	->	5.0	n	+5	+1.13446	+2.003
2.0	n	+5	->	5.0	n	+5	+1.04720	+1.991
2.0	n	+5	->	5.0	n	+5	+0.95993	+2.002
2.0	n	+5	->	5.0	n	+5	+0.87266	+2.002
2.0	n	+5	->	5.0	n	+5	+0.78540	+2.000
5.0	n	+5	->	1.0	n	+6	+1.57080	+2.002
5.0	n	+5	->	1.0	n	+6	+1.48353	+2.008
5.0	n	+5	->	1.0	n	+6	+1.39626	+2.008
5.0	n	+5	->	1.0	n	+6	+1.30900	+2.000
5.0	n	+5	->	1.0	n	+6	+1.22173	+2.016
5.0	n	+5	->	1.0	n	+6	+1.13446	+1.997
5.0	n	+5	->	1.0	n	+6	+1.04720	+2.002
5.0	n	+5	->	1.0	n	+6	+0.95993	+2.002
5.0	n	+5	->	1.0	n	+6	+0.87256	+2.057
5.0	n	+5	->	1.0	n	+6	+0.78540	+2.001
1.0	n	+6	->	2.0	n	+6	+1.57080	+2.000
1.0	n	+6	->	2.0	n	+6	+1.48353	+2.001
1.0	n	+6	->	2.0	n	+6	+1.39626	+1.996
1.0	n	+6	->	2.0	n	+6	+1.30900	+2.002
1.0	n	+6	->	2.0	n	+6	+1.22173	+2.005
1.0	n	+6	->	2.0	n	+6	+1.13446	+2.003
1.0	n	+6	->	2.0	n	+6	+1.04720	+2.001
1.0	n	+6	->	2.0	n	+6	+0.95993	+1.991
1.0	n	+6	->	2.0	n	+6	+0.87266	+1.947
1.0	n	+6	->	2.0	n	+6	+0.78540	+1.996
2.0	n	+6	->	5.0	n	+6	+1.57080	+2.001
2.0	n	+6	->	5.0	n	+6	+1.48353	+1.983
2.0	n	+6	->	5.0	n	+6	+1.39626	+2.001
2.0	n	+6	->	5.0	n	+6	+1.30900	+2.000
2.0	n	+6	->	5.0	n	+6	+1.22173	+2.000
2.0	n	+6	->	5.0	n	+6	+1.13446	+1.993
2.0	n	+6	->	5.0	n	+6	+1.04720	+2.006
2.0	n	+6	->	5.0	n	+6	+0.95993	+2.010
2.0	n	+6	->	5.0	n	+6	+0.87266	+2.018
2.0	n	+6	->	5.0	n	+6	+0.78540	+2.004

MOD range				ARG	Coeff
5.0	n	+6	-> 1.0 n +7	+1.57080	+2.000
5.0	n	+6	-> 1.0 n +7	+1.48353	+2.043
5.0	n	+6	-> 1.0 n +7	+1.39626	+1.997
5.0	n	+6	-> 1.0 n +7	+1.30900	+2.000
5.0	n	+6	-> 1.0 n +7	+1.22173	+1.997
5.0	n	+6	-> 1.0 n +7	+1.13446	+2.012
5.0	n	+6	-> 1.0 n +7	+1.04720	+2.000
5.0	n	+6	-> 1.0 n +7	+0.95993	+1.996
5.0	n	+6	-> 1.0 n +7	+0.87266	+1.989
5.0	n	+6	-> 1.0 n +7	+0.78540	+2.037

Sub - table (MOD = 50 - 5000)

MOD		ARG	mod Y	arg Y
5.0	n	+1	+1.57080	6.000 n +0 -0.2138
5.0	n	+1	+1.48353	6.109 n +0 -0.1312
5.0	n	+1	+1.39626	6.226 n +0 -0.0471
5.0	n	+1	+1.30900	6.350 n +0 +0.0386
5.0	n	+1	+1.22173	6.479 n +0 +0.1261
5.0	n	+1	+1.13446	6.615 n +0 +0.2154
5.0	n	+1	+1.04720	6.755 n +0 +0.3066
5.0	n	+1	+0.95993	6.899 n +0 +0.4001
5.0	r	+1	+0.87266	7.045 n +0 +0.4959
5.0	n	+1	+0.78540	7.190 n +0 +0.5939
6.4	n	+1	+1.57080	7.536 n +0 -0.2694
6.4	n	+1	+1.48353	7.705 n +0 -0.1897
6.4	n	+1	+1.39626	7.888 n +0 -0.1083
6.4	n	+1	+1.30900	8.087 n +0 -0.0252
6.4	n	+1	+1.22173	8.298 n +0 +0.0600
6.4	n	+1	+1.13446	8.525 n +0 +0.1475
6.4	n	+1	+1.04720	8.764 n +0 +0.2376
6.4	n	+1	+0.95993	9.016 n +0 +0.3305
6.4	n	+1	+0.87266	9.278 n +0 +0.4265
6.4	n	+1	+0.78540	9.549 n +0 +0.5258
8.0	n	+1	+1.57080	9.178 n +0 -0.3293
8.0	n	+1	+1.48353	9.421 n +0 -0.2535
8.0	n	+1	+1.39626	9.689 n +0 -0.1762
8.0	n	+1	+1.30900	9.983 n +0 -0.0969
8.0	n	+1	+1.22173	1.030 n +1 -0.0153
8.0	n	+1	+1.13446	1.066 n +1 +0.0688
8.0	n	+1	+1.04720	1.104 n +1 +0.1557
8.0	n	+1	+0.95993	1.146 n +1 +0.2463
8.0	n	+1	+0.87266	1.190 n +1 +0.3407
8.0	n	+1	+0.78540	1.238 n +1 +0.4397
1.0	n	+2	+1.57080	1.105 n +1 -0.3984
1.0	n	+2	+1.48353	1.139 n +1 -0.3278
1.0	n	+2	+1.39626	1.175 n +1 -0.2562
1.0	r	+2	+1.30900	1.217 n +1 -0.1827
1.0	n	+2	+1.22173	1.264 n +1 -0.1073
1.0	n	+2	+1.13446	1.317 n +1 -0.0293
1.0	n	+2	+1.04720	1.378 n +1 +0.0520
1.0	n	+2	+0.95993	1.442 n +1 +0.1363
1.0	n	+2	+0.87266	1.516 n +1 +0.2256
1.0	n	+2	+0.78540	1.599 n +1 +0.3204
1.2	n	+2	+1.57080	1.271 n +1 -0.4603
1.2	n	+2	+1.48353	1.312 n +1 -0.3956
1.2	n	+2	+1.39626	1.359 n +1 -0.3298
1.2	n	+2	+1.30900	1.412 n +1 -0.2628
1.2	n	+2	+1.22173	1.473 n +1 -0.1943
1.2	n	+2	+1.13446	1.542 n +1 -0.1239

MOD			ARG	mod Y			arg Y
1.2	n	+2	+1.04720	1.622	n	+1	-0.0510
1.2	n	+2	+0.95993	1.720	n	+1	+0.0260
1.2	n	+2	+0.87266	1.827	n	+1	+0.1075
1.2	n	+2	+0.78540	1.951	n	+1	+0.1946
1.6	n	+2	+1.57080	1.548	n	+1	-0.5641
1.6	n	+2	+1.48353	1.600	n	+1	-0.5095
1.6	n	+2	+1.39626	1.660	n	+1	-0.4550
1.6	n	+2	+1.30900	1.729	n	+1	-0.4004
1.6	n	+2	+1.22173	1.808	n	+1	-0.3459
1.6	n	+2	+1.13446	1.900	n	+1	-0.2915
1.6	n	+2	+1.04720	2.023	n	+1	-0.2414
1.6	n	+2	+0.95993	2.158	n	+1	-0.1854
1.6	n	+2	+0.87266	2.322	n	+1	-0.1275
1.6	n	+2	+0.78540	2.523	n	+1	-0.0670
2.0	n	+2	+1.57080	1.763	n	+1	-0.6445
2.0	n	+2	+1.48353	1.820	n	+1	-0.5978
2.0	n	+2	+1.39626	1.885	n	+1	-0.5523
2.0	n	+2	+1.30900	1.960	n	+1	-0.5077
2.0	n	+2	+1.22173	2.046	n	+1	-0.4646
2.0	n	+2	+1.13446	2.149	n	+1	-0.4353
2.0	n	+2	+1.04720	2.275	n	+1	-0.3983
2.0	n	+2	+0.95993	2.426	n	+1	-0.3629
2.0	n	+2	+0.87266	2.610	n	+1	-0.3299
2.0	n	+2	+0.78540	2.839	n	+1	-0.2992
2.5	n	+2	+1.57080	1.969	n	+1	-0.7189
2.5	n	+2	+1.48353	2.027	n	+1	-0.6802
2.5	n	+2	+1.39626	2.093	n	+1	-0.6424
2.5	n	+2	+1.30900	2.166	n	+1	-0.6066
2.5	n	+2	+1.22173	2.227	n	+1	-0.5879
2.5	n	+2	+1.13446	2.324	n	+1	-0.5633
2.5	n	+2	+1.04720	2.438	n	+1	-0.5426
2.5	n	+2	+0.95993	2.575	n	+1	-0.5266
2.5	n	+2	+0.87266	2.739	n	+1	-0.5171
2.5	n	+2	+0.78540	2.936	n	+1	-0.5142
3.2	n	+2	+1.57080	2.155	n	+1	-0.7857
3.2	n	+2	+1.48353	2.198	n	+1	-0.7555
3.2	n	+2	+1.39626	2.248	n	+1	-0.7281
3.2	n	+2	+1.30900	2.303	n	+1	-0.7049
3.2	n	+2	+1.22173	2.366	n	+1	-0.6857
3.2	n	+2	+1.13446	2.446	n	+1	-0.6759
3.2	n	+2	+1.04720	2.515	n	+1	-0.6636
3.2	n	+2	+0.95993	2.605	n	+1	-0.6624
3.2	n	+2	+0.87266	2.709	n	+1	-0.6695
3.2	n	+2	+0.78540	2.828	n	+1	-0.6867
4.0	n	+2	+1.57080	2.326	n	+1	-0.8264
4.0	n	+2	+1.48353	2.355	n	+1	-0.7992

MOD		ARG	mod Y		arg Y
4.0	x +2	+1.39626	2.386	x +1	-0.7753
4.0	x +2	+1.30900	2.419	x +1	-0.7556
4.0	x +2	+1.22173	2.453	x +1	-0.7398
4.0	x +2	+1.13446	2.490	x +1	-0.7297
4.0	x +2	+1.04720	2.527	x +1	-0.7261
4.0	x +2	+0.95993	2.566	x +1	-0.7294
4.0	x +2	+0.87266	2.605	x +1	-0.7417
4.0	x +2	+0.78540	2.646	x +1	-0.7637
5.0	x +2	+1.57080	2.501	x +1	-0.8488
5.0	x +2	+1.48353	2.513	x +1	-0.8214
5.0	x +2	+1.39626	2.525	x +1	-0.7972
5.0	x +2	+1.30900	2.544	x +1	-0.7810
5.0	x +2	+1.22173	2.538	x +1	-0.7598
5.0	x +2	+1.13446	2.540	x +1	-0.7478
5.0	x +2	+1.04720	2.535	x +1	-0.7413
5.0	x +2	+0.95993	2.525	x +1	-0.7414
5.0	x +2	+0.87266	2.507	x +1	-0.7484
5.0	x +2	+0.78540	2.479	x +1	-0.7651
6.4	x +2	+1.57080	2.720	x +1	-0.8541
6.4	x +2	+1.48353	2.728	x +1	-0.8279
6.4	x +2	+1.39626	2.706	x +1	-0.7956
6.4	x +2	+1.30900	2.691	x +1	-0.7699
6.4	x +2	+1.22173	2.669	x +1	-0.7467
6.4	x +2	+1.13446	2.638	x +1	-0.7264
6.4	x +2	+1.04720	2.596	x +1	-0.7099
6.4	x +2	+0.95993	2.541	x +1	-0.6974
6.4	x +2	+0.87266	2.472	x +1	-0.6897
6.4	x +2	+0.78540	2.395	x +1	-0.6935
8.0	x +2	+1.57080	2.959	x +1	-0.8468
8.0	x +2	+1.48353	2.944	x +1	-0.8123
8.0	x +2	+1.39626	2.923	x +1	-0.7784
8.0	x +2	+1.30900	2.906	x +1	-0.7496
8.0	x +2	+1.22173	2.856	x +1	-0.7138
8.0	x +2	+1.13446	2.819	x +1	-0.6869
8.0	x +2	+1.04720	2.749	x +1	-0.6520
8.0	x +2	+0.95993	2.672	x +1	-0.6225
8.0	x +2	+0.87266	2.576	x +1	-0.5942
8.0	x +2	+0.78540	2.457	x +1	-0.5661
1.0	x +3	+1.57080	3.254	x +1	-0.8337
1.0	x +3	+1.48353	3.233	x +1	-0.7946
1.0	x +3	+1.39626	3.207	x +1	-0.7554
1.0	x +3	+1.30900	3.176	x +1	-0.7159
1.0	x +3	+1.22173	3.135	x +1	-0.6751
1.0	x +3	+1.13446	3.088	x +1	-0.6335
1.0	x +3	+1.04720	3.028	x +1	-0.5898
1.0	x +3	+0.95993	2.953	x +1	-0.5431

MOD		ARG	mod Y		arg Y
1.0	n +3	+0.87266	2.862	n +1	-0.4929
1.0	n +3	+0.78540	2.748	n +1	-0.4374
1.2	n +3	+1.57080	3.539	n +1	-0.8230
1.2	n +3	+1.48353	3.520	n +1	-0.7810
1.2	n +3	+1.39626	3.498	n +1	-0.7383
1.2	n +3	+1.30900	3.470	n +1	-0.6946
1.2	n +3	+1.22173	3.437	n +1	-0.6490
1.2	n +3	+1.13446	3.401	n +1	-0.6016
1.2	n +3	+1.04720	3.356	n +1	-0.5506
1.2	n +3	+0.95993	3.304	n +1	-0.4955
1.2	n +3	+0.87266	3.242	n +1	-0.4339
1.2	n +3	+0.78540	3.172	n +1	-0.3642
1.6	n +3	+1.57080	4.076	n +1	-0.8106
1.6	n +3	+1.48353	4.065	n +1	-0.7663
1.6	n +3	+1.39626	4.053	n +1	-0.7215
1.6	n +3	+1.30900	4.041	n +1	-0.6753
1.6	n +3	+1.22173	4.030	n +1	-0.6286
1.6	n +3	+1.13446	4.022	n +1	-0.5791
1.6	n +3	+1.04720	4.017	n +1	-0.5269
1.6	n +3	+0.95993	4.018	n +1	-0.4714
1.6	n +3	+0.87266	4.032	n +1	-0.4113
1.6	n +3	+0.78540	4.063	n +1	-0.3455
2.0	n +3	+1.57080	4.559	n +1	-0.8056
2.0	n +3	+1.48353	4.554	n +1	-0.7616
2.0	n +3	+1.39626	4.551	n +1	-0.7171
2.0	n +3	+1.30900	4.549	n +1	-0.6720
2.0	n +3	+1.22173	4.550	n +1	-0.6271
2.0	n +3	+1.13446	4.557	n +1	-0.5807
2.0	n +3	+1.04720	4.573	n +1	-0.5338
2.0	n +3	+0.95993	4.602	n +1	-0.4861
2.0	n +3	+0.87266	4.651	n +1	-0.4379
2.0	n +3	+0.78540	4.726	n +1	-0.3857
2.5	n +3	+1.57080	5.096	n +1	-0.8036
2.5	n +3	+1.48353	5.093	n +1	-0.7604
2.5	n +3	+1.39626	5.093	n +1	-0.7168
2.5	n +3	+1.30900	5.095	n +1	-0.6735
2.5	n +3	+1.22173	5.098	n +1	-0.6304
2.5	n +3	+1.13446	5.105	n +1	-0.5876
2.5	n +3	+1.04720	5.120	n +1	-0.5454
2.5	n +3	+0.95993	5.142	n +1	-0.5046
2.5	n +3	+0.87266	5.172	n +1	-0.4665
2.5	n +3	+0.78540	5.217	n +1	-0.4322
3.2	n +3	+1.57080	5.756	n +1	-0.8022
3.2	n +3	+1.48353	5.753	n +1	-0.7595
3.2	n +3	+1.39626	5.751	n +1	-0.7167
3.2	n +3	+1.30900	5.748	n +1	-0.6740

MOD		ARC	mod Y		arg Y
3.2	x +3	+1.22173	5.746	x +1	-0.6317
3.2	x +3	+1.13446	5.749	x +1	-0.5907
3.2	x +3	+1.04720	5.740	x +1	-0.5491
3.2	x +3	+0.95993	5.733	x +1	-0.5093
3.2	x +3	+0.87266	5.719	x +1	-0.4712
3.2	x +3	+0.78540	5.691	x +1	-0.4350
4.0	x +3	+1.57080	6.421	x +1	-0.8008
4.0	x +3	+1.48353	6.417	x +1	-0.7581
4.0	x +3	+1.39626	6.412	x +1	-0.7150
4.0	x +3	+1.30900	6.407	x +1	-0.6723
4.0	x +3	+1.22173	6.401	x +1	-0.6296
4.0	x +3	+1.13446	6.408	x +1	-0.5922
4.0	x +3	+1.04720	6.378	x +1	-0.5462
4.0	x +3	+0.95993	6.360	x +1	-0.5027
4.0	x +3	+0.87266	6.331	x +1	-0.4625
4.0	x +3	+0.78540	6.296	x +1	-0.4145
5.0	x +3	+1.57080	7.166	x +1	-0.7991
5.0	x +3	+1.48353	7.161	x +1	-0.7561
5.0	x +3	+1.39626	7.157	x +1	-0.7129
5.0	x +3	+1.30900	7.151	x +1	-0.6698
5.0	x +3	+1.22173	7.145	x +1	-0.6266
5.0	x +3	+1.13446	7.156	x +1	-0.5870
5.0	x +3	+1.04720	7.117	x +1	-0.5398
5.0	x +3	+0.95993	7.121	x +1	-0.4954
5.0	x +3	+0.87266	7.085	x +1	-0.4508
5.0	x +3	+0.78540	7.060	x +1	-0.4044

Interpolation for sub-table

MOD range				ARG	Coeff	
5.0	x	+1	-> 6.4	x +1	+1.57080	+1.083
5.0	x	+1	-> 6.4	x +1	+1.48353	+1.064
5.0	x	+1	-> 6.4	x +1	+1.39626	+1.043
5.0	x	+1	-> 6.4	x +1	+1.30900	+1.021
5.0	x	+1	-> 6.4	x +1	+1.22173	+0.998
5.0	x	+1	-> 6.4	x +1	+1.13446	+0.973
5.0	x	+1	-> 6.4	x +1	+1.04720	+0.948
5.0	x	+1	-> 6.4	x +1	+0.95993	+0.922
5.0	x	+1	-> 6.4	x +1	+0.87266	+0.896
5.0	x	+1	-> 6.4	x +1	+0.78540	+0.870
6.4	x	+1	-> 8.0	x +1	+1.57080	+1.132
6.4	x	+1	-> 8.0	x +1	+1.48353	+1.110
6.4	x	+1	-> 8.0	x +1	+1.39626	+1.085
6.4	x	+1	-> 8.0	x +1	+1.30900	+1.059
6.4	x	+1	-> 8.0	x +1	+1.22173	+1.032
6.4	x	+1	-> 8.0	x +1	+1.13446	+1.000
6.4	x	+1	-> 8.0	x +1	+1.04720	+0.965
6.4	x	+1	-> 8.0	x +1	+0.95993	+0.932
6.4	x	+1	-> 8.0	x +1	+0.87266	+0.895
6.4	x	+1	-> 8.0	x +1	+0.78540	+0.860
8.0	x	+1	-> 1.0	x +2	+1.57080	+1.205
8.0	x	+1	-> 1.0	x +2	+1.48353	+1.178
8.0	x	+1	-> 1.0	x +2	+1.39626	+1.155
8.0	x	+1	-> 1.0	x +2	+1.30900	+1.125
8.0	x	+1	-> 1.0	x +2	+1.22173	+1.089
8.0	x	+1	-> 1.0	x +2	+1.13446	+1.055
8.0	x	+1	-> 1.0	x +2	+1.04720	+1.009
8.0	x	+1	-> 1.0	x +2	+0.95993	+0.969
8.0	x	+1	-> 1.0	x +2	+0.87266	+0.922
8.0	x	+1	-> 1.0	x +2	+0.78540	+0.871
1.0	x	+2	-> 1.2	x +2	+1.57080	+1.296
1.0	x	+2	-> 1.2	x +2	+1.48353	+1.284
1.0	x	+2	-> 1.2	x +2	+1.39626	+1.254
1.0	x	+2	-> 1.2	x +2	+1.30900	+1.226
1.0	x	+2	-> 1.2	x +2	+1.22173	+1.195
1.0	x	+2	-> 1.2	x +2	+1.13446	+1.154
1.0	x	+2	-> 1.2	x +2	+1.04720	+1.117
1.0	x	+2	-> 1.2	x +2	+0.95993	+1.037
1.0	x	+2	-> 1.2	x +2	+0.87266	+0.980
1.0	x	+2	-> 1.2	x +2	+0.78540	+0.918
1.2	x	+2	-> 1.6	x +2	+1.57080	+1.462
1.2	x	+2	-> 1.6	x +2	+1.48353	+1.451
1.2	x	+2	-> 1.6	x +2	+1.39626	+1.440
1.2	x	+2	-> 1.6	x +2	+1.30900	+1.424
1.2	x	+2	-> 1.6	x +2	+1.22173	+1.402
1.2	x	+2	-> 1.6	x +2	+1.13446	+1.377

MOD range				ARG		Coeff		
1.2	n	+2	->	1.6	n	+2	+1.04720	+1.304
1.2	n	+2	->	1.6	n	+2	+0.95993	+1.267
1.2	n	+2	->	1.6	n	+2	+0.87266	+1.199
1.2	n	+2	->	1.6	n	+2	+0.78540	+1.119
1.6	n	+2	->	2.0	n	+2	+1.57080	+1.717
1.6	n	+2	->	2.0	n	+2	+1.48353	+1.738
1.6	n	+2	->	2.0	n	+2	+1.39626	+1.752
1.6	n	+2	->	2.0	n	+2	+1.30900	+1.775
1.6	n	+2	->	2.0	n	+2	+1.22173	+1.806
1.6	n	+2	->	2.0	n	+2	+1.13446	+1.810
1.6	n	+2	->	2.0	n	+2	+1.04720	+1.898
1.6	n	+2	->	2.0	n	+2	+0.95993	+1.906
1.6	n	+2	->	2.0	n	+2	+0.87266	+1.909
1.6	n	+2	->	2.0	n	+2	+0.78540	+1.888
2.0	n	+2	->	2.5	n	+2	+1.57080	+2.011
2.0	n	+2	->	2.5	n	+2	+1.48353	+2.065
2.0	n	+2	->	2.5	n	+2	+1.39626	+2.133
2.0	n	+2	->	2.5	n	+2	+1.30900	+2.231
2.0	n	+2	->	2.5	n	+2	+1.22173	+2.632
2.0	n	+2	->	2.5	n	+2	+1.13446	+2.857
2.0	n	+2	->	2.5	n	+2	+1.04720	+3.222
2.0	n	+2	->	2.5	n	+2	+0.95993	+3.750
2.0	n	+2	->	2.5	n	+2	+0.87266	+4.614
2.0	n	+2	->	2.5	n	+2	+0.78540	+6.675
2.5	n	+2	->	3.2	n	+2	+1.57080	+2.747
2.5	n	+2	->	3.2	n	+2	+1.48353	+3.052
2.5	n	+2	->	3.2	n	+2	+1.39626	+3.459
2.5	n	+2	->	3.2	n	+2	+1.30900	+4.047
2.5	n	+2	->	3.2	n	+2	+1.22173	+4.081
2.5	n	+2	->	3.2	n	+2	+1.13446	+4.840
2.5	n	+2	->	3.2	n	+2	+1.04720	+7.990
2.5	n	+2	->	3.2	n	+2	+0.95993	+21.253
2.5	n	+2	->	3.2	n	+2	+0.87266	-22.155
2.5	n	+2	->	3.2	n	+2	+0.78540	-6.608
3.2	n	+2	->	4.0	n	+2	+1.57080	+2.911
3.2	n	+2	->	4.0	n	+2	+1.48353	+3.236
3.2	n	+2	->	4.0	n	+2	+1.39626	+3.749
3.2	n	+2	->	4.0	n	+2	+1.30900	+4.516
3.2	n	+2	->	4.0	n	+2	+1.22173	+6.132
3.2	n	+2	->	4.0	n	+2	+1.13446	+12.412
3.2	n	+2	->	4.0	n	+2	+1.04720	+44.305
3.2	n	+2	->	4.0	n	+2	+0.95993	-14.793
3.2	n	+2	->	4.0	n	+2	+0.87266	-5.735
3.2	n	+2	->	4.0	n	+2	+0.78540	-3.352
4.0	n	+2	->	5.0	n	+2	+1.57080	+3.078
4.0	n	+2	->	5.0	n	+2	+1.48353	+3.428

MOD range				ARG	Coeff	
4.0	n	+2	-> 5.0	n +2	+1.39626	+3.950
4.0	n	+2	-> 5.0	n +2	+1.30900	+4.436
4.0	n	+2	-> 5.0	n +2	+1.22173	+6.585
4.0	n	+2	-> 5.0	n +2	+1.13446	+11.324
4.0	n	+2	-> 5.0	n +2	+1.04720	+71.386
4.0	n	+2	-> 5.0	n +2	+0.95993	-13.794
4.0	n	+2	-> 5.0	n +2	+0.87266	-5.798
4.0	n	+2	-> 5.0	n +2	+0.78540	-3.423
5.0	n	+2	-> 6.4	n +2	+1.57080	+2.939
5.0	n	+2	-> 6.4	n +2	+1.48353	+3.184
5.0	n	+2	-> 6.4	n +2	+1.39626	+3.552
5.0	n	+2	-> 6.4	n +2	+1.30900	+4.404
5.0	n	+2	-> 6.4	n +2	+1.22173	+4.895
5.0	n	+2	-> 6.4	n +2	+1.13446	+6.503
5.0	n	+2	-> 6.4	n +2	+1.04720	+10.417
5.0	n	+2	-> 6.4	n +2	+0.95993	+37.684
5.0	n	+2	-> 6.4	n +2	+0.87266	-17.583
5.0	n	+2	-> 6.4	n +2	+0.78540	-7.184
6.4	n	+2	-> 8.0	n +2	+1.57080	+2.651
6.4	n	+2	-> 8.0	n +2	+1.48353	+2.766
6.4	n	+2	-> 8.0	n +2	+1.39626	+2.902
6.4	n	+2	-> 8.0	n +2	+1.30900	+2.902
6.4	n	+2	-> 8.0	n +2	+1.22173	+3.295
6.4	n	+2	-> 8.0	n +2	+1.13446	+3.352
6.4	n	+2	-> 8.0	n +2	+1.04720	+3.902
6.4	n	+2	-> 8.0	n +2	+0.95993	+4.443
6.4	n	+2	-> 8.0	n +2	+0.87266	+5.441
6.4	n	+2	-> 8.0	n +2	+0.78540	+8.708
8.0	n	+2	-> 1.0	n +3	+1.57080	+2.352
8.0	n	+2	-> 1.0	n +3	+1.48353	+2.383
8.0	n	+2	-> 1.0	n +3	+1.39626	+2.399
8.0	n	+2	-> 1.0	n +3	+1.30900	+2.515
8.0	n	+2	-> 1.0	n +3	+1.22173	+2.400
8.0	n	+2	-> 1.0	n +3	+1.13446	+2.451
8.0	n	+2	-> 1.0	n +3	+1.04720	+2.311
8.0	n	+2	-> 1.0	n +3	+0.95993	+2.234
8.0	n	+2	-> 1.0	n +3	+0.87266	+2.119
8.0	n	+2	-> 1.0	n +3	+0.78540	+1.998
1.0	n	+3	-> 1.2	n +3	+1.57080	+2.166
1.0	n	+3	-> 1.2	n +3	+1.48353	+2.144
1.0	n	+3	-> 1.2	n +3	+1.39626	+2.105
1.0	n	+3	-> 1.2	n +3	+1.30900	+2.056
1.0	n	+3	-> 1.2	n +3	+1.22173	+1.982
1.0	n	+3	-> 1.2	n +3	+1.13446	+1.888
1.0	n	+3	-> 1.2	n +3	+1.04720	+1.770
1.0	n	+3	-> 1.2	n +3	+0.95993	+1.621

MOD range				ARG		Coeff	
1.0	n	+3	-> 1.2	n	+3	+0.87266	+1.459
1.0	n	+3	-> 1.2	n	+3	+0.78540	+1.269
1.2	n	+3	-> 1.6	n	+3	+1.57080	+2.037
1.2	n	+3	-> 1.6	n	+3	+1.48353	+1.998
1.2	n	+3	-> 1.6	n	+3	+1.39626	+1.953
1.2	n	+3	-> 1.6	n	+3	+1.30900	+1.889
1.2	n	+3	-> 1.6	n	+3	+1.22173	+1.805
1.2	n	+3	-> 1.6	n	+3	+1.13446	+1.717
1.2	n	+3	-> 1.6	n	+3	+1.04720	+1.601
1.2	n	+3	-> 1.6	n	+3	+0.95993	+1.471
1.2	n	+3	-> 1.6	n	+3	+0.87266	+1.320
1.2	n	+3	-> 1.6	n	+3	+0.78540	+1.162
1.6	n	+3	-> 2.0	n	+3	+1.57080	+1.994
1.6	n	+3	-> 2.0	n	+3	+1.48353	+1.964
1.6	n	+3	-> 2.0	n	+3	+1.39626	+1.925
1.6	n	+3	-> 2.0	n	+3	+1.30900	+1.884
1.6	n	+3	-> 2.0	n	+3	+1.22173	+1.841
1.6	n	+3	-> 2.0	n	+3	+1.13446	+1.786
1.6	n	+3	-> 2.0	n	+3	+1.04720	+1.720
1.6	n	+3	-> 2.0	n	+3	+0.95993	+1.645
1.6	n	+3	-> 2.0	n	+3	+0.87266	+1.564
1.6	n	+3	-> 2.0	n	+3	+0.78540	+1.476
2.0	n	+3	-> 2.5	n	+3	+1.57080	+2.005
2.0	n	+3	-> 2.5	n	+3	+1.48353	+1.997
2.0	n	+3	-> 2.5	n	+3	+1.39626	+1.982
2.0	n	+3	-> 2.5	n	+3	+1.30900	+1.967
2.0	n	+3	-> 2.5	n	+3	+1.22173	+1.962
2.0	n	+3	-> 2.5	n	+3	+1.13446	+1.964
2.0	n	+3	-> 2.5	n	+3	+1.04720	+1.977
2.0	n	+3	-> 2.5	n	+3	+0.95993	+2.012
2.0	n	+3	-> 2.5	n	+3	+0.87266	+2.102
2.0	n	+3	-> 2.5	n	+3	+0.78540	+2.260
2.5	n	+3	-> 3.2	n	+3	+1.57080	+2.026
2.5	n	+3	-> 3.2	n	+3	+1.48353	+2.026
2.5	n	+3	-> 3.2	n	+3	+1.39626	+2.032
2.5	n	+3	-> 3.2	n	+3	+1.30900	+2.050
2.5	n	+3	-> 3.2	n	+3	+1.22173	+2.063
2.5	n	+3	-> 3.2	n	+3	+1.13446	+2.078
2.5	n	+3	-> 3.2	n	+3	+1.04720	+2.159
2.5	n	+3	-> 3.2	n	+3	+0.95993	+2.270
2.5	n	+3	-> 3.2	n	+3	+0.87266	+2.453
2.5	n	+3	-> 3.2	n	+3	+0.78540	+2.837
3.2	n	+3	-> 4.0	n	+3	+1.57080	+2.040
3.2	n	+3	-> 4.0	n	+3	+1.48353	+2.042
3.2	n	+3	-> 4.0	n	+3	+1.39626	+2.050
3.2	n	+3	-> 4.0	n	+3	+1.30900	+2.055

MOD range				ARG	Coeff	
3.2	n	+3	-> 4.0	n +3	+1.22173	+2.066
3.2	n	+3	-> 4.0	n +3	+1.13446	+2.056
3.2	n	+3	-> 4.0	n +3	+1.04720	+2.117
3.2	n	+3	-> 4.0	n +3	+0.95993	+2.149
3.2	n	+3	-> 4.0	n +3	+0.87266	+2.195
3.2	n	+3	-> 4.0	n +3	+0.78540	+2.207
4.0	n	+3	-> 5.0	n +3	+1.57080	+2.034
4.0	n	+3	-> 5.0	n +3	+1.48353	+2.035
4.0	n	+3	-> 5.0	n +3	+1.39626	+2.031
4.0	n	+3	-> 5.0	n +3	+1.30900	+2.031
4.0	n	+3	-> 5.0	n +3	+1.22173	+2.029
4.0	n	+3	-> 5.0	n +3	+1.13446	+2.023
4.0	n	+3	-> 5.0	n +3	+1.04720	+2.035
4.0	n	+3	-> 5.0	n +3	+0.95993	+1.974
4.0	n	+3	-> 5.0	n +3	+0.87266	+1.984
4.0	n	+3	-> 5.0	n +3	+0.78540	+1.948

The final program shown in the next few pages performs the operations described in Section 3.1. The results for the coupled values of γ are printed in cartesian form and a small subsidiary program (not shown) was used to convert these to polar form as presented in Section 3.2.

B.3. Algol programme for integration procedure

The Algol programme shown in the next few pages performs the procedure described in Section B.1. The results for the complex values of Y are punched in cartesian form and a small subsidiary programme (not shown) was used to convert these to polar form as presented in Section B.2.

→ESTABLISH DA1201000AFU;
CYLINDRICAL PROPAGATION;
O/P L;→

begin library A0,A6;
real x,h,P,Q,mod,arg,M,B; integer k,s,t,u,v,n,l,I,A,N,NI;
boolean f1;
array y1[1:2], y2[1:2], F[1:2], f[1:2], T[0:500],
MOD[1:50], ARG[1:50],Z[1:2,0:500], Y1[1:2];

real procedure DE(ya,yb,t,n);
value ya,yb,t,n;
real ya,yb,t; integer n;

begin if n=1 then DE:=3xya/(t+1)+2xyaxyb+modxsln(arg)
else DE:=3xyb/(t+1)+yb↑2-ya↑2+modxcos(arg);

end DE ;

procedure RKOST(x,h,y1,y2);

value x,h,y1;
real x,h; array y1, y2;

begin real xe; array k[1:2,0:4]; integer p,q;

k[1,0]:=k[2,0]:=0;
for q:=1 step 1 until 4 do
begin
xe:=x+((q+2)/2)xh;
for p:=1 step 1 until 2 do
y2[p]:=y1[p]+k[p,q-1]x((q+2)/2);

for p:=1 step 1 until 2 do
k[p,q]:=hxDE(y2[1],y2[2],xe,p);
end q;

for p:=1 step 1 until 2 do
y2[p]:=y1[p]+k[p,1]/6+k[p,2]/3+k[p,3]/3+k[p,4]/6;

end RKOST ;

open(10); open(20);
u:=0; M:=p-4;
A:=0;
A:=read(20);

n:=read(20);

B:=read(20);
NI:=read(20);


```

N:=read(20);
for k:=n step -1 until 1 do MOD[k]:=read(20);
for k:=NI step -1 until 1 do ARG[k]:=read(20);
N:=N+1;
data: h:=0.01; N:=N-1;
if N=0 then begin
n:=n-1;
N:=NI;
end;

if u>2 then M:=M/10;
if u=1 then M:=M*10;
if u>0 then h:=2*T[1];
if h>0.01 then h:=0.01;
if M>n-3 then M:=n-3;
x:=y1[1]; y1[2]:=T[0]:=0;

k:=u:=0; s:=1;
l:=0;
mod:=MOD[n]; arg:=ARG[N];
I:=0;

if mod>n4 then h:=0.00125;

L: RKOST(x,h,y1,y2);
I:=I+1;
if u>0 then goto RR;
if k:=k+1;
k:=1 if k=1 then begin F[1]:=y2[1];
if F[2]:=y2[2];
F[2]:=y2[2];
h:=h/2;
end;

if k=2 then begin
y1[1]:=y1[1];
y1[2]:=y1[2];
y1[1]:=f[1]:=y2[1];
y1[2]:=f[2]:=y2[2];
x:=x+h;
end;

if k=1 then goto L else if k=2 then goto L;
if ((y2[1]-F[1])/y2[1])2+((y2[2]-F[2])/y2[2])2<M
then begin
l:=0;
k:=0;
x:=x+h; h:=4*xh;

T[s]:=x;
y1[1]:=Z[1,s]:=y2[1];

```

```

y1[2]:=Z[2,s]:=y2[2];
end

```

```

else begin k:=1; x:=x-h; h:=h/2;
l:=l+1;
F[1]:=f[1]; F[2]:=f[2];
y1[1]:=Y1[1]; y1[2]:=Y1[2];
end;

```

```

if k=1 then goto L else if x>B+0.0002
then goto repeat else t:=s:=s+1;

```

```

if s<498 then goto L else goto data;
repeat: s:=1; u:=u+1; v:=0;
P:=Q:=0; Z[1,0]:=Z[2,0]:=0;
y1[1]:=y1[2]:=y2[1]:=y2[2]:=0;

```

```

RR: v:=v+1;
if v-1<2tu then begin
x:=T[s-1]+(T[s]-T[s-1])x(v-1)/2tu;

```

```

y1[1]:=y2[1];
y1[2]:=y2[2];
end;

```

```

if v-1=2tu then begin
P:=Z[1,s]; Q:=Z[2,s];
x:=T[s];
y1[1]:=Z[1,s]:=y2[1];
y1[2]:=Z[2,s]:=y2[2];
s:=s+1; v:=1;
end;

```

```

if s=t+1 and ((P-Z[1,s-1])/Z[1,s-1])2+((Q-Z[2,s-1])/Z[2,s-1])2<=8
then goto out;

```

```

T[t+1]:=0;
h:=(T[s]-T[s-1])/2tu;
if s=t+1 then goto repeat else goto L;

```

```

out:

```

```

s:=0;

```

```

X: s:=s+1;

```

```

if T[s]<B-0.0001 then goto X;

```

```

if T[s]>B+0.0001 then begin

```

```

h:=B-T[s-1]; f1:=true;

```

```

y1[1]:=Z[1,s-1];

```

```

y1[2]:=Z[2,s-1];

```

```

RKOST (T[s-1],h,y1,y2);

```

```

end

```

```

else f1:=false;

```

```

if not f1 then begin

```



```
y2[1]:=Z[1,s];y2[2]:=Z[2,s];end;
```

```
A:=A+1;
```

```
if A=47 then A:=1;
```

```
if A>1 then goto NOPAGE;
```

```
h:=arctan(y2[2]/y2[1]);
```

```
write text (10,[[2c2s]MOD[9s]ARG[8s]mod*Y  
[6s]arg*Y[7s]INT[2c]]);
```

```
if y2[1] < 0 then h:=if y2[2]<0 then h-3.14159265
```

```
else h+3.14159265;
```

```
NOPAGE: write (10, format([d.ds,nd;]),mod);
```

```
write (10, format([ss+d.ddddd;]), arg);
```

```
write (10, format([ssd.ddds,nd;]), sqrt(y2[1]2+y2[2]2));
```

```
write (10, format([ss+d.dddd;c]), h);
```

```
if n+N>2 then goto data;
```

```
close(10); close(20);
```

```
end→
```

APPENDIX C

Calculation of the cylindrical impedance z.

From equation 3.9, we have

$$\frac{h}{\Delta Z_E} = \frac{Z_o \cdot h}{K^2} - \frac{Z_o^2}{K^2 z} \quad \text{C.1}$$

where h is the change of liquid height in the annulus, causing a change ΔZ_E in the electrical impedance. K^2 is the transducer constant, z is the contribution to the torsional impedance of unit height of liquid and Z_o is an unknown background impedance.

$$\text{Let } z = |z| e^{-j\alpha}, \quad Z_o = |Z_o| e^{j\beta}$$

$$\begin{aligned} \text{Then } \operatorname{Re}\left(\frac{h}{\Delta Z_E}\right) &= \frac{h}{K^2} |Z_o| \cos \beta - \frac{|Z_o|^2}{K^2 |z|} \cos(2\beta + \alpha) \\ \operatorname{Im}\left(\frac{h}{\Delta Z_E}\right) &= \frac{h}{K^2} |Z_o| \sin \beta - \frac{|Z_o|^2}{K^2 |z|} \sin(2\beta + \alpha) \end{aligned}$$

If graphs are drawn of the real and imaginary parts of $(h/\Delta Z_E)$ vs. h , let the slopes and intercepts of the resulting straight lines be S and I with suffices 1 and 2 to represent real and imaginary quantities respectively.

$$\begin{aligned} \text{Then, } S_1 &= \frac{|Z_o|}{K^2} \cos \beta; & I_1 &= -\frac{|Z_o|^2}{K^2 |z|} \cos(2\beta + \alpha) \\ S_2 &= \frac{|Z_o|}{K^2} \sin \beta; & I_2 &= -\frac{|Z_o|^2}{K^2 |z|} \sin(2\beta + \alpha) \end{aligned}$$

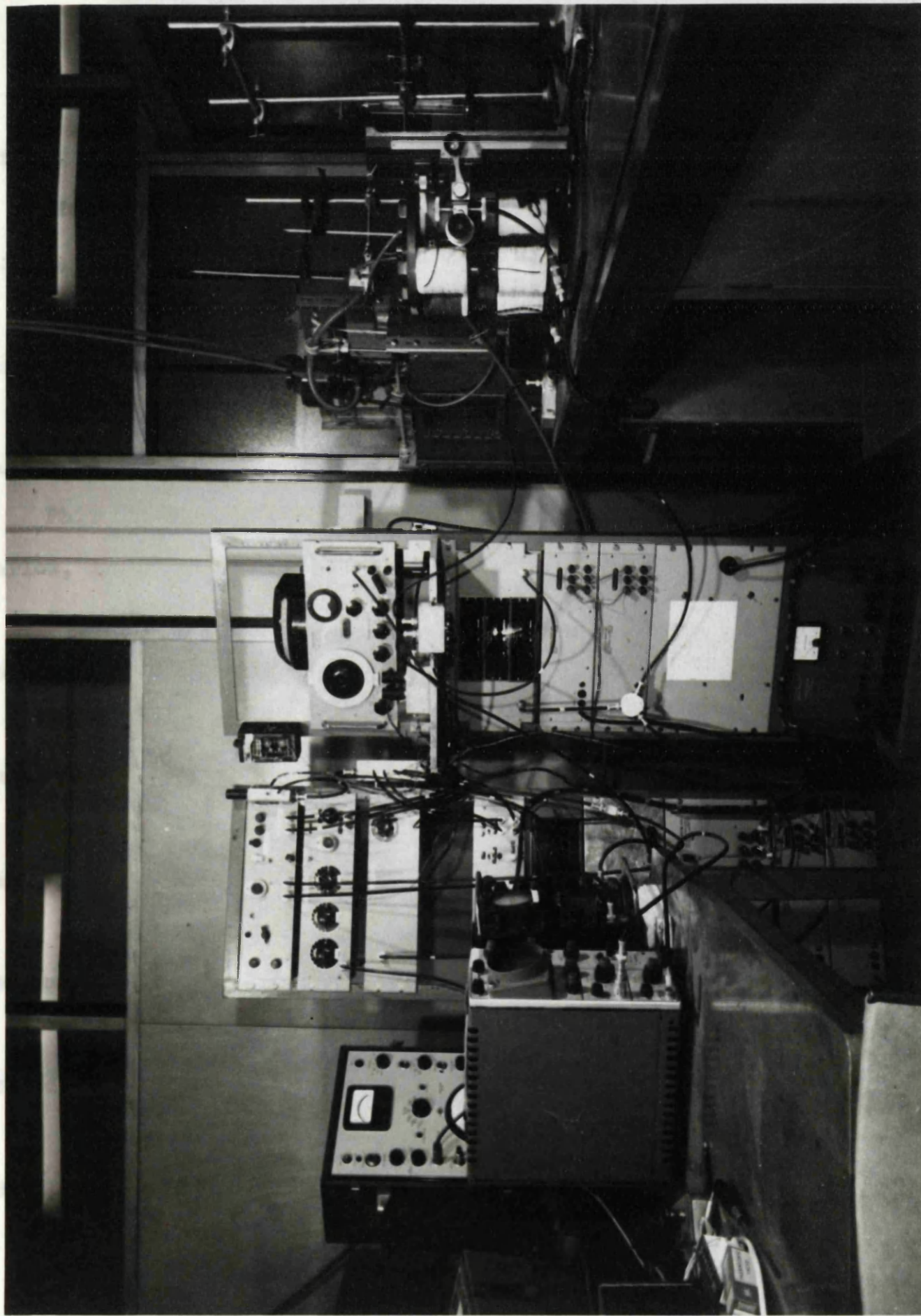
$$\text{Whence, } \tan \beta = S_2/S_1 \quad \text{C.2}$$

$$\tan(2\beta + \alpha) = I_2/I_1 \quad \text{C.3}$$

where $\alpha = -\angle z = \arg Y$ and $|z| = \frac{k^2(s_1^2 + s_2^2)}{\sqrt{I_1^2 + I_2^2}}$ C.4

From equations C.2 and C.3, the unknown β may be eliminated to give $\angle z$. Together with equation C.4, z is thus determined.

General View of the Apparatus



REFERENCES

Alfrey, T., 1948

'Mechanical Behaviour of High Polymers', Interscience, New York.

Alfrey, T. and Doty, P.M., 1945

J. Appl. Phys., 16, 700.

Barber, E.M., Muenger, J.R. and Villforth, F.J., 1955

Anal. Chem., 27, 425.

Barlow, A.J., 1959

Ph.D. Thesis, University of London.

Barlow, A.J., Harrison, G.H. and Lamb, J., 1964

Proc. Roy. Soc., A, 282, 228.

Barlow, A.J. and Lamb, J., 1959

Proc. Roy. Soc., A, 253, 52.

Barlow, A.J., Harrison, G.H., Richter, J., Seguin, H. and Lamb, J., 1961

Lab. Pract., 10, 786.

Barry, A.J., 1946

J. Appl. Phys., 17, 1020.

Benbow, J.J., 1953

J. Sci. Instr., 30, 412.

Bland, D.R., 1960

'The Theory of Linear Viscoelasticity', Pergamon, London.

Boyd, R.H., 1958

J. Appl. Phys., 29, 953.

Bueche, F., 1952

J. Chem. Phys., 20, 1959.

Bueche, F., 1954

J. Chem. Phys., 22, 603.

Coleman, B.D. and Markovitz, H., 1964

J. Appl. Phys., 35, 1.

Coleman, B.D. and Noll, W., 1956

Arch. Ration. Mech. Anal., 3, 289.

Collatz, L., 1960

'The Numerical Treatment of Differential Equations', Springer, Berlin.

Cox, W.P. and Merz, E.H., 1958

J. Poly. Sci., 28, 619.

Cox, W.P. and Merz, E.H., 1959

MSS., Monsanto Chemical Co., Springfield, Mass.

Curie, P., 1908

'Oevres'

de Groot, S.R. and Mazur, P., 1962

'Non-equilibrium Thermodynamics', North Holland, Amsterdam.

de Witt, T.W., 1955

J. Appl. Phys., 26, 889.

den Otter, J.L., 1965

Private communication.

Dyson, A., 1965

Phil. Trans. Roy. Soc., (to be published).

Ferguson, W.A., 1954

Mullard Tech. Comm., 6, 137.

Ferry, J.D., 1958

'Rheology' (Ed. Eötvös, F.R.) Vol. 2.

Ferry, J.D., 1961

'Viscoelastic Properties of Polymers', Wiley, New York.

Ferry, J.D., Fitzgerald, E.R., Grandine, L.D. and Williams, M.L., 1952

Industr. Engng. Chem., 44, 702.

Ferry, J.D., Landel, R.F. and Williams, M.L., 1955

J. Appl. Phys., 26, 359.

Fitzgerald, E.R. and Ferry, J.D., 1953

J. Coll. Sci., 8, 1.

Flory, P.J., 1953

'Principles of Polymer Chemistry', Cornell University Press, New York.

Fujita, H., 1958

J. Appl. Phys., 29, 943.

Goldberg, H. and Sandvik, O., 1947

Anal. Chem., 19, 123.

Gross, B., 1953

'Mathematical Structure of the Theories of Viscoelasticity',
Hermann, Paris.

Guillemin, E.A., 1957

'Synthesis of Passive Networks', Wiley, New York.

Harrison, G., 1964

Ph.D. Thesis, University of London.

Harrison, V.G.W., 1953

Ed. of Proc. of 2nd Int. Congr. Rheol., Butterworths, London.

Hopkins, I.L., 1951

Trans. Am. Soc. Mech. Eng., 73, 195.

Hunter, S.C., 1960

'Progress in Solid Mechanics', (Ed. Sneddon, I.N., Hill, R.),

North Holland, Amsterdam.

Hutton, J.F., 1963

Nature, 200, 646.

Leademann, H., 1943

'Elastic and Creep Properties of Filamentous Materials',

Textile Foundation, Washington.

Lodge, A.S., 1964

'Elastic Liquids', Academic Press, New York.

Long, R.R., 1961

'Mechanics of Solids and Fluids', Prentice-Hall, London.

Lovitt, W.V., 1950

'Linear Integral Equations', Dover

McLachlan, N.W., 1934

'Bessel Functions for Engineers', Oxford University Press.

McSkimin, H.J., 1952

J. Acoust. Soc. Amer. 24, 355.

Mark, H. and Tobolsky, A.V., 1950

'Physical Chemistry of High Polymeric Systems', Interscience,

New York.

Markovitz, H., 1952

J. Appl. Phys., 23, 1070.

Markovitz, H., 1960

'Viscoelasticity', Ed. J.T. Bergen, p.133, Academic Press, New York.

Markovitz, H., and Williamson, B., 1957

Trans. Soc. Rheol., 1, 25.

Mason, W.P., 1948

'Electromechanical Transducers and Wave Filters', Van Nostrand,
New York.

Maxwell, J.C., 1867

Phil. Trans. 157, 52.

Morrisson, T.E., Zapas, L.J. and de Witt, T.W., 1955

Rev. Sci. Instr., 26, 357.

Murnaghan, F.D., 1951

'Finite Deformation of an Elastic Solid', Wiley, New York.

Oldroyd, J.G., 1950

Proc. Roy. Soc., A, 200, 523.

Oldroyd, J.G., 1958

Proc. Roy. Soc., A, 245, 278.

Oldroyd, J.G., 1961

Sonderdruck aus Rheol. Acta., 1, 337.

Oldroyd, J.G., Strawbridge, D.J. and Toms, B.A., 1951

Proc. Phys. Soc., B, 64, 44.

Oliner, A.A., 1948

J. Appl. Phys., 19, 109.

Onogi, S., Hamana, I. and Hirai, H., 1958

J. Appl. Phys. 29, 1053.

Padden, F.J. and de Witt, T.W., 1954

J. Appl. Phys., 25, 1086.

Pao, Y.H., 1957

J. Appl. Phys., 28, 591.

Philipoff, W., 1954

J. Appl. Phys., 25, 9.

Redish, K.A., 1961

'An Introduction to Computational Methods', English Universities
Press, London.

Reiner, M., 1949

'Deformation and Flow', Lewis,

Rivlin, R.S., 1956

'Rheology', (Ed. Eirich, F.R.), Vol. 1, Academic Press, New York.

Roesler, F.C., 1955

Proc. Phys. Soc., B, 68, 89.

Roesler, F.C. and Pearson, J.R.A., 1954

Proc. Phys. Soc., MB, 67, 338.

Roesler, F.C. and Twyman, W.A., 1955

Proc. Phys. Soc., B, 68, 97.

Roscoe, R., 1964

Brit. J. Appl. Phys., 15, 1095.

Rouse, P.E., 1953

J. Chem. Phys., 21, 1272.

Russell, R.J., 1946

Ph.D. Thesis, University of London.

Schwarzl, F. and Staverman, A.J., 1953

Appl. Sci. Res., A, 4, 127.

Sittel, K., Rouse, P.E. and Bailey, E.D., 1954

J. Appl. Phys., 25, 10.

Smith, T.L., Ferry, J.D. and Schremp, F.W., 1949

J. Appl. Phys., 20, 144.

Tobolsky, A.V. and Andrews, R.D., 1943

J. Chem. Phys., 11, 125.

Tschoegl, N.W., 1963

MSS., Dept. of Chemistry, University of Wisconsin.

Valley, G.E. and Wallman, H., 1948

'Vacuum Tube Amplifiers', Vol. 18, M.I.T. Radiation Lab. Series,
McGraw-Hill, New York.

van der Pol, B. and Bremmer, H., 1955

'Operational Calculus', Cambridge University Press.

Weissenberg, K., 1947

Nature, 159, 310.

Weissenberg, K., 1949

Proc. 1st Int. Congr. Rheol., North Holland, Amsterdam.

Williams, M.L. and Ferry, J.D., 1953

J. Poly. Sci., 11, 169.

Zimm, B.H., 1956

J. Chem. Phys., 24, 269.

Table 8.1 Inverse of Matrix M (elements to be multiplied by 100)

[illegible]

